Summer 2015

Combustion and pollutant characteristics of IC engines fueled with hydrogen and diesel/hydrogen mixtures using 3D computations with detailed chemical kinetics

Hassan A. Khairallah

Department: Mechanical and Aerospace Engineering

COMBUSTION AND POLLUTANT CHARACTERISTICS OF IC ENGINES FUELED WITH HYDROGEN AND DIESEL/ HYDROGEN MIXTURES USING 3D COMPUTATIONS WITH DETAILED CHEMICAL KINETICS

by

HASSAN A. KHAIRALLAH

A DISSERTATION

Presented to the Faculty of the Graduate School of the

MISSOURI UNIVERSITY OF SCIENCE AND TECHNOLOGY

In Partial Fulfillment of the Requirements for the Degree

DOCTOR OF PHILOSOPHY

in

MECHANICAL ENGINEERING

2015

Approved
Umit O. Koylu, Advisor
John W. Sheffield
James A. Drallmeier
Lian Duan
Jagannathan Sarangapani

PUBLICATION DISSERTATION OPTION

This dissertation has been prepared in the form of four papers for publication as follows:

Pages 4-34 have been submitted to Journal of Energy and Fuels journal.

Pages 35-57 have been presented at ASME IMECE and being finalized for submission to International Journal of Hydrogen Energy.

Pages 58-83 have been presented at Society of Automotive Engineers conference and to be submitted to Journal of Energy.

Pages 83-112 have recently been presented at the ASME Power and Energy Conference (ASME 2015).

ABSTRACT

In order to develop design guidelines for optimum operations of internal combustion engines fueled with alternative fuels, a comprehensive understanding combustion behavior and the pollutant formation inside the cylinder are needed. The first part of this thesis aimed to numerically study the engine performance and in-cylinder pollutant formation in a spark ignition engine fueled with hydrogen. Advanced simulations were performed using multi- dimensional software AVL FIRE coupled with CHEMKIN. The detailed chemical reactions with 29 steps of hydrogen oxidation with additional nitrogen oxidation reactions were also employed. Formation rates of nitrogen oxides (NO_x) within the engine were accurately predicted using the extended Zeldovich mechanism with parameters adjusted for a carbon-free fuel. The computational results were first validated against experimental results with different equivalence ratios and then employed to examine a spark-ignition engine fueled with hydrogen under different operating conditions. Strategies that could have significant effects on the engine performance and emissions, such as exhaust gas recirculation (EGR) and ignition timing were also investigated. Furthermore, the maximization of engine power and minimization of NO_x emissions were considered as conflicting objectives for preliminary optimization. Finally, a skeletal reaction mechanism was developed to include the reaction kinetics of diesel and hydrogen fuel mixtures to investigate in-cylinder combustion processes of such a dual fuel compression-ignition engine. The model was then employed to examine the effects of exhaust gas recirculation (EGR) and N_2 dilution on NO_x emissions.

ACKNOWLEDGMENTS

First, I hereby take the opportunity to thank my advisor, Prof. Koylu for his extensive help and suggestions as well as for providing valuable information regarding my research. I am also deeply indebted to my committee members for their time and effort in reviewing this work.

I would like to extend my sincerest thanks and appreciation to all of the faculty and staff in the Department of Mechanical and Aerospace Engineering at Missouri University of Science and Technology for their help and input.

I must express my special thanks to my wife, Maria, for her moral support and precious love while always standing by me in my hard times during my study.

. Finally, I feel especially indebted to my parents for their love and support. They are my first teachers, and without their encouragement throughout my entire life, I would never have been successful.

TABLE OF CONTENTS

LIST OF ILLUSTRATION

Page

PAPER I

PAPER II

PAPER III

PAPER IV

LIST OF TABLES

1. INTRODUCTION

Due to the depletion of fossil fuels and environmental degradation in recent years, there is considerable global effort to ensure continued availability of supplies of hydrocarbon fuels and to reduce exhaust emissions from all combustion devices, particularly internal combustion engines. Many studies by a number of research groups worldwide have focused attention on alternative transportation fuels to replace or supplement hydrocarbon fuels. In this regard, hydrogen is considered one of the most promising alternate fuels due to its clean burning characteristics and better overall performance as compared to hydrocarbons fuel.

The hydrogen has numerous excellent combustion characteristics when burned in internal combustion (IC). Hydrogen's composition does not include any carbon specie. This means that a hydrogen engine does not produce toxic products, such as hydrocarbons (HC), carbon monoxide (CO), and carbon dioxide (CO_2); instead, its main products are water (H_2O) and nitrogen oxide (NOx). Hydrogen has a wide flammability range in comparison with all other fuels. This is a significant advantage that permits the use of an ultra-lean mixture. Generally, fuel economy will be greater when an IC engine is run with a lean mixture. Hydrogen has a very low ignition energy. The amount of energy needed to ignite hydrogen is less than that needed for conventional fuels. This permits hydrogen engines to ignite lean mixtures and ensures prompt ignition. Hydrogen also has a high flame speed. This means that hydrogen engines can more closely approach the thermodynamically ideal engine cycle. The higher flame speed results in a high rate of pressure rise in hydrogen-fueled engines; therefore, combustion is almost instantaneous. The auto-ignition temperature of hydrogen is very high (858°K). This permits hydrogen to be more suitable as a fuel for spark ignition (SI) engines. Moreover, hydrogen's high auto-ignition temperature encourages the use of larger compression ratios, such as the ones prevalent in diesel engines.

Hydrogen-fueled IC engines also have negative aspects that need to emphasis on them and suggest the technologies for overcoming on these challenges. Increasing the equivalence ratio for a higher power demand increases NOx emissions, which are higher than those from conventional engines. Due to hydrogen's lower ignition energy, the hot

gases and hot spots in the cylinder, such as deposits, residual gas, exhaust valves, spark plugs, etc., can serve as sources of ignition, generating problems of pre-ignition (undesired ignition) and backfire. The pre-ignition can be prevented by using dilution techniques, such as exhaust gas recirculation (EGR); charge dilution by inert gases, such as helium (He) and nitrogen (N_2); and by water (H_2O) injection. Hydrogen has a very low density. This result in two problems when it is used in an internal combustion engine: (1) a very large volume is required to store enough hydrogen to give an adequate running time for the vehicle, and (2) the low energy density of a hydrogen-air mixture reduces the power output of the hydrogen-fueled engine. Hydrogen has a small quenching distance, smaller than other conventional fuels. Consequently, this allows flame propagation nearer to the cylinder walls before they extinguish than is possible with other fuels. The smaller quenching distance can also increase the chance for backfire. Hydrogen has very high diffusivity. This ability to disperse in air is advantageous for the formation of a uniform mixture of fuel and air, and to curb the problem of hydrogen leaks.

Hydrogen can be adapted to power both spark ignition (SI) and compression ignition (CI) engines. In SI engines, hydrogen can be used directly as the sole fuel. However in the case of a CI engine, hydrogen cannot be used directly, because it is very difficult to ignite it by only the compression process due to its auto-ignition temperature (858 K) being so much higher than that of diesel fuel (525 K) . Therefore, some auxiliary ignition sources (spark plugs, glow plugs, or pilot fuel) have to be used inside the CI engine combustion chamber to ensure the ignition of hydrogen. Hydrogen can also be used in compression ignition (CI) engines under dual-fuel combustion mode with H2 supplemented into the intake air. In dual-fuel engines, the combustion of gaseous fuel with high ignition temperature such as H_2 is achieved with the ignition of a fuel with low ignition temperature such as diesel.

Numerous experiments have been established on IC fueled with hydrogen to investigated and understand the in-cylinder combustion processes under different operating conditions. However, there are difficult to obtain better knowledge about the in-cylinder combustion processes and pollutant experimentally. Also reduce the development costs and minimizing the time is needed with experimental investigations. In the past few years numerous studies focused on how to create an engine models in order to obtain an insight

into the complex phenomena in-cylinder processes, and furthermore optimize engines development.

Today Computational Fluid Dynamics (CFD) has become an essential tool in the process of designing and developing engineering devices. In the past few decades, the 3D CFD code has become a commonly used tool to gain a better knowledge about the combustion processes inside the engine cylinder. CFD offers successful assessment of new technologies, e. g., new fuel preparation methods, new combustion concepts, and/or alternative fuels. With the recent development of computer processors and the expansion of allowable memory, researchers and engineers are now able to integrate detailed chemical kinetics with a computational fluid dynamics (CFD) code to simulate IC engines.

The layout of the dissertation is as follows. The first part investigates in-cylinder combustion processes in a SI engine using a 3D Model with Chemical Kinetics. The model was validated by the experimental results and employed to examine important parameters that have significant effects on the engine performance. The second part investigates in-cylinder combustion processes in a diesel engine fueled with hydrogen using a 3D Model with Chemical Kinetics. The model was then employed to examine the effects of exhaust gas recirculation (EGR) and N2 dilution on NO_X emissions.

I. COMPUTATIONAL INVESTIGATION OF IN-CYLINDER COMBUSTION CHARACTERISTICS AND EMISSION OF HYDROGEN IC ENGINE USING A 3D MODEL WITH CHEMICAL KINETICS

Hassan A. Khairallah and Umit O. Koylu
Department of Mechanical and Aerospace Engineering, Missouri University of Science and Technology, Rolla, MO 65409 USA.

ABSTRACT

During the past decade, considerable effort has been made to introduce alternative energy sources for use in conventional diesel and gasoline engines. Many researchers have attempted to use hydrogen as a fuel in the diesel engine due to its ability to reduce pollutant emissions, such as carbon monoxide and unburned hydrocarbons. With the rapid increase in computational capabilities, 3D computational fluid dynamics CFD codes become essential tools for practical design, control and optimization of hydrogen engines. In the present study, detailed chemical kinetic reactions with twenty nine steps of hydrogen oxidation with additional nitrogen oxidation reactions were coupled with CFD code to study combustion processes in a diesel engine using hydrogen as the fuel. Moreover, a spark ignition model built by C++ program was incorporated into the model to simulate the hydrogen ignition behavior. The NO formation within the engine was computed using the extended Zel'dovic mechanism with parameters adjusted for a carbon-free fuel such as hydrogen. The model was validated by the experimental results and employed to examine important parameters that have significant effects on the engine performance. The simulation results show that the variations of peak in-cylinder pressure, heat release rate, brake thermal efficiency, flame development period, combustion duration, and NO emissions reasonably agree with the experimental findings. In order to reduce NO_x

emission an exhaust gas recirculation (EGR) system has been employed in the engine model. The computations are consistent with the hypothesis that gas cylinder temperature decreases with adding EGR and that the decrease in gas cylinder temperature results in the reduction in NO_x emissions.

KEYWORDS: chemical kinetics, spark ignition engine, hydrogen engine and exhaust gas recirculation (EGR), emissions.

Corresponding Author: Umit O. Koylu* , Tel: (001) 573-341-6601, E-mail: koyluu@mst.edu

1. INTRODUCTION

Due to the rapid depletion of fossil fuels and their detrimental effect on the environment, many researchers have put considerable effort into developing and introducing alternative transportation fuels to replace conventional fuels, such as gasoline and diesel.1 Hydrogen is one of the most promising alternative fuels for internal combustion (IC) engines due to its positive effects and its limited number of negative effects. In the absence of carbon and sulfur the hydrogen-operated engine produces water as its main combustion product. It does not produce significant amounts of carbon monoxide (CO), hydrocarbon (HC), smoke, Sulphur oxides (SOX), or carbon dioxide (CO2). The only undesirable emissions are the nitrogen oxides (NOx), specifically nitric oxide (NO) and nitrogen dioxide (NO2). This high level of NOx is due to the high combustion temperature in hydrogen-fuelled engines.2 Hydrogen has good properties as a fuel for internal combustion engines.3-5 Hydrogen has a wide flammability range in comparison with all other fuels. Hydrogen also has a high flame speed. This means that hydrogen engines can more closely approach the thermodynamically ideal engine cycle. The higher flame speed results in a high rate of pressure rise in hydrogen fueled engines; therefore, combustion is almost instantaneous. The higher flame speed and wider

flammability limits make hydrogen engines more efficient in stop-and-start driving. The high burning rate of hydrogen produces high pressures and temperatures during combustion in chamber combustion when operating in near-stoichiometric mixtures. This will lead to high exhaust emissions of oxides of nitrogen.

The ignition energy required to ignite the hydrogen is very low, which allows hydrogen engine to ignite lean mixtures and ensures prompt ignition. However, the low ignition energy leads to uncontrolled pre-ignition/backfire problems.[6,7] Hydrogen's high diffusivity quickly spreads fuel leaks, therefore reducing the explosion hazards associated with hydrogen engine operation. Hydrogen has a very low density. This means that the hydrogen engine needs a tank of very large volume to store enough hydrogen to give the vehicle an adequate driving range.

Hydrogen's high auto-ignition temperature (858°K) makes it more suitable as a fuel for spark ignition (SI) engines8[-10] than for compression ignition engines (IC) engines. However, the hydrogen cannot be used directly in a diesel engine, because it is very difficult to ignite hydrogen just by the compression process, due to its auto-ignition temperature (858°K) being so much higher than that of diesel fuel (525°K).[11] Therefore, some sources of ignition (spark plugs, glow plugs, or pilot fuel),[12-18] have to be generated inside the combustion chamber to ensure the ignition of hydrogen.

2. BACKGROUND AND MOTIVATION

During the past few years, numerous researchers have made an effort to use hydrogen as fuel compression ignition engines. Some researchers have used diesel as an ignition source to ignite hydrogen,[14-16,18,19] and others have used glow plugs or spark plugs as an ignition source. Homan et al.[12] carried out experiments on a diesel engine converted for hydrogen operation without providing a timed ignition system. A glow plug and a multiple-strike spark plug were tested as ignition sources. It was found that glow plug ignition was an attractive way to operate hydrogen-fueled engines with direct cylinder injection late in the compression stroke. Welch et al.[13] performed hydrogen injection investigations using a glow plug for ignition assist and found that the use of hydrogen

provided higher power than the same engine could provide on diesel. Wong[17] has tried using a ceramic part as a glow plug to retain heat as the ignition source.

Several experiments have been established on SI engine fueled with hydrogen to investigated and understand the in-cylinder combustion processes under different operating conditions. Lee et al. [20] conducted that flame propagation under the stoichiometric condition was faster than that under the lean mixture condition. They also found that the flame kernel was made at the central area near the spark plug. Tang et al. [21, 22] investigated the shape of flame kernel in hydrogen–air mixture ignited through a spark plug. The results showed that at 0.1 MPa, the shape of flame kernel was found as a disk whose diameter increases with crank angles. However, there are difficult to obtain better knowledge about the in-cylinder combustion processes and pollutant experimentally. Also reduce the development costs and minimizing the time is needed with experimental investigations. In the past few years numerous studies focused on how to create an engine models in order to obtain an insight into the complex phenomena in-cylinder processes, and furthermore optimize engines development.

Moreover, today Computational Fluid Dynamics (CFD) has become an essential tool in the process of designing and developing engineering devices. In the past few decades, the 3D CFD code has become a commonly used tool to gain a better knowledge about the combustion processes inside the engine cylinder. CFD offers successful assessment of new technologies, e. g., new fuel preparation methods, new combustion concepts, and/or alternative fuels. With the recent development of computer processors and the expansion of allowable memory, researchers and engineers are now able to integrate detailed chemical kinetics with a computational fluid dynamics (CFD) code to simulate IC engines. Many statistical studies have focused on using three-dimensional computational fluid dynamics (CFD) tools to understand the in-cylinder flow field and mixing process.[23-30] Rakopoulos et al.[23,26,27] have recently developed combustion model, which is incorporated in an in-house CFD code using RNG k-ε turbulence model for the simulation of a hydrogen spark-ignition engine. That model is composed of various sub-models used for the simulation of combustion of conventional fuels in SI engines; it has been adjusted for simulation of hydrogen combustion engine. They have investigated the combustion

processes inside cylinder, especially with varying equivalence ratios. Kosmadakis et al.[28] have investigated the variation of EGR rates in that model in order to decrease the exhaust nitrogen oxides emissions. Many studies have also focused on integrated chemical kinetics details with CFD code.[30-33] AVL FIRE® software has been widely used in predicting the performance of diesel engines.[32,33] However, few studies have investigated and reported on hydrogen using chemical kinetics.

In the present model, detailed chemical kinetic reactions for hydrogen oxidation with additional nitrogen oxidation reactions were combined with the AVL FIRE® CFD code using k-ζ-f turbulence model to run a hydrogen-fuelled diesel engine. Also, a spark ignition model was built using C++ programming and incorporated into the model to simulate the hydrogen ignition behavior. An advantage of this model is the FIRE General Gas Phase Reactions Module was used for simulation of spark-ignition engines that run on either hydrogen fuel or conventional fuels, contrary to what it is done in most existing engines models. The present simulation provides better knowledge about the in-cylinder combustion processes that are difficult to determine experimentally.

3. COMPUTATIONAL METHOD

AVL FIRE® presents a general species transport model to allow the implementation of a detailed kinetic model.[31] FIRE® solves species transport equations for an arbitrary number of chemical species. The species mass conservation equation is expressed as:

$$\frac{\partial(\rho w_i)}{\partial t} + \frac{\partial}{\partial x_k}(\rho(U_k - U_{\delta k})w_i) = \frac{\partial}{\partial x_k}\left(\left(\rho D_i + \frac{\mu}{\sigma_{ci}}\right)\frac{\partial}{\partial x_k}\right) + S_{w_i} \quad (1)$$

$$at\ S_{w_i} = r_i$$

Where w_i is the mass fraction, S_{w_i} is the source term of species i by taking into account homogeneous chemical reactions, σ_{ci} is the stress tenser, and μ is the viscosity. Based on parameters extracted from a database, the physical properties (viscosity, density, specific heat, diffusion coefficient, thermal conductivity) shown in the equation above are

calculated for each species and for gas mixtures by using the chemical kinetic databases (CHEMKIN™).

The chemistry effect (level of elementary reactions) is taken into account such that at the beginning of each CFD time step (Δt), a single zone reactor model is calculated for each computational cell. At the latest CFD time step for the properties (pressure, volume, temperature), the following conservation equations are integrated by the model for the time step (Δt), considering the volume cell as a function of time $\{V = V(t)\}$. The species conservation equation is computed using:

$$\rho \frac{\partial w_i}{\partial t} = M_i \omega_i \qquad (2)$$

Here M_i is the molecular weight of ith species, and ω_i is the molar species production rate. In this case, only the source term, S_{w_i}, is taken into account due to the homogeneity assumption. The energy conservation equation is expressed as:

$$\rho c_v \frac{\partial T}{\partial t} + \frac{P}{V}\frac{\partial V}{\partial t} = -\sum_{i=1}^{N_y} u_i M_i \omega_i \qquad (3)$$

On the left-hand side, the first term represents the temporal change of energy content, and the second term represents the volume work. The terms on the right-hand side represent the consideration of the change of inner energy due to production and consumption of chemical species. By using an interface to the CHEMKIN™ libraries, the molar species production rates, ω_i, can be calculated, and the source terms can be calculated by neglecting any effect of turbulence/mixing on the chemical reaction as follows:

$$r_i = \frac{\rho^{n+1} w_i^{n+1} - \rho^n w_i^n}{\Delta t} \qquad (4)$$

Here the superscripts n and n+1 indicate the first and the last values of the single zone reactor model. Keeping the source terms constant for the following CFD time step is the most important advantage of this approach because it makes the CFD simulation 100 percent conservative, fast, and valid.

The following approach considers the effects of both mixing and chemical kinetics by assuming that the reaction rate is determined via a kinetic time scale τ_{kin} (an equilibrium assumption under perfect mixed conditions) and turbulent time scale τ_{turb} (an eddy break up assumption). Furthermore, it assumes that the equilibrium concentration of the fuel is zero and the kinetic time scale is equal to the scale used for the fuel for all the species. By taking these assumptions into account, the above equation becomes:

$$r_i = \frac{\tau_{kin}}{\tau_{kin} + f\tau_{turb}} \frac{\rho^{n+1} w_i^{n+1} - \rho^n w_i^n}{\Delta t} \quad (5)$$

$$\tau_{kin,i} = \Delta t \frac{\rho^{n+1} w_i^{n+1}}{\rho^{n+1} w_i^{n+1} - \rho^n w_i^n} \quad (6)$$

$$\tau_{kin} = \max\left(\tau_{kin,f}, \tau_{kin,CO}\right) \quad (7)$$

The turbulent time scale τ_{turb} can be calculated using the following:

$$\tau_{turb} = C_t \frac{k}{\varepsilon} \quad (8)$$

The variable f is a delay coefficient that uses to simulate the influence of turbulence on combustion after ignition has occurred[34] and can be calculated as:

$$f = \frac{1 - e^{-r}}{0.632} \quad (9)$$

$$r = \frac{w_{co_2} - w_{H_2O} - w_{co} - w_{H_2}}{1 - w_{N_2}} \quad (10)$$

In this study the k-zeta-f model was chosen. This model recently developed by Hanjalic et al.[35] For IC-engine flows the k-z-f model leads to more accurate results than the much simpler two-equation eddy viscosity models of the k-e type by simultaneously exhibiting a high degree of numerical robustness. This model is based on Durbin's elliptic

relaxation concept, which solves a transport equation for the velocity scales ratio $\zeta = \frac{\overline{v^2}}{k}$ instead of the equation for $\overline{v^2}$.[35] The $\overline{v^2}$ is the velocity scale and k is the turbulence kinetic energy. Durbin's model is described in refereance.[36] The detailed chemical kinetics for hydrogen was integrated with the multidimensional CFD code to investigate SI engine fueled with hydrogen. The detailed chemical kinetic reactions for hydrogen consist of 29 steps with additional oxidation reactions involving nitrogen.[37] The CHEMKIN chemistry solver was integrated into the CFD code for solving the chemistry during multidimensional engine simulation. The AVL FIRE® code provides CHEMKIN the species and thermodynamic information of each computation cell, and the CHEMKIN utilities return the new species information and energy release after solving for the chemistry. The FIRE internal interpreter first reads the user's symbolic description of the reaction mechanism. It then extracts thermodynamic information for the species involved from the Thermodynamic Database. The FIRE General Gas Phase Reactions Module was used to enable the simulations of kinetic problems, the detailed chemistry modeling scheme shown in the figure 1.

User-function was applied to use the spark ignition model. A spark ignition model was built using C++ programming and incorporated into the model to simulate the hydrogen ignition behavior. The piston geometry and computational grid used for the simulations were built up using the commercial CFD tool AVL ESEDiesel. The mesh was composed of about 12960 computational cells with mesh size was 3.33 ×3.33×3.56 mm and nodes number 14167. An et al.[44] considered the effect of mesh size in detail and showed that 3.4 mm was sufficient for typical IC engine. Wang et al[45]. also used similar mesh size for reasonable spatial resolution.

The convergence criterion is either maximum number of iterations 60 or reduction of residuals as 0.01 whichever achieves first. In this paper, the boundary conditions were as follows: the piston temperature was 423 K, cylinder liner temperature was 423 K, and cylinder head temperature was 453 K. The computational domain consists of one section of the modeled engine cylinder, which was used for simulations between inlet valve closing (IVC) and exhaust valve opening (EVO). This means that only the closed volume part of the engine cycle is computed. The spark plug located in the center of cylinder head. The

spark duration is equal to 4.5 ^{o}CA (almost 1.33 ms). The computational time step used for simulation, during the compression stroke was 1 ^{o}CA. However during the combustion period, the time step was further decreased and becomes equal to 0.25 ^{o}CA. This occurs in order to increase the accuracy of the computational results.

4. RESULTS AND DISCUSSIONS

The operating conditions of the hydrogen IC engine modeled and simulated in this investigation were chosen similar to the independent study by Subramanian et. al.4 because their reported test conditions and experimental data were well documented. Specifications for the spark-ignition hydrogen engine used in this computational study and engine's initial operating conditions are listed in Table 1. The spark-timing was set to its MBT (Minimum advance for best torque) value, and the engine speed was kept constant at 2500 rpm.

4.1. A comparison between hydrogen and gasoline IC engines

Before a comparison to experimental data, the computational model for hydrogen engine was first compared to the computational model for gasoline engine with the same geometry and operating conditions. The spark-timing is set to their MBT value (5 ^{o}CA BTDC for hydrogen and 18 ^{o}CA BTDC for gasoline), and the engine speed was kept constant at 2500 rpm. This exercise revealed the general features of a hydrogen engine relative to a traditional engine. Figure 2 illustrate the variation of cylinder pressure versus crank angle for both types of engines at full load. As expected, in comparison to the gasoline engine, the hydrogen engine had both a higher rate of pressure rise and a higher maximum pressure in the cylinder than did the gasoline engine because the hydrogen had a significantly higher burning speed. The peak pressure for hydrogen was advanced by 3^{o} crank angle as compared to the peak pressure for gasoline because the hydrogen undergoes instantaneous combustion.

Additionally, the flame development period (time interval between instant of spark and the inflammation of the air-fuel mixture) and combustion duration, for the hydrogen and gasoline engines under identical operating conditions are compared in terms of crank angle. The flame development period and combustion duration for the hydrogen engine were 6^{o} and 27^{o} crank angles respectively. On the other hand, for the gasoline engine, the

flame development period and combustion duration were recorded as 12º and 60º crank angles respectively. The faster ignition and shorter combustion duration were responsible for the optimal spark timing (MBT) to be close to the top dead center (5 ºCA BTDC) for hydrogen and to be 18 ºCA BTDC for gasoline operation. Figure 3 shows in-cylinder temperature profiles as the flame propagates out from the spark plug, depicting how the flame propagates inside the cylinder after the ignition timing for hydrogen and gasoline. At the start of the ignition, the flame kernel shape was found as a disk whose diameter increases with time, which agrees with Tang et al.[21,22] It is seen that hydrogen has shorter burn compared to that of gasoline, wherein the flame covered the entire cylinder at a crank angle of 16 ºCA AIT (After Ignition Time). However, for gasoline at a crank angle of 24º AIT the flame is still propagating. This is due to higher flame speed of hydrogen, which is five times that of gasoline, and the wider flammability range of hydrogen compared to gasoline. This leads to faster burning velocity of hydrogen and an extended flame limit than gasoline, which can achieve a shorter burning duration and a more complete burning.

4.2. Model validation-comparison of simulations to experiments

Several engine combustion cases were studied, and an in-cylinder emissions formation process and engine performance were predicted. The simulations provide values of indicated work (W_i), indicated mean effective pressure (IMEP) and indicated power (P_i), which was calculated from in-cylinder pressure trace as following equations:

$$W_i\ (kj) = \int_{IVC}^{EVO} pdV \tag{11}$$

$$IMEP\ (kPa) = \frac{1}{V_d} \int_{IVC}^{EVO} pdV \tag{12}$$

$$P_i\ (kW) = \frac{W_i\ .N}{2\ \times 60} \tag{13}$$

Indicated thermal efficiency (ITE) would be a more relevant comparison as this study was more concerned with the combustion process instead of the power transmission. The experimental data4 were obtained for brake thermal efficiency (after friction) instead of indicated thermal efficiency (before friction). To compute brake thermal efficiency of the hydrogen engine, the Chen-Flynn friction model 46 has been used as shown in the following equation:

$$FMEP\ (kPa) = 0.7 + 0.008\ \times\ P_{\max\_cylindr} + 0.21\ \times \bar{S}_p + 0.0015\ \times\ \bar{S}_p^2 \tag{14}$$

So friction power (P_f) was calculated as follows:

$$P_f\ (kW) = \frac{FMEP\ \times\ V_d\ \times N}{2 \times 60} \tag{15}$$

where N is engine speed (rpm), $\bar{S}_p$ is mean piston speed (m/s) and V_d is displacement volume (m^3). Then the brake power (P_b) was obtained as the difference in between indicated power (P_i) and the friction power (P_f). Table 2 shows validated model results against independent experiments for performance and engine out exhausts. It was found that the peak pressure increase almost linearly with equivalence ratio (or brake power) as shown in the table, which were in agreement with one dimensional model reported by Vudumu et al.[46] This is because the flame speed increased as both the equivalence ratio (and brake power) increased and the time required completing the combustion decreased. The predicted peak pressure was in good agreement with the experimental data collected at equivalence ratios of 0.3 and 0.55. However the predicted results were 5 % higher than the experiments at equivalence ratio of 0.84.

From the table was observed that the brake thermal efficiency increased as the equivalence ratio increased. The brake thermal efficiency of an engine is defined as the ratio of the engine brake power to the input fuel energy.

$$\eta_{\mathrm{BTE}} = \frac{P_b}{(\dot{m}_{f.hydrogen} \times CV_{hydrogen})} \tag{16}$$

Here $\dot{m}_{f.hydrogen}$ is hydrogen flow rate (kg/s) and $CV_{hydrogen}$ is the lower heating value of hydrogen fuel (kg/kJ) with a value of 120 MJ/kg. The maximum brake thermal efficiency was nearly 30 % at an equivalence ratio of 0.84 (7.4 kW) and 19 % at 0.3 equivalence ratio (2 kW). At high brake power flame speed increases as the equivalence ratio increases and therefore nearly constant volume combustion is achieved with hydrogen, which results in higher brake thermal efficiency.

The predicted heat release rates as a function with the crank angle for hydrogen and gasoline operation at maximum are illustrated in Fig. 4. The predicted peak heat release in the hydrogen operation was higher (83 J/deg) compared to gasoline operation. These results indicate that hydrogen's faster burning speed produces a relatively high rate of heat release within a small time interval. Several of the simple divergences that occurred in predicting the heat release rate (HRR) could have been caused either by deficiencies in the computer models or differences in the boundary conditions between the simulations and the experiments.

In-cylinder temperature profiles, as the flame propagated out from the spark plug with different equivalence ratios (0.84, 0.55, and 0.3) are illustrated in Fig. 7. The equivalence ratio had a significant influence on the flame propagation. The highest flame intensity was obtained at $\phi = 0.84$, where the flame covered the entire combustion chamber at a crank angle of 16 ^{o}CA AIT. The flame's intensity was weaker at $\phi = 0.55$ than it was at $\varphi = 0.84$. Here the flame covered the entire combustion chamber at a crank angle of 24 ^{o}CA AIT. The flame's intensity was very weak at $\phi = 0.3$, since at a crank angle of 32 ^{o}CA AIT the flame still propagates towards the chamber walls. This might be caused due to lesser thermal energy liberated from the leaner mixture which increases the flame development period and slows the flame propagation. These results were in agreement with experimental observations reported by Lee et al.[20] and with numerical observations reported by Rakopoulos et al.[26,27].

The undesirable emission produced by hydrogen engines only the nitric oxide. Any carbon emissions (e.g., CO, CO_2 and HC) will be very little. Thus, they are omitted in emission discussions. The NO formation can be described by reactions R6, R7, and R8. These reactions are typically known as the extended Zel'dovich mechanism:

$$N2 + O = N + NO \quad (R1)$$

$$N + O2 = NO + O \quad (R2)$$

$$N + OH = NO + H \quad (R3)$$

In general, these three reactions are only important at high temperatures because, the radicals O and OH are created in high temperature gases.

The other path to formation NO can be described by reactions the following reactions:

$$N2O + O = N2 + O2 \quad (R4)$$

$$N2O + O = NO + NO \quad (R5)$$

$$N2O + H = N2 + OH \quad (R8)$$

$$N2O + OH = N2 + HO2 \quad (R7)$$

$$N2O + M = N2 + O + M \quad (R8)$$

The nitrogen reaction constants which were used in reference[37], were derived for hydrocarbon fuels, and so their accuracy not well to predict quantitative results for hydrogen-fuelled engines. In the present study the chemical reaction constants for extended Zel'dovic mechanism (R1, R2 and R3) was adjusted for a carbon-free fuel, where the constants in reference[38] have been applied to predict the NOx emissions for hydrogen-fuelled engines. The Table 3 shows the chemical reaction constants used for NO calculations with both the hydrocarbon fuel and the carbon-free fuel. As depicted in Table 4, with carbon-free fuel, the predicted results were more accurate compared with that at hydrocarbon fuel. Where the difference between experiment and computation with free carbon were approximately 0.26% and 2.22%, while with hydrocarbon were 22.2% and 62% for equivalence ratios of 0.84 and 0.55 respectively.

The one important scope of the present computational was to provide a better understanding of the NO emissions production, in association with the mean in-cylinder gas temperature and oxygen availability at the same instants of time. Figure 6 shows the changes of NO, O_2, N_2O and OH concentrations depending on crank angle, for three

equivalence ratios at 0.84, 0.55 and 0.3. The CFD results confirmed that, as the equivalence ratio decreased, the oxygen concentrations increased, and the in parallel cylinder temperature decreased. Thus, the NO emissions decreased as illustrated in the contour plot. The NO formation was influenced, primarily, by a reduction in temperature rather than the availability of O_2. For equivalence ratio of 0.84, NO formation occurred near the spark-plug where the local temperature was very high (at flame region), and start to diffuse inside the cylinder until reached its maximum. Then can be observed that NO began to decline as the crank angle increased during the expansion stroke. As result of the decline in-cylinder temperature, the rate of NO decomposition rapidly decreases, and after crank angle of 50 ^{o}CA AIT, the NO kinetics was effectively frozen. It is due to the rates of R1, R2 and R3 becoming small after 50 ^{o}CA AIT. For equivalence ratios of 0.55, the NO formation shows a similar trend at equivalence ratio of 0.84, where it formed near spark plug and reached its maximum than start to decline, but less diffusion inside the cylinder, where its concentration just observed at the center of cylinder compared to that at equivalence ratio of 0.84. For an equivalence ratio of 0.3, the NO formation reaches its maximum value and was essentially "frozen" at that value, and does not change during the remainder of the expansion stroke. The simulations of NO emissions conducted in this study agree with the experimental data of Subramanian et al.[4] on a single hydrogen engine.

Also figure 6 shows N_2O and OH formation. These species was selected as the most important for driving the NO formation.[39] The formation of both species increased as equivalence ratio increases. For an equivalence ratio of 0.84, the peak N_2O formation occurred at crank angle of 20 ^{o}CA AIT. Immediately after 20 ^{o}CA AIT, more N_2O formed was converted to NO by the reaction $N_2O + O = NO + NO$, due to the high activation energy of this reaction.40 For an equivalence ratio of 0.55, it observed that the peak N_2O formation occurred at crank angle of 30 ^{o}CA AIT, this is may be due to longer flame development period period and combustion duration. Also it observed that OH radical has strong influence on combustion presses and NO formation. As equivalence ratio increased the in-cylinder temperature increases, and that leading to create the OH radical. As shown in figure 6, that with three different equivalence ratio (0.84, 0.55 and 0.3), the OH radical gradually decreased as the crank angle increased during the expansion stroke; hence, the

rate of HO decomposition rapidly increased and that lead to enhance produce the NO via N+OH = NO+H reaction.

After its development and validation, the computational model could be employed to investigate various aspects of hydrogen engines which have a major effect on engine performance and emission. One possibility is to use the model to study the effect of exhaust gas recirculation (EGR) and ignition timing on engine performance and NOx emissions.

4.3. Effect of exhaust gas recirculation (EGR) on engine performance and emission.

One of the methods to decreasing the exhaust nitrogen oxides (NO_x), is the use of exhaust gas recirculation (EGR). An exhaust gas recirculation system was used to reduce NO emissions. The EGR rate of hydrocarbon fuels was generally calculated from a molar CO_2 balance. However, this cannot be used for hydrogen engines as no CO_2 emissions occur. Three methods are available that can calculate the amount of EGR in a hydrogen engine.[41] The first is based upon a volume balance in the mixing section of exhaust gases and fresh air. The second method uses a molar balance of O_2 and third one uses a molar balance of H_2O. The third method was used in this study, the mass fraction of EGR (EGR %) is defined as the mass flow of EGR ($\dot{m}_{EGR}$) divided by the mass flows of EGR, fresh air and fuel ($\dot{m}_{EGR} + \dot{m}_{air} + \dot{m}_{H_2}$) :

$$EGR\ \% = \frac{\dot{m}_{EGR}}{\dot{m}_{EGR} + \dot{m}_{air} + \dot{m}_{H_2}} \tag{17}$$

The information in Table 5 suggests that at equivalence ratio of 0.84 and constant ignition timing at 5 ^{o}CA BTDC, the peak NO was 5600 ppm and 313 ppm with addition of 5 % EGR and 15 % EGR respectively in comparison to 7620 ppm without EGR. It is generally known that the main reasons to formulation the NO_x emissions are high in-cylinder temperature and oxygen availability. Recirculating a portion of the exhaust gases back into the intake manifold, is a convenient way to decrease in-cylinder oxygen, at the same time to increases the amount of combustion-accompanying gases, which in turn increases the heat capacity, and hence to lower in-cylinder temperatures for the same

amount of heat addition. This will reduce NO_x emissions, the possibility of pre-ignition, knock, and backfire.

The CFD results are consistent with the hypothesis that gas cylinder temperature decrease when EGR was added. The decrease in gas cylinder temperature results in the reduction in NO emission as illustrated in Fig. 7. From the figure it is observed that for the 5% EGR, the flame has covered the whole combustion chamber at 30 oCA AIT. At that moment the NO formation has its peak value, and starts to decrease as crank angle increased during expansion stroke until reached its final value 5600 as shown in the Table 5. This is due to reduction in in-cylinder temperature, which leads to decrease the rate of reactions R1, R2 and R3. For 15% EGR, the flame propagation velocity was lower than that at 5% EGR, since at 30 ^{o}CA AIT the flame still propagates towards the chamber walls, and the local temperature is very low especially near to the sides of cylinder. This led to produced small amount of NO in cylinder's center. These results were agreed with observations of Kosmadakis et al.[28] It is observed that with 5% EGR the N_2O and OH formation higher than that at 15% EGR. The N_2O was primarily formed by the reactions of molecular nitrogen with some radicals, with $N_2O+M = N_2+O+M$ dominating. With EGR, there is less O_2 in the oxidizer, and thus less O radicals to react with N_2 to form N_2O. Then part of the formed N_2O start to decline and converting to NO primarily by the reaction $N_2O+O = 2NO$.

In general, as EGR percentage increases the in-cylinder temperature decrease, hence there are more OH radical inside the cylinder with 5% EGR compared to 15% EGR operation, because the OH radical is created in high temperature gases. However, with 5% EGR the almost of the OH will oxidize N and convert to NO according to N + OH = NO + H reaction, just 7.5% of OH formation (318.4 ppm) will remain and exhausted as out emission, contrary to what occurs with 15% EGR, where 50% of OH formation (403 ppm) will remain and exhausted as shown in the Table 5.

The performance of the engine, in terms of IMEP, indicated efficiency and indicated power are shown as a function of EGR percentage in the Table 5. As expected, the IMEP, indicated efficiency and indicated power was decreased by increase EGR. This may be due to the fact that the amount of fresh oxygen available for combustion gets

decreased due to replacement by exhaust gas, which lead to combustion degradation and changes in intake charge. With the increase in EGR, the combustion is expected to occur later, and consequently lower the in-cylinder peak pressure and temperature, and hence the engine power decreases and IMEP take values from 100 kPa down to 50 kPa with 15% EGR. Also as Table 5 shows, when EGR rate was high (15%), the indicated efficiency decrease. The main cause for decreasing the indicated efficiency are attributed to increased combustion duration and no time for a constant volume combustion close to TDC.[27]

4.4. Effect of ignition timing on engine performance and emission.

Also in the present study after validated with experiments, the effect of ignition timing has been investigated, because the spark timing is another parameter that has a major effect on engine performance and emission. According to experiments data the ignition timing was 5 ^{o}CA BTDC at full load (7.4 kW). As shown from the Table 5, that with ignition timing of 10 ^{o}CA BTDC, the NO formation was high, where it was 9470 ppm compared to 7600 ppm and 2020 ppm at 5 ^{o}CA BTDC and 5 ^{o}CA ATDC respectively. This is because as ignition timing was advanced relative to the TDC, the combustion occurs earlier and consequently increase the in-cylinder peak pressure and temperature, thus increases NO formation.[42,43] Figure 8 shows the effect of ignition timing on in-cylinder NO, N_2O and OH formation, with two different ignition timing at 10 ^{o}CA BTDC and at 5 ^{o}CA ATDC. At ignition timing of 10 ^{o}CA BTDC, the in-cylinder NO, N_2O and OH formation have similar trends to that at 5 ^{o}CA BTDC which were observed in Figure 6. As ignition timing was advanced, there is increase in in-cylinder temperature and enough time to complete combustion, which leads to created high O and OH radicals close to TDC, and consequently the O radical will react with nitrogen and produce N_2O early, and reached its peak value at crank angle of 20 ^{o}CA AIT, than after that crank angle, the N_2O start to decline and converting to NO via of $N_2O+O = 2NO$, and just 25% of N_2O formation (1.23 ppm) will remain and exhausted as shown in the Table 5. The OH formation have similar trends, it reached its peak value and start to decline and oxidize N to NO, and just 20% of N_2O formation (88 ppm) will remain and exhausted.

Table 5 presents the predicted results of the engine power, IMEP and indicated thermal efficiency with different ignition timing. The operation at ignition timing of 10

^{o}CA BTDC showed the highest value in IMEP was 1008 kPa compared to 722 kPa and 656.6 kPa with 5 ^{o}CA BTDC and 5 ^{o}CA ATDC respectively. The lower power and indicated thermal efficiency were achieved at ignition timing of 5 ^{o}CA ATDC. Because as ignition timing was retard, most of the combustion occurs when the piston is moving down and, in this case, the power and the thermal efficiency decrease.[43]

5. SUMMARY AND CONCLUSIONS

In this study, the CFD simulation work carried out using AVL FIRE software for an IC Engine fueled with hydrogen at three equivalence ratios at MBT timing and constant engine speed (2500 rpm). A detailed reaction mechanism was developed to include the chemical kinetics of twenty nine steps of hydrogen oxidation and eight nitrogen oxidation reactions. The extended Zel'dovic mechanism was adjusted for a carbon-free fuel to quantitatively predict the NO_x emissions.

The computational predictions were compared to independent and well documented experimental data, in order to evaluate accuracy and suitability for widespread implementation. To understand the general features of a SI engine fueled with hydrogen relative to a traditional engine, the computational model for hydrogen engine was first compared to the computational model for gasoline engine with the same geometry and operating conditions. As expected, the hydrogen engine had both a higher rate of pressure rise and a higher maximum pressure in the cylinder, because the hydrogen had a significantly higher burning speed compared to the gasoline engine operation. The model results (engine performance and exhaust nitric oxide emissions) have been compared with the experimental data and showed a good agreement. The NOx predicted was more accurate with reaction constants which were derived for carbon-free fuel compared with that at hydrocarbon fuel.

Once validated, the model provides an insight into the combustion and pollutant formation processes occurring in inside the cylinder. Also after the validation, the computational model was employed to quantify the effect of (EGR) exhaust gas recirculation and ignition timing on engine performance and emission. EGR and retard ignition timing were found to be an effective method to reduce NO_X. However, a

remarkable reduction of engine power output and thermal efficiency with increase EGR ratio, and showed a similar trend when retarding ignition timing. This reveals that the adjusting EGR ratios and ignition timings are needed to optimize the performance and NO_x emission.

6. REFERENCES

1- Verhelst, S. Recent progress in the use of hydrogen as a fuel for internal combustion engines *Int. J. Hydrogen Energy* **2014**, 39, 1071-1085.

2- Jongtai, L.; Kwangju, L.; Jonggoo, L.; Byunghoh, A. High power performance with zero NOx emission in a hydrogen-fueled park ignition engine by valve timing and lean boosting. *Fuel* **2014,** 128, 381-389.

3- Barreto L.; Makihira A. The hydrogen economy in the 21st century: a sustainable development scenario. *Int. J. Hydrogen Energy* **2003,** 28, 267-284.

4- Subramanian, V.; Mallikarjuna, JM.; Ramesh, A. Performance, emission and combustion characteristics of a hydrogen fueled SI engine-an experimental study. *SAE Technical Paper* **2005** -26-349.

5- Verhelst, S.; Wallner, T. Hydrogen-fueled internal combustion engines. *Prog Energy Combust. Sci.* **2009,** 35,490-527.

6- White, C.; Steeper, R.; Lutz, A. The hydrogen-fueled internal combustion engine: a technical review. *Int. J. Hydrogen Energy* **2006**, 31, 1292-305.

7- Verhelst, S.; Sierens, R.; Verstraeten, S. A critical review of experimental research on hydrogen fueled SI engines. *SAE Technical Paper* **2006**-01-0430.

8- Karim, GA. Hydrogen as a spark ignition engine fuel. *Int. J. Hydrogen Energy* **2003,** 28, 569–77.

9- Mohammadi, A.; Shioji, M.; Nakai, Y.; Ishikura, W.; Tabo, E. Performance and combustion characteristics of a direct injection SI hydrogen engine. *Int. J. Hydrogen Energy* **2007,** 32, 296–304.

10- Kawahara, N.; Tomita, E. Visualization of auto-ignition and pressure wave during knocking in a hydrogen spark-ignition engine. *Int. J. Hydrogen Energy* **2009**, 34, 3156–63.

11- Das, LM. Hydrogen engine: research and development (R&D) programmers in Indian Institute of Technology (IIT), Delhi. *Int. J. Hydrogen Energy* **2002,** 27, 953–65.

12- Homan, H.; Reynolds, R.; DeBoer, P.; McLean, W. Hydrogen-fueled diesel engine without timed ignition. *Int. J. Hydrogen Energy* **1979,** 4, 315-325.

13- Welch, A.; Wallace, J.; Performance characteristics of a hydrogen-fueled diesel engine with ignition assist. *SAE Technical Paper*. **1990**-90-2070.

14- Adrian, B.; Iulian, V.; Cristian, P.; Radu, C.; Nicolae, A. Effects of air-hydrogen induction on performance and combustion of a diesel engine. *SAE Technical Paper* **2011**-24-0094

15- Saravanan, N.; Nagarajan, G. Performance and emission study in manifold hydrogen injection with diesel as an ignition source for different start of injection. *Renewable Energy* **2009,** 34, 328-334.

16- Saravanan, N.; Nagarajan, G. Experimental investigation in optimizing the hydrogen fuel on a hydrogen diesel dual-fuel engine. *Energy Fuels* **2009**, 23 (5), 2646–2657.

17- Wong, JKS., Compression ignition of hydrogen in a direct injection diesel engine modified to operate as a low-heat rejection engine. *Int. J. Hydrogen Energy* **1990**, 15, 507–14.

18- Horng-Wen, W.; Zhan-Yi, W. Investigation on combustion characteristics and emissions of diesel/hydrogen mixtures by using energy-share method in a diesel engine. *Appl. Therm. Eng.* **2012,** 42, 154-162.

19- Lee, K.; Kim, Y.R. Feasibility of compression ignition for hydrogen fueled engine with neat hydrogen-air pre-mixture by using high compression. *Int. J. hydrogen energy* **2013**, 38, 255-264.

20- Lee, K.; Bae, C.; Kang, K. The effects of tumble and swirl flows on flame propagation in a four-valve S.I. engine. *Applied Thermal Eng.* **2007**, 27, 2122–2130

21- Tang, C.; He, J.; Huang, Z.; Jin, C.; Wang, J.; Wang, X. Measurement of laminar burning velocities and Markstein lengths of propane–hydrogen–air mixtures at elevated pressures and temperatures. *Int. J. Hydrogen Energy* **2008**, 33,7274–85.

22- Lamoureux N, Djebaili-Chaumeix N, Paillard CE. Laminar flame velocity determination for H_2–air–He-CO_2 mixtures using the spherical bomb method. *Experimental Thermal and Fluid Sci.* **2003**,27,385–93.

23- Rakopoulos, CD.; Kosmadakis, GM.; Pariotis, EG. Evaluation of a new computational fluid dynamics model for internal combustion engines using hydrogen under motoring conditions. *Energy* **2009**, 12, 2158-66.

24- Arash, H.; Pavlos, A. Computational study of hydrogen direct injection for internal combustion engines. *SAE Technical Paper* **2013**-01-2524.

25- Zhenzhong, Y.; Aiguo, S.; Fei, W.; Nan, G., "Research into the formation process of hydrogen air mixture in hydrogen fueled engines based on CFD. *Int. J. Hydrogen Energy* **2010,** 35, 3051-7.

26- Rakopoulos, CD.; Kosmadakis, GM.; Pariotis, EG. Evaluation of a combustion model for the simulation of hydrogen spark ignition engines using a CFD code. *Int. J. Hydrogen Energy* **2010**, 35,12545-60.

27- Rakopoulos, CD.; Kosmadakis, GM.; Demuynck, J.; Paepe, M.; Verhelst, S. A combined experimental and numerical study of thermal processes, performance and nitric oxide emissions in a hydrogen-fueled spark-ignition engine. *Int. J. Hydrogen Energy* **2011,** 36, 5163-80.

28- Kosmadakis, GM.; Rakopoulos, CD.; Demuynck, J.; Paepe, M.; Verhelst, S. CFD modeling and experimental study of combustion and nitric oxide emissions in hydrogen-fueled spark-ignition engine operating in a very wide range of EGR rates. *Int. J. Hydrogen Energy* **2012**, 37, 10917-10934.
29- Vincent, K.; Adle`ne, B. Modelling of combustion and nitrogen oxide formation in hydrogen-fuelled internal combustion engines within a 3D CFD code. *Int. J. Hydrogen Energy* **2008,** 33, 5083-5097.
30- Pitsch, H.; Peters, N., Three-Dimensional Modeling of NOx and Soot Formation in DI-Diesel Engines Using Detailed Chemistry Based on the Interactive Flamelet Approach. *SAE Technical Paper* **1996**-96-2057.
31- Wang H.; Mingfa Y.; Reitz, R. Development of a Reduced Primary Reference Fuel Mechanism for Internal Combustion Engine Combustion Simulations. *Energy Fuels* **2013**, 27, 7843−7853.
32- Priesching, P.; Wanker, R., "Detailed and reduced chemistry CFD modeling of premixed charge compression ignition engine combustion. Int. Multidimensional Engine Modeling User's Group Meeting 2003.
33- Khairallah, H.; Koylu, U. Combustion simulation of hydrogen-fuelled diesel engines using detailed chemical kinetics. *ASME*, IMECE**2013**-65194
34- Kong, S.; Marriott, C.; Reitz, R.; Christensen, M. Modeling and Experiments of HCCI Engine Combustion using Detailed Chemical Kinetics with Multidimensional CFD. *SAE Technical Paper* **2001**-01-1026.
35- Hanjalic, K.; Popovac, M.; Hadziabdic, M. A robust near-wall elliptic relaxation eddy-viscosity turbulence model for CFD. *Int. J. Heat and Fluid Flow*, **2004**, 25, 1047–1051.
36- Durbin, P. Near-wall turbulence closure modelling without damping functions. Theoretical and Computational Fluid Dynamics, **1991**-31–13.
37- https://github.com/OpenCFD/OpenFOAM1.7.x/blob/master/tutorials/combustion/dieselFoam/aachenBomb/chemkin/chem.inp_15.
38- Knop, V.; Benkenida A.; Jay, S.; Colin O. Modelling of combustion and nitrogen oxide formation in hydrogen-fuelled internal combustion engines within a 3D CFD code. *In.t J. Hydrogen Energy* **2008**, 19, 5083-97.
39- Cuoci, A.; Frassoldati, A.; Stagni, A.; Faravelli, T.; Ranzi, E.; Buzzi-Ferraris, G. Numerical modeling of NOx formation in turbulent flames using a kinetic post-processing echnique. *Energy Fuels* **2013**, 27, 1104−1122.
40- Sung, K.; Je-Hyung, L. Combustion process analysis in a HSDI diesel engine using a reduced chemical kinetics. *SAE Technical Paper **2004**-01-0108.*
41- Verhelst, S.; Vancoillie, J. Setting a best practice for determining the EGR rate in hydrogen internal combustion engines. *Int. J. hydrogen energy* **2013**, 38, 2490-2503.

42- Farhad, S.; Amir, S.; Ali P. Effects of spark advance, A/F ratio and valve timing on emission and performance characteristics of hydrogen internal combustion engine. *SAE Technical Paper* **2009**-01-1424.
43- Erjiang, H.; Zuohua, H. Optimization on ignition timing and EGR ratio of a spark-ignition engine fuelled with natural gas-hydrogen blends. *SAE Technical Paper* ***2011****-01-0918.*
44- An, H.; Yang W.; Maghbouli, A.; Li, J.; Chou, S.; Chua, K.; Wang J.; Li, L. Numerical investigation on the combustion and emission characteristics of a hydrogen assisted biodiesel combustion in a diesel engine. *Fuel* **2014**, 120, 186–194.
45- Wang, Z.; Wang, Y.; Reitz, R. Pressure oscillation and chemical kinetics coupling during knock processes in gasoline engine combustion. *Energy Fuels* **2012**, 26, 7107-7119.
46- Vudumu S.; Koylu, U. Computational modeling, validation, and utilization for predicting the performance, combustion and emission characteristics of hydrogen IC engines. *Energy* **2011**, 36, 647-655.

Table 1 Specifications of the IC engine modeled

Fuel	Hydrogen
Number of cylinders	1
Bore × Stroke	85 × 95 mm
Displacement volume	530 cm3
Compression ratio	9:1
Engine speed	2500 rpm
Initial operating conditions of engine	
Start angle (BTDC)	540 degree
End angle (ATDC)	850 degree
Piston surface temperature	423 K
EGR levels	5 % and 15 %
Swirl ratio	1.2
Turbulence model	k-ζ-f model
Turbulence kinetic energy	2 m2/s2
Turbulence length scale	4.5 mm
Initial temperature	330 K
Initial pressure	1 bar

Table 2 Simulations validated

	Simulation			Experimental		
	Φ = 0.84	Φ = 0.55	Φ = 0.3	Φ = 0.84	Φ = 0.55	Φ = 0.3
Peak pressure (bar)	52.3	40.2	32	50	39.5	32
Brake power (kW)	7.37	5	2	7.4	5	2
Brake thermal eff. (%)	28	26	16.8	27	26	17
NO (ppm)	7620	500	11.9	7600	489	0

Table 3 Chemical reaction constants used for NO

$k = A.T^b.e^{\left(\frac{-E}{RT}\right)}$				
	Reaction	A	b	E
Hydrocarbon fuel	R1	3.270E+12	0.3	0
	R2	6.400E+09	1	6280
	R3	7.333E+13	0	1120
Carbon-free fuel	R1	2.700E+13	0	1500
	R2	9.000E+09	1	27200
	R3	3.600E+13	0	1600

Table 4 Compared of NO emissions with different chemical reaction constant at different equivalence ratio

	0% EGR			5% EGR	15% EGR
Ignition timing	10BTDC	MBT	5 ATDC	MBT	MBT
Peak pressure (bar)	60.2	52.2	45	40	24
Indicate Power (kW)	11.13	7.9	7.25	6.8	5.7
Indicate thermal eff. (%)	41.5	29.7	27.1	25.4	22
IMEP (KPA)	1008	722.1	656.6	617	525
NO (ppm)	9470	7620	2020	7500	313
OH (ppm)	88	105.81	315.3	318.4	403
N2O (ppm)	1.2	1	0.6	0.5	0.3

Table 4 Computed the engine performance and out emissions at different EGR level and ignition timing with equivalence ratio 0.84

	Φ = 0.84	Φ = 0.55	Φ = 0.3
Experimental	7600	500	0
NO (ppm) - Hydrocarbon fuel	9500	950	19
NO (ppm) - Carbon-free	7620	489	11.9

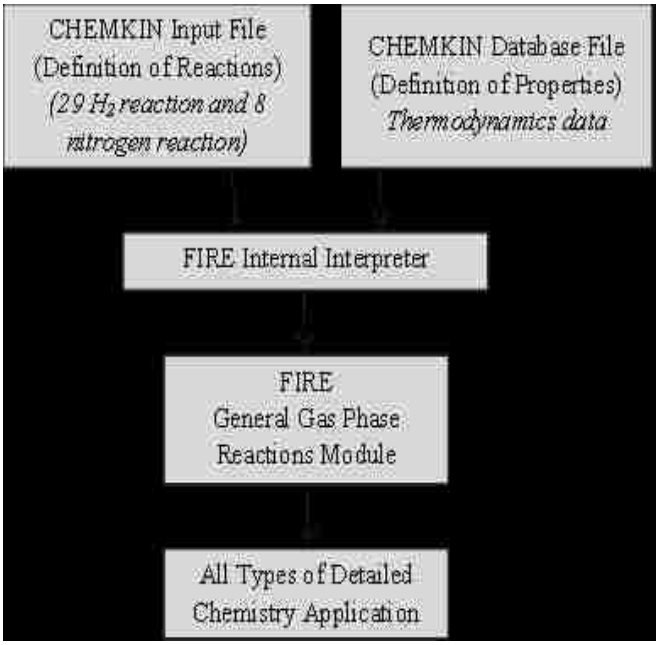

Figure 1 Detailed chemistry modeling scheme

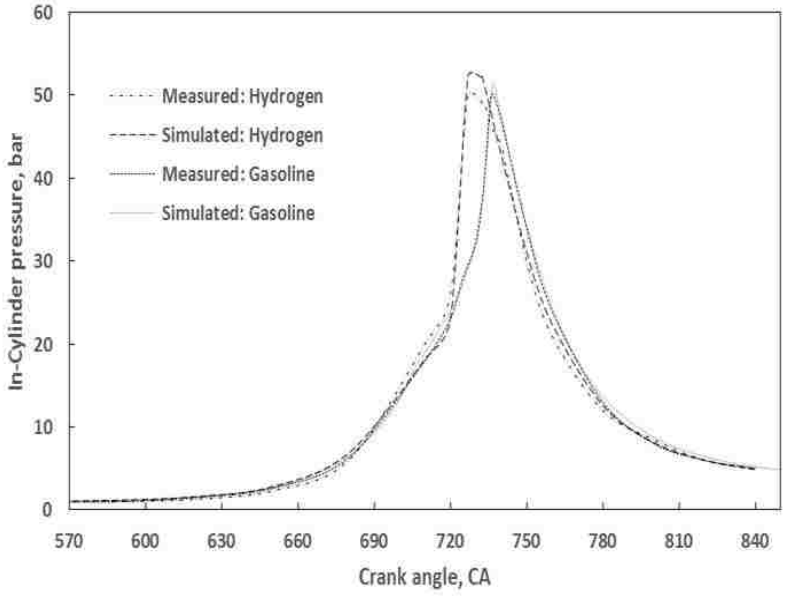

Figure 2 Variation in cylinder pressure as crank angle varies

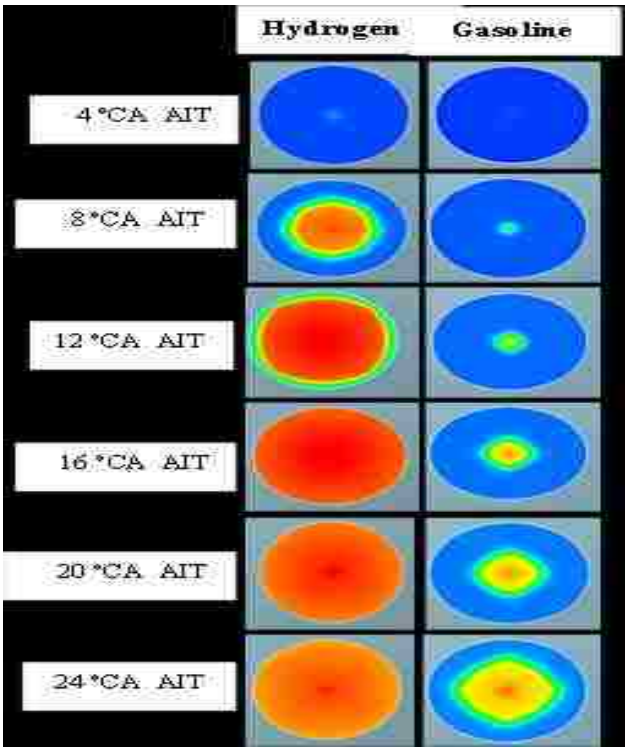

Figure 3 Flame developed for the hydrogen and gasoline examined

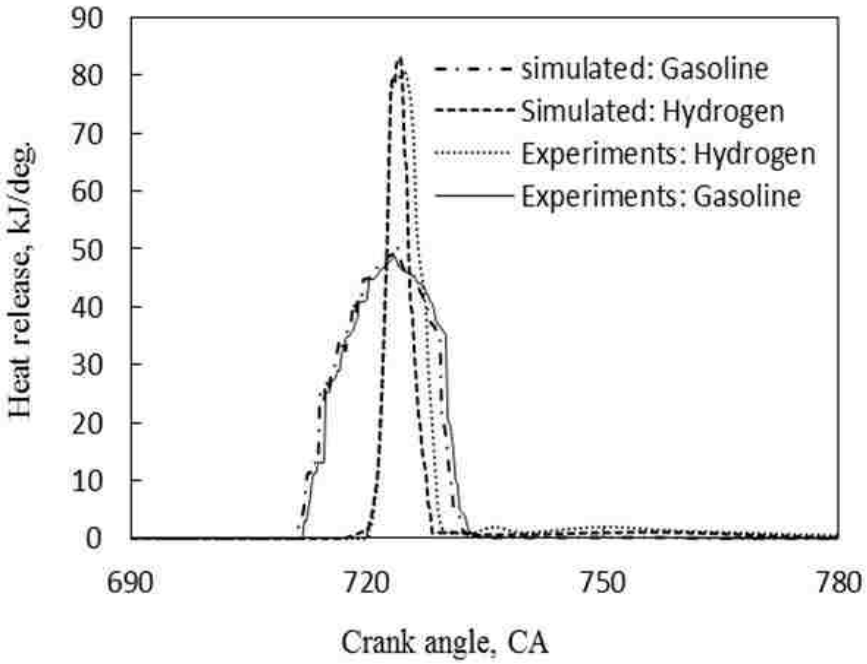

Figure 4 Variation in heat release as crank angle varies for hydrogen and gasoline operation at full load

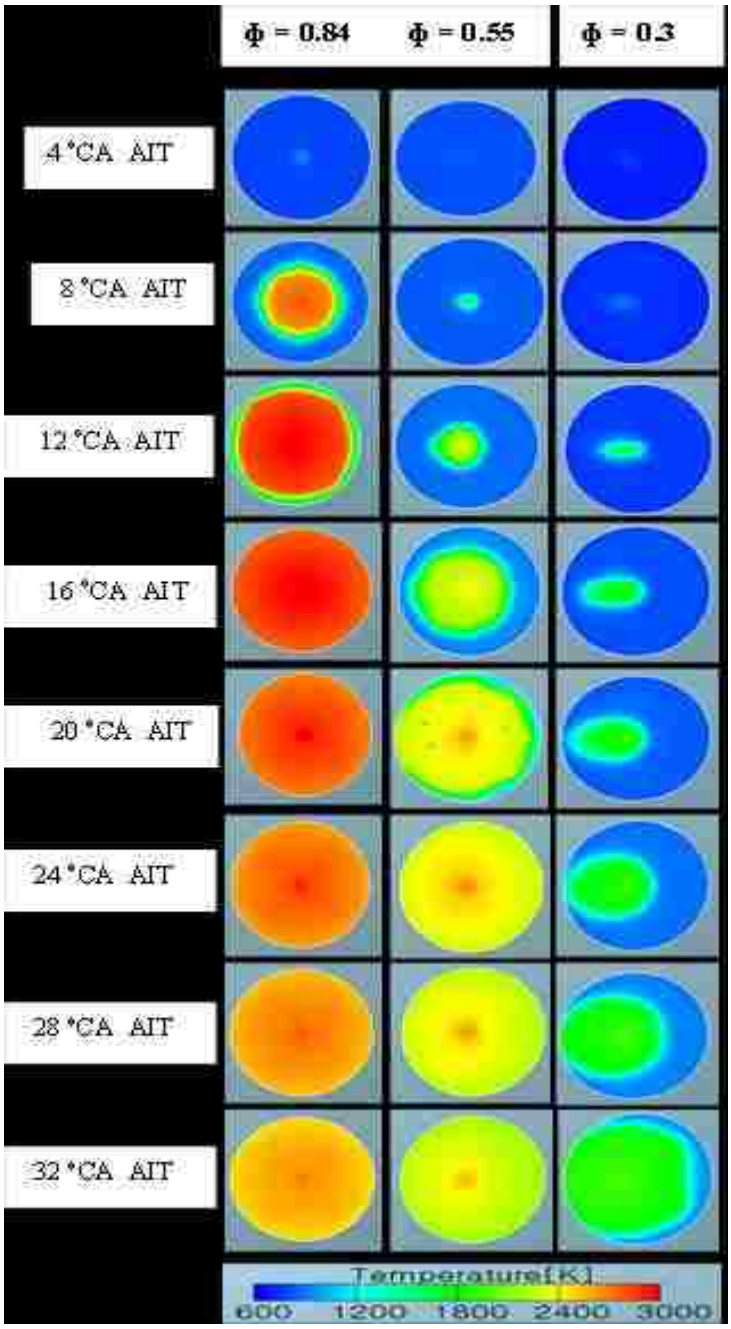

Figure 5 Hydrogen flame developed for the three equivalence ratios examined

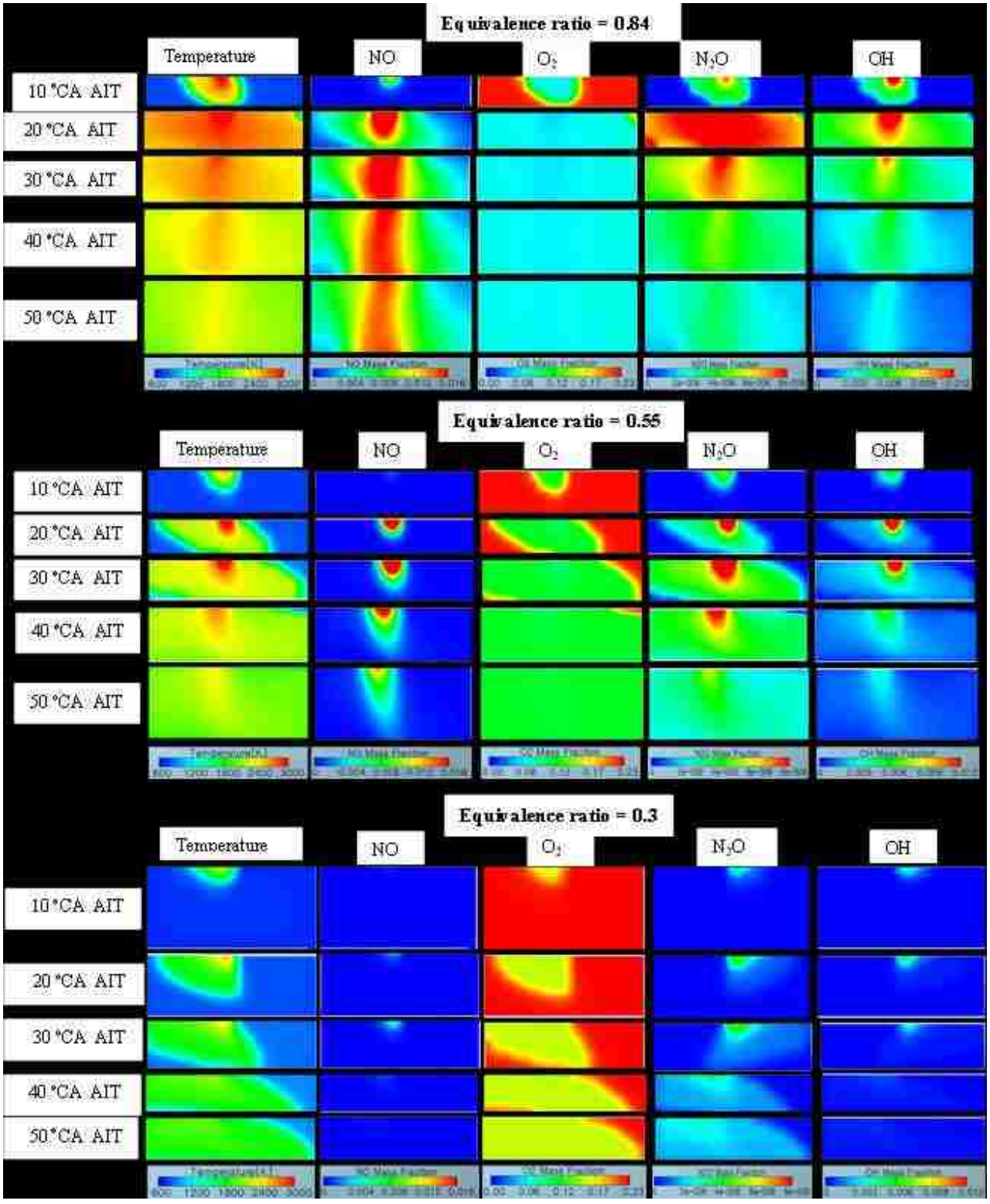

Figure 6 NO, O2 mass fraction and temperature during combustion process for three equivalence ratios

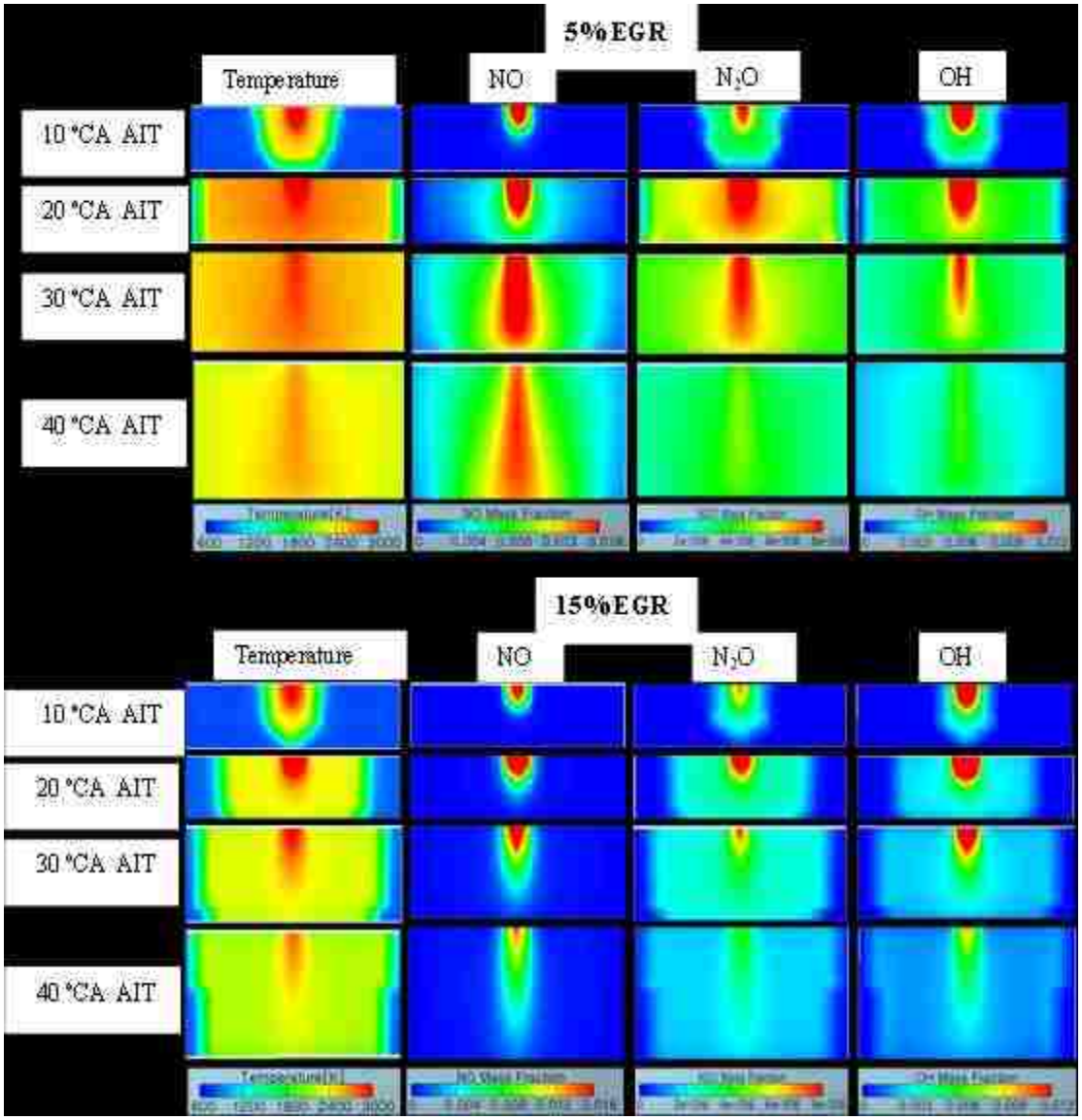

Figure 7 NO, N2O and OH mass fraction and temperature during combustion process with 5 % EGR and 15 % EGR

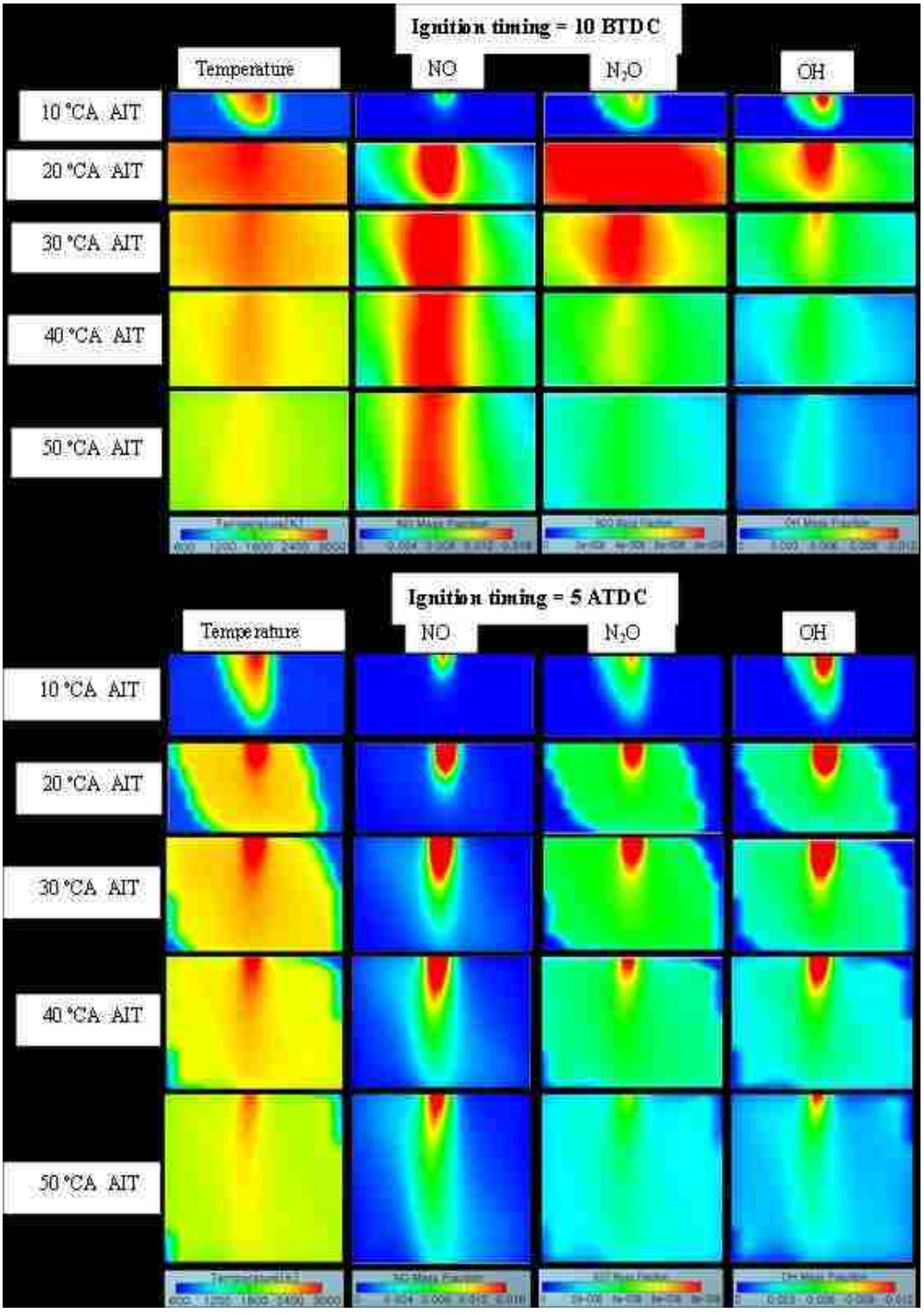

Figure 8 NO, N2O and OH mass fraction and temperature during combustion process with, ignition timing at 10o BTDC and 5o ATDC

II. INFLUENCE OF IGNITION TIMING AND EGR ON THE NOx EMISSION AND THE PERFORMANCE OF AN SI ENGINE FUELED WITH HYDROGEN

Hassan A. Khairallah
Department of Mechanical and Aerospace Engineering
Missouri University of Science and Technology
Rolla, MO, USA

Warren S. Vaz
Department of Mechanical and Aerospace Engineering
Missouri University of Science and Technology
Rolla, MO, USA

Umit O. Koylu
Department of Mechanical and Aerospace Engineering
Missouri University of Science and Technology
Rolla, MO, USA

ABSTRACT

Exhaust gas recirculation (EGR) and ignition timing have strong effects on engine performance and exhaust emissions. In the present study, detailed chemical reactions with 29 steps of hydrogen oxidation with additional nitrogen oxidation reactions were coupled with an advanced CFD code to investigate the engine performance and emission characteristics of a SI engine fueled with hydrogen. The NO_x formation within the engine was computed using the extended Zeldovich mechanism with parameters adjusted for a carbon-free fuel such as hydrogen. The computational results were validated against experimental results with equivalence ratio of 0.84 and fixed ignition timing at crank angle of 5º BTDC (before top dead center). The simulations were then employed to examine the effects of EGR and ignition timing on the engine performance and NO_x formation and emission. The EGR ratio was varied between 5% and 15% while the ignition timings considered were 5º, 10º, 15º, and 20º BTDC. It was found that NO_x emission increased with advancing the ignition timing away from TDC while the indicated engine power showed an increasing trend with further advancing the ignition timing. Higher indicated mean effective pressure (IMEP) and indicated thermal efficiency were obtained with an advanced ignition timing of 20º BTDC. The model was also run with three different EGR ratios of 5%, 10% and 15% with fixed ignition timing at 5º BTDC. The simulation results quantified the reduction in NO_x and the indicated engine power with the increase in the EGR ratio. The computations were consistent with the hypothesis that the combustion

duration increases with the EGR ratio. Finally, the maximization of engine power and minimization of NOx emissions were considered as conflicting objectives. The different data points were plotted in the objective space. Using the concept of "knee", (5º BTDC, 0% EGR) was selected as the optimal operating point representing the best trade-off between maximum engine power and minimum NO_x emissions.
KEYWORDS: Spark-ignition engine, hydrogen, ignition timing, exhaust gas recirculation, CFD, knee.

1. Introduction

Due to the acceleration of depletion and pollution of fossil fuels in recent years, many studies have been conducted to address the growing concerns about shortage of fossil fuel supply as well as reduction in greenhouse gas emissions. Hydrogen is considered as one of the most promising alternative fuels for internal combustion (IC) engines due to its unique combustion characteristics, especially when compared to other alternative fuels like biodiesel, CNG, LPG, and ethanol. Hydrogen can be adapted to power both spark ignition (SI) and compression ignition (CI) engines. In SI engines, hydrogen can be used directly as the sole fuel, but in the case of a CI engine, hydrogen cannot be used directly, because it is very difficult to ignite it by only the compression process due to its auto-ignition temperature (858 K) being so much higher than that of diesel fuel (525 K) [1]. Therefore, some auxiliary ignition sources (spark plugs, glow plugs, or pilot fuel) [2-5] have to be used inside the CI engine combustion chamber to ensure the ignition of hydrogen.

Hydrogen has interesting properties as a fuel for internal combustion engines [6-8]. It has the widest flammability range in comparison to all other fuels, and this allows a hydrogen engine to run a lean mixture at a high efficiency. This can also lead to reduced NOX at equivalence ratios lower than about 0.5 [9, 10]. The ignition energy required to ignite the hydrogen is very low, which allows a hydrogen engine to ignite lean mixtures and ensures prompt ignition even with a relatively weak spark. Due to the higher flame speed of hydrogen, the combustion duration of hydrogen-air mixture is significantly shorter relative to other fuel-air mixtures. Hydrogen is a carbon-free fuel, so hydrogen engines do

not produce any carbon dioxide or carbon-based emissions. Nitrogen oxides (NOx) are the only undesirable emissions. Numerous studies on internal combustion engines using hydrogen as a fuel have been undertaken in recent years. Within this field, experimental and numerical investigations have been constructed in order to investigate the combustion process and the performance of an SI engine fueled with hydrogen under different operating conditions and strategies. Many studies have been performed to investigate the effects of exhaust gas recirculation (EGR) on engine performance and NO_x emission [11-15]. While the EGR technique was found to be very effective in reducing the NO_x emission. It has an adverse effect on the engine power. Several studies also focused on the effects of ignition timing on power and NO_x [16-18,12] because the relatively high flame speed of hydrogen makes a hydrogen engine more sensitive to the ignition timing for both power as well NO_x emission. On advancing the ignition timing, the engine power output increases significantly, but NO_x emissions also increase. However, few studies reported the effects of combining the ignition timing with EGR on NO_x emission and engine power output. Erjiang et al. [19] investigated the effect of ignition timing and EGR ratio on the performance and emissions of an SI engine fueled with natural gas-hydrogen mixtures. They reported that advancing the ignition timing at a specified EGR ratio increased the engine power. However, a remarkable increase in NO_x emission was observed. Therefore, the optimization of ignition timing and EGR can lead to an improvement for an SI engine.

Computational fluid dynamics (CFD) has become an essential tool in the process of designing and developing engineering devices. In the past few decades, 3D CFD code has become a commonly used tool to gain better knowledge about the combustion processes inside the engine cylinder. CFD offers successful assessment of new technologies, e.g. fuel preparation methods, combustion concepts, especially for alternative fuels. With the recent development in computer processors and the expansion of allowable memory, researchers and engineers are now able to integrate detailed chemical kinetics with CFD code to simulate IC engines. Many statistical studies have focused on using 3D CFD tools to understand the in-cylinder flow field and mixing process [20-23].

2. Methodology

In the present study, hydrogen chemical reactions with 29 steps of hydrogen oxidation with additional nitrogen oxidation reactions were coupled with 3D CFD software AVL FIRE® to validate the predicted engine performance and NOx emission results against independent experimental data. Extended Zeldovich model to predict the NO formation with carbon-free fuel constants was adapted. The simulations were then employed to examine the effects of combing the ignition timing with EGR on the engine performance and NO_x formation which the cylinder and emission from the engine exhaust.

3. Computational methods

Simulations were conducted using 3D CFD software AVL FIRE® coupled with the detailed chemical kinetics for hydrogen. The detailed chemical kinetic reactions for hydrogen consist of 29 steps with additional oxidation reactions involving nitrogen [24]. NO formation can be described by reactions R1, R2, and R8. These reactions are typically known as the extended Zeldovich mechanism.

$$N_2 + O = N + NO \qquad (R1)$$

$$N + O_2 = NO + O \qquad (R2)$$

$$N + OH = NO + H \qquad (R3)$$

In general, these three reactions are only important at high temperatures because the radicals O and OH are created in high-temperature gases. The other path to NO formation can be described by the following reactions.

$$N_2O + O = N_2 + O_2 \qquad (R4)$$

$$N_2O + O = NO + NO \qquad (R5)$$

$$N_2O + H = N_2 + OH \qquad (R8)$$

$$N_2O + OH = N_2 + HO_2 \qquad (R7)$$

$$N_2O + M = N_2 + O + M \qquad (R8)$$

The nitrogen reaction constants that were used in reference [24] were derived for hydrocarbon fuels, so they may not be suited to predict quantitative results for hydrogen-

fueled engines. In the present study, the chemical reaction constants for the extended Zeldovich mechanism (R1, R2, and R3) were adjusted for a carbon-free fuel. The constants in reference [25] have been applied to predict the NO_x emissions for hydrogen-fueled engines. The Table 1 shows the chemical reaction constants used for NO calculations with both the hydrocarbon fuel and the carbon-free fuel.

The CHEMKIN chemistry solver was integrated into the CFD code for solving the chemistry during multidimensional engine simulations. The AVL FIRE® code provides CHEMKIN with the species and thermodynamic information of each computational cell. The CHEMKIN utilities return the new species information and energy release after solving for the chemistry. The FIRE® internal interpreter first reads the user's symbolic description of the reaction mechanism. It then extracts thermodynamic information for the species involved from the Thermodynamic Database. The FIRE® General Gas Phase Reactions Module was used to enable the simulation of kinetic problems, the detailed chemistry modeling scheme shown in the figure 1.

A user-supplied function was applied to incorporate the SI model. The model was built using C++ and incorporated into the model to simulate the hydrogen ignition behavior. The piston geometry and computational grid used for the simulations were built using the commercial CFD tool AVL ESEDiesel. An et al. [26] considered the effect of mesh size in detail and showed that 3.4 mm was sufficient for a typical IC engine. Wang et al [27] also used similar mesh size for reasonable spatial resolution. The convergence criterion was either maximum number of iterations (60) or reduction of residuals (0.01), whichever was achieved first. In this paper, the boundary conditions were as follows: the piston temperature was 423 K, the cylinder liner temperature was 423 K, and cylinder head temperature was 453 K. The computational domain consisted of one section of the modeled engine cylinder, which was used for simulations between the inlet valve closing (IVC) and the exhaust valve opening (EVO). This meant that only the closed volume part of the engine cycle was computed. The spark plug located in the center of the cylinder head. The spark duration was 4.5º (almost 1.33 ms). The computational time step used for simulation during the compression stroke was 1º. However, during the combustion period, the time step was further decreased to 0.25º, in order to increase the accuracy of the computational results.

The simulations provided values for indicated work (W_i) indicated mean effective pressure (IMEP), indicated thermal efficiency (%), and indicated power (P_i). These were calculated from in-cylinder pressure traces as follows.

$$W_i\ (kj) = \int_{IVC}^{EVO} pdV \tag{1}$$

$$IMEP\ (kpa) = \frac{1}{V_d} \int_{IVC}^{EVO} pdV \tag{2}$$

$$P_i\ (kW) = \frac{W_i\ .N}{2\ \times 60} \tag{3}$$

$$\eta_{\mathrm{ITE}} = \frac{P_i}{(\dot{m}_{f.hydrogen} \times CV_{hydrogen})} \tag{4}$$

Here $\dot{m}_{f.hydrogen}$ is the hydrogen flow rate (kg/s) and $CV_{hydrogen}$ is the lower heating value of hydrogen (kg/kJ) with a value of 120 MJ/kg.

4. Results and discussion

The operating conditions of the hydrogen IC engine in this investigation were chosen similar to the independent study by Subramanian et al. [28] because their reported test conditions and experimental data were well documented. Specifications for the SI hydrogen engine used in this computational study and the engine's initial operating conditions are listed in Table 2.

4.1 Model validation: comparison of simulations to experiments

Table 3 shows the validated model results against independent experiments for engine performance and exhausts emissions. It was found that the peak pressure increased almost linearly with the equivalence ratio (or brake power) as shown in the table. This is because the flame speed increased as the equivalence ratio increased and the time required to complete the combustion decreased. The predicted peak pressure was in good agreement with the experimental data collected at equivalence ratios of 0.3 and 0.55. The predicted results were only 3% higher than the experiments at an equivalence ratio of 0.84. From the table, it was observed that the brake thermal efficiency increased as the equivalence ratio increased. The brake thermal efficiency of an engine is defined as the ratio of the engine brake power to the input fuel energy. The maximum brake thermal efficiency was nearly 30% at an equivalence ratio of 0.84 (7.4 kW) and 19% at an equivalence ratio of 0.3 (2 kW). At high brake power, the flame speed increases as the equivalence ratio increases and therefore nearly constant-volume combustion can be achieved with hydrogen, resulting in higher brake thermal efficiency. The only undesirable emission produced by hydrogen engines is NOx. Any carbon emissions (e.g. CO, CO_2, and HC) will be very little. As the equivalence ratio decreased, the oxygen concentration increased, and the in-parallel cylinder temperature decreased. Hence, the NOx emitted from the engine decreased, as shown in Table 3.

The Table 4 shows the chemical reaction constants used for NO calculations with both the hydrocarbon fuel and the carbon-free fuel. As depicted in Table 4, the predicted NO emissions were more accurate with the kinetic parameters from carbon-free fuels, compared to ones obtained for hydrocarbon fuels. The difference between experiments and computations with carbon-free fuel was approximately 0.26% and 2.22%, while it was 22.2% and 62% for equivalence ratios of 0.84 and 0.55, respectively with hydrocarbon fuel. In general, the computational results showed good agreements with the experimental results for peak pressure, brake thermal efficiency, NO_x emissions with different equivalence ratios at constant engine speed.

4.2 Effect of EGR and ignition timing on engine performance and emissions

After its development and validation, the computational model was employed to investigate various aspects of an SI engine fueled with hydrogen. It was used to examine the effects of the combination of the ignition timing and EGR on the engine performance and NOx formation and emission. The operation with an equivalence ratio of 0.84 was selected to study those effects.

Figure 2 illustrates the variation of indicated mean effective pressure (IMEP) with ignition timing for different EGR levels. IMEP is a parameter that is a response of the engine's working capability and therefore a measure of the effectiveness of a given displacement volume in producing network. The results showed that IMEP decreased with an increase in the EGR level because the addition of EGR led to the decrease in the amount of air and fuel in the cylinder along with the flame propagation speed. It was also observed that the IMEP increased with advancing the ignition timing. However, the effect of late ignition timing (relative to TDC) on IMEP was clearly more than that of early ignition.

Figure 3 illustrates the variation of indicated thermal efficiency with ignition timing for different EGR levels. The indicated thermal efficiency decreased with an increase in the EGR level. This is attributed to the decreased combustion work (i.e. indicated work) with EGR addition. The decreased combustion work is a consequence of combustion degradation due to lower combustion temperatures. The figure also reveals that the indicated thermal efficiency highly depends on ignition timing. The indicated thermal efficiency increased with advanced ignition timing, similar to the way the IMEP increased. The increase of the indicated thermal efficiency with advanced ignition timing can be explained by the fact that combustion occurs earlier increases the in-cylinder peak pressure and temperature, and consequently increases the indicated thermal efficiency.

Figure 4 illustrates NO_x emission versus ignition timing for different EGR levels. NO_x emission decreased with an increase in the EGR level and also increased with the advancing of ignition timing. The main reasons for reduction in NO_x emissions with EGR are reduced oxygen concentration and decreased in-cylinder temperature. The NO_x increase with advanced ignition timing is attributed to the rise in the in-cylinder pressure and temperature with advancing ignition timing during the combustion process.

The CFD results were consistent with the hypothesis that combustion duration increases with the EGR level increased. Figure 5 illustrates the in-cylinder temperature profiles, as the flame propagates out from the spark plug with different EGR levels (0%, 5%, 10%, and 15% EGR) with a fixed ignition timing of 5º BTDC. As seen from the figure, without EGR, the flame propagates very fast and covered entire the cylinder at a crank angle of 25º AIT (After Ignition Timing), while at the same crank angle with 10% and 15% EGR, the flame is still propagating. This is because, with the increase of the EGR ratio, the specific heat capacity increases and the in-cylinder temperature are decreases [29]. This will lead to a decrease in the mixture burning velocity and an increase in the combustion duration.

The present computational methods provide a better understanding of the NO formation, in relation to the mean in-cylinder gas temperature and oxygen availability at the same instants of time. In Figure 5, the spatial distributions of NO, O2, and the temperatures inside the cylinder are shown at crank angles of 15º, 20º, and 25º AIT for three EGR levels. The CFD results confirmed that, as EGR increased, the oxygen concentration as well as the in-cylinder gas temperature decreased. Hence, the formation of NO reduced. The NO formation was shown in the central region of the cylinder near the spark plug where the local temperature was very high (in the flame region) [20], and then it started to diffuse throughout the cylinder until it reached its maximum. Without EGR operation, the rate of NO formation was very fast compared with EGR operations, due to high in-cylinder pressure and temperature, and hence the rates of R1, R2 and R3 became high. As seen in the figure without EGR operations at 20 ºCA AIT, the NO covered a significant portion of the cylinder compared to EGR operations at the same crank angle.

Figure 6 illustrates the in-cylinder temperature profiles, as the flame propagated out from the spark plug with different EGR levels (5%, 10%, and 15% EGR) and with different ignition timings of 5º, 10º, and 20º BTDC. The decrease in burning velocity with advanced ignition timing was observed in agreement with [19]. Also, it could be seen that the effect of advancing the ignition timing on the burning velocity becames more obvious at advancing the ignition to 20º BTDC.

As shown in Figure 6, for an ignition timing of 20º BTDC with 5% and 10% EGR, the burning velocity was very high since the flame covered whole the cylinder at 25º AIT. For 15% EGR, just a few crank angle degrees were required for the entire combustion process. As expected, an increase in burning velocity leads to reduction of the combustion duration. On the contrary, for an ignition timing of 5º BTDC and 10º BTDC, at 25º AIT, the flame still propagates towards the chamber walls and more crank angle degrees are required for the whole combustion process. This was especially visible especially for 15% EGR with an ignition timing of 5º BTDC. Advancing the ignition timing causes combustion to occur early in the cycle that in turn, moves the peak pressure closer to TDC increases the temperature during the combustion process, and hence, increases the burning velocity.

In Figure 7, the spatial distribution of NO concentration inside the combustion chamber was shown at crank angles of 15º, 20º, and 25º AIT for three levels of EGR with different ignition timings. The formation rate of NO, decreased as the EGR level was increased. By advancing the ignition timing, NO formation was increased, as discussed above in Figure 4. NO formation occurred near the spark plug where the local temperature was very high. And, as observed in Figure 7, with an ignition timing of 5º BTDC, the region where NO was actually formed became significantly restricted as the EGR level was increased. With further advancement of the ignition timing, the in-cylinder temperature increases during the combustion process and that leads to the extended the region of NO towards the chamber walls.

5. Selection of the optimal operating point

In the preceding section, the effects of EGR and ignition timing on the engine power, NOx emissions, efficiency, and IMEP were considered. The engine power, NO_x emissions, and efficiency are typical optimization objectives [30-32]. In general, it is desirable to increase the engine power and efficiency while reducing the NO_x emissions. In the present study, the decision variables that affect these objectives are EGR and the ignition timing. However, if the three objectives are plotted against each other, it becomes evident that improving the engine power also improves (increases) the efficiency whereas

improving the engine power worsens (increases) the NO_x emissions. Therefore, engine power and efficiency are correlated objectives, but engine power and NO_x are conflicting objectives. Figure 8shows a plot of the engine power and the NO_x emissions. Each EGR series has four points representing the four ignition timing values. It can be seen that there is a general trend that, as the power increases, so does the NOx. However, when Point A is compared with Point B, it can be seen that the latter has a lower engine power as well as a higher NO_x value. This is called a dominated solution [33]. After discarding all such solutions, the concept of "knee" [34] was applied to choose the best operating point from amongst the non-dominated solutions. This point represents the best trade-off between power and NO_x: it is not extreme as either objective and moving from this point to either the preceding point or the succeeding point causes the least increase in NOx for the corresponding gain in power compared to doing so for any other point. The knee point for Figure 8 is (7.9 kW, 7620 ppm), corresponding to 0% EGR and an ignition timing of 5º BTDC

6. Conclusions

The combined effects of the ignition timing with EGR on the combustion characteristics and NO formation in a spark ignition engine fueled with hydrogen were numerically investigated through advanced CFD calculations in this paper. The conclusions from this work are summarized as follows:

1. The present model successfully demonstrated the capability of describing a hydrogen-fueled IC engine with different ignition timings and EGR levels.
2. The IMEP and indicated thermal efficiency decreased with an increase in the EGR level. The effect of ignition timing on IMEP and indicated thermal efficiency was clearer at late ignition timing compared to early ignition.
3. NOx emission decreased with an increase in the EGR level while it increased with advancement of the ignition timing.
4. The combustion duration decreased with the advancing of ignition timing and increased with the increase of the EGR level.

It should be noted that there is a need to investigate the effect of combing the ignition timing with other important parameters such as engine speed and equivalence ratio and to find an optimized range of operation conditions.

7. References

1- Das, L.M., "Hydrogen Engine: Research and Development (R&D) Programmes in Indian Institute of Technology (IIT), Delhi," International Journal Hydrogen Energy, 27:953–65, 2002.

2- Homan, H., Reynolds R., DeBoer, P., McLean, W., "Hydrogen-fueled Diesel Engine without Timed Ignition," International Journal Hydrogen Energy, 4:315-325, 1979.

3- Naber, J.D., and Siebers, D.L., "Hydrogen Combustion under Diesel Engine Conditions," International Journal Hydrogen Energy, 23(5):363-371, 1998.

4- Welch, A.B., and Wallace, J.S., "Performance Characteristics of a Hydrogen-fueled Diesel Engine with Ignition Assist," SAE Technical Paper 902070, 1990, doi:10.4271/902070.

5- Saravanan, N., and Nagarajan, G., "Performance and Emission Study in Manifold Hydrogen Injection with Diesel as an Ignition Source for Different Start of Injection," Renewable Energy, 34:328-334, 2009.

6- Verhelst, S. "Recent progress in the use of hydrogen as a fuel for internal combustion engines," International Journal Hydrogen Energy 2014, 39, 1071-1085.

7- Jongtai, L., Kwangju, L., Jonggoo, L., Byunghoh, A. "High power performance with zero NOx emission in a hydrogen-fueled park ignition engine by valve timing and lean boosting," Fuel 2014, 128, 381-389.

8- Kunal, R., Saravanan, N. , Srinivas J., "Potential of Hydrogen Fuelled IC Engine to Achieve the Future Performance and Emission Norms," SAE Technical Paper, 2015-26-0050, 2015, doi:10.4271/2015-26-0050

9- Knop, V., Benkenida A., Jay, S., Colin O. "Modelling of combustion and nitrogen oxide formation in hydrogen-fuelled internal combustion engines within a 3D CFD code," International Journal Hydrogen Energy, 2008, 19, 5083-97.

10- Rakopoulos, CD., Kosmadakis, GM., Demuynck, J., Paepe, M., Verhelst, S. "A combined experimental and numerical study of thermal processes, performance and nitric oxide emissions in a hydrogen-fueled spark-ignition engine," International Journal Hydrogen Energy, 2011, 36, 5163-80.

11- Callan, B., Simon B. "Dilution Strategies for Load and NOx Management in a Hydrogen Fuelled Direct Injection Engine," SAE Technical Paper, 2007-01-4097.

12- Abhijeet, N., Stanislaw S., Jeffrey, N. "Impact of EGR on Combustion Processes in a Hydrogen Fuelled SI Engine," SAE Technical Paper, 2008-01-1039.

13- Kosmadakis, GM., Rakopoulos, CD., Demuynck, J., Paepe, M., Verhelst, S. "CFD modeling and experimental study of combustion and nitric oxide emissions in

hydrogen-fueled spark-ignition engine operating in a very wide range of EGR rates," International Journal Hydrogen Energy 2012, 37, 10917-10934.

14- Vudumu S., Koylu, U. "Computational modeling, validation, and utilization for predicting the performance, combustion and emission characteristics of hydrogen IC engines," Energy 2011, 36, 647-655.

15- Verhelst, S., Vancoillie, J. "Setting a best practice for determining the EGR rate in hydrogen internal combustion engines," International Journal Hydrogen Energy, 2013, 38, 2490-2503.

16- Sierens, R., Verhelst, S. "Experimental Study of a Hydrogen-Fueled Engine," Journal of Engineering for Gas Turbines and Power- ASME, 2001, Vol. 123 -211.

17- Farhad, S., Amir, S., Ali P. "Effects of spark advance, A/F ratio and valve timing on emission and performance characteristics of hydrogen internal combustion engine," SAE Technical Paper 2009-01-1424.

18- Rana K., Saravanan, N., Mathew, A., Lalit, D. "Effects of governing parameters on the Performance and emissions of hydrogen engine for automotive application," SAE Technical Paper 2013-01-2891.

19- Erjiang, H., Zuohua, H." Optimization on ignition timing and EGR ratio of a spark-ignition engine fuelled with natural gas-hydrogen blends," SAE Technical Paper 2011-01-0918.

20- Rakopoulos, CD., Kosmadakis, GM., Pariotis, EG. "Evaluation of a combustion model for the simulation of hydrogen spark ignition engines using a CFD code," International Journal Hydrogen Energy, 2010, 35(22),12545-60.

21- Arash, H., Pavlos, A. "Computational study of hydrogen direct injection for internal combustion engines," SAE Technical Paper 2013-01-2524.

22- Vincent, K., Adle`ne, B. "Modelling of combustion and nitrogen oxide formation in hydrogen-fuelled internal combustion engines within a 3D CFD code," International Journal Hydrogen Energy, 2008 (33)5083-5097.

23- Zhenzhong, Y., Aiguo, S., Fei, W., Nan, G., "Research into the formation process of hydrogen air mixture in hydrogen fueled engines based on CFD," International Journal Hydrogen Energy, 2010, 35, 3051-7.

24- https://github.com/OpenCFD/OpenFOAM1.7.x/blob/master/tutorials/combustion/dieselFoam/aachenBomb/chemkin/chem.inp_15.

25- Knop, V., Benkenida A., Jay, S., Colin O. "Modelling of combustion and nitrogen oxide formation in hydrogen-fuelled internal combustion engines within a 3D CFD code," International Journal Hydrogen Energy, 2008, 19, 5083-97.

26- An, H., Yang W., Maghbouli, A., Li, J., Chou, S., Chua, K., Wang J., Li, L. "Numerical investigation on the combustion and emission characteristics of a hydrogen assisted biodiesel combustion in a diesel engine," Fuel 2014, 120, 186–194.

27- Wang, Z., Wang, Y., Reitz, R. "Pressure oscillation and chemical kinetics coupling during knock processes in gasoline engine combustion," Energy Fuels 2012, 26, 7107-7119.

28- Subramanian, V., Mallikarjuna, JM., Ramesh, A. “Performance, emission and combustion characteristics of a hydrogen fueled SI engine-an experimental study,” SAE Technical Paper 2005 -26-349.
29- Heywood, JB. Internal combustion engine fundamentals. McGraw-Hill book company, 1988:383-390.
30- Hiroyasu, T., Miki, M., Kim, M., Watanabe, S., Hiroyasu, H., Miao, H. “Reduction of heavy duty diesel engine emission and fuel economy with multi-objective genetic algorithm and phenomenological model,” SAE Technical Papers (2004-01-0531), 2004.
31- Deb, M., Banerjee, R., Majumder, A., Sastry, G.R.K. “Multi objective optimization of performance parameters of a single cylinder diesel engine with hydrogen as a dual fuel using pareto-based genetic algorithm,” International Journal of Hydrogen Energy 39 (15), pp. 8063-8077, 2014.
32- Hiroyasu, T., Miki, M., Kamiura, J., Watanabe, S., Hiroyasu, H. “Multi-objective optimization of diesel engine emissions and fuel economy using genetic algorithms and phenomenological model,” SAE Technical Papers (2002-01-2778), 2002.
33- Deb K., Pratap, A., Agarwal S., Meyarivan, T. “A fast elitist non-dominated sorting genetic algorithm for multi-objective optimization,” NSGA-II. IEEE Transactions on Evolutionary Computation 2002,6 (2), 182-197.
34- Branke, J., Deb, K., Dierolf, H., Osswald, M. “Finding knees in multi-objective optimization,” Yao, X., et al. (eds.) PPSN 2004, LNCS 3242, Springer, Heidelberg, 722–731.

Table 1 Chemical reaction constants used for NO calculations

$k = A.T^{b}.e^{\left(\frac{-E}{RT}\right)}$				
	Reaction	A	b	E
Hydrocarbon fuel	R1	3.270E+12	0.3	0
	R2	6.400E+09	1	6280
	R3	7.333E+13	0	1120
Carbon-free fuel	R1	2.700E+13	0	1500
	R2	9.000E+09	1	27200
	R3	3.600E+13	0	1600

Table 2 Specifications of the IC engine modeled

Fuel	Hydrogen
Number of cylinders	1
Bore × Stroke	85 × 95 mm
Displacement volume	530 cm3
Compression ratio	9:1
Engine speed	2500 rpm
Initial operating conditions	
Start angle (BTDC)	540 degrees
End angle (ATDC)	850 degrees
Piston surface temperature	423 K
EGR levels	5 %, 10% and 15 %
Turbulence model	k-ζ-f model
Turbulence kinetic energy	2 m2/s2
Turbulence length scale	4.5 mm
Initial temperature	330 K
Initial pressure	1 bar

Table 3 Validation of simulation results

	Simulation			Experimental		
Equivalence ratio	0.84	0.55	0.3	0.84	0.55	0.3
Peak pressure (bar)	52.3	40.2	32	50	39.5	32
Brake power (kW)	7.37	5	2	7.4	5	2
Brake thermal eff. (%)	28	26	16.8	27	26	17
NO (ppm)	7620	500	11.9	7600	489	0

Table 4 Compared of NO emissions with different chemical reaction constant at different equivalence ratio

	Equivalence ratio		
	0.84	0.55	0.3
Experimental	7600	500	0
NO (ppm) Hydrocarbon fuel	9500	950	19
NO (ppm) Carbon-free	7620	489	11.9

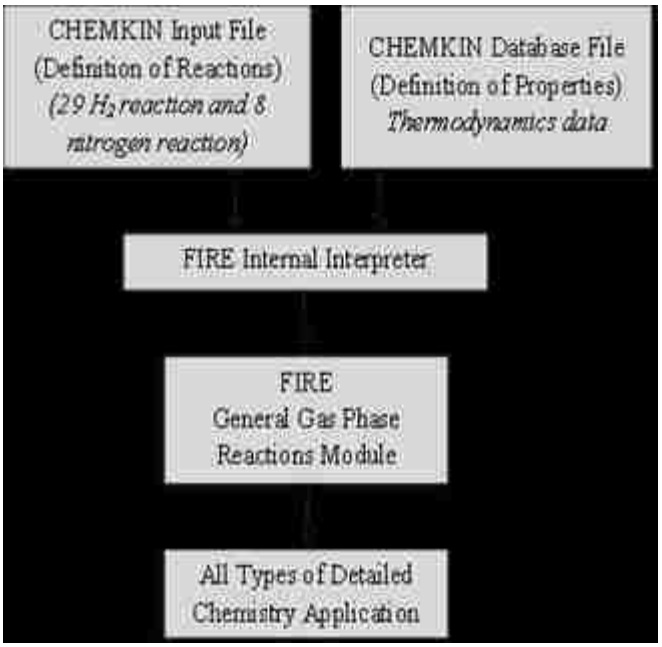

Figure 1 Detailed chemistry modeling scheme

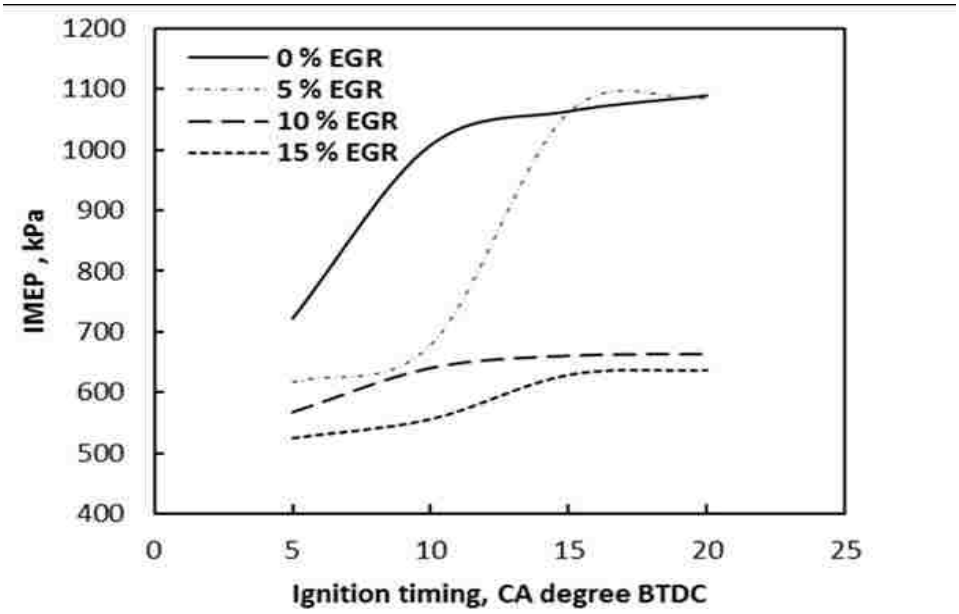

Figure 2 Variation of IMEP with ignition timing for various EGR levels

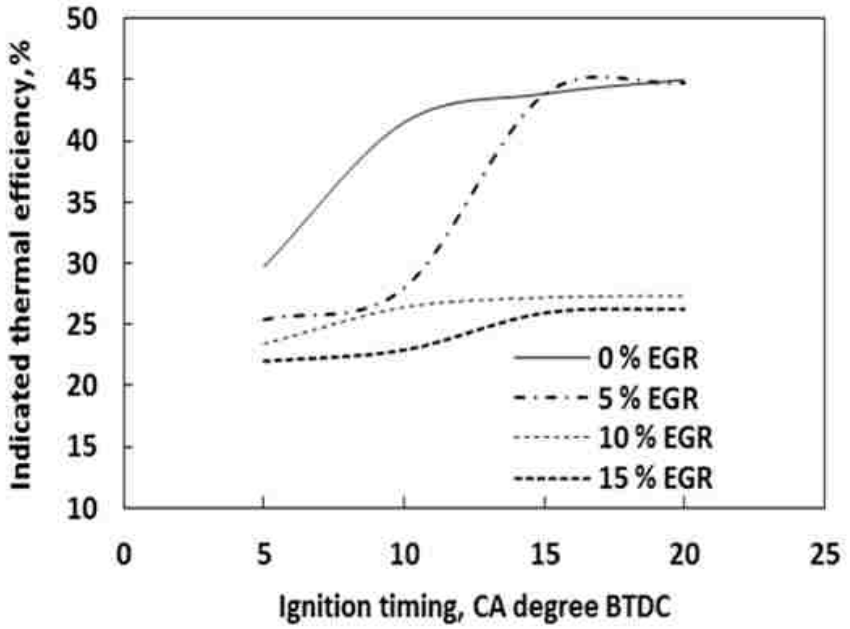

Figure 3 Variation of indicated thermal efficiency with ignition timings for various level of EGR

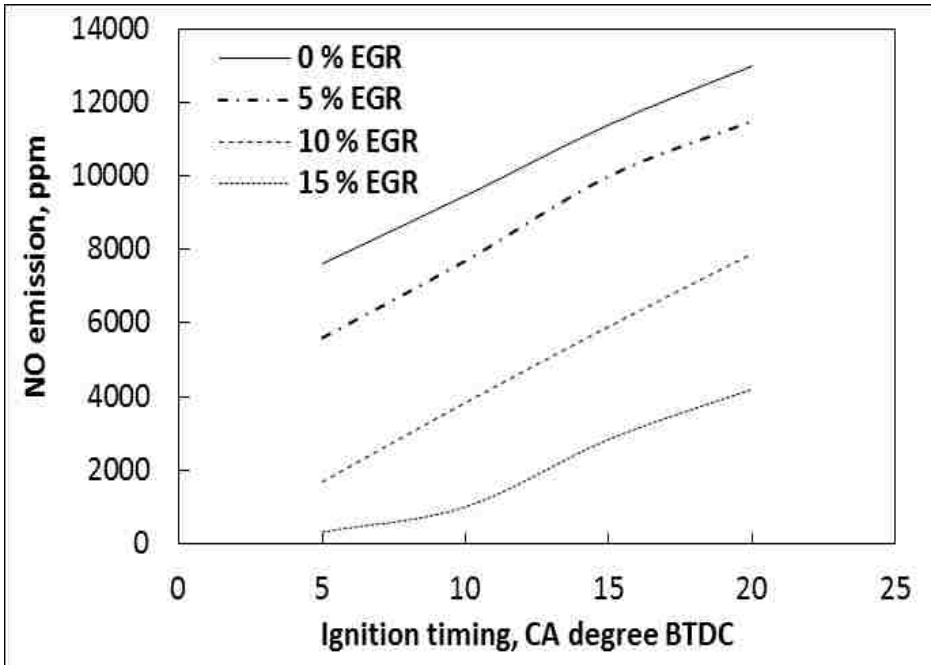

Figure 4 Variation of nitrogen oxides with ignition timing for various EGR levels

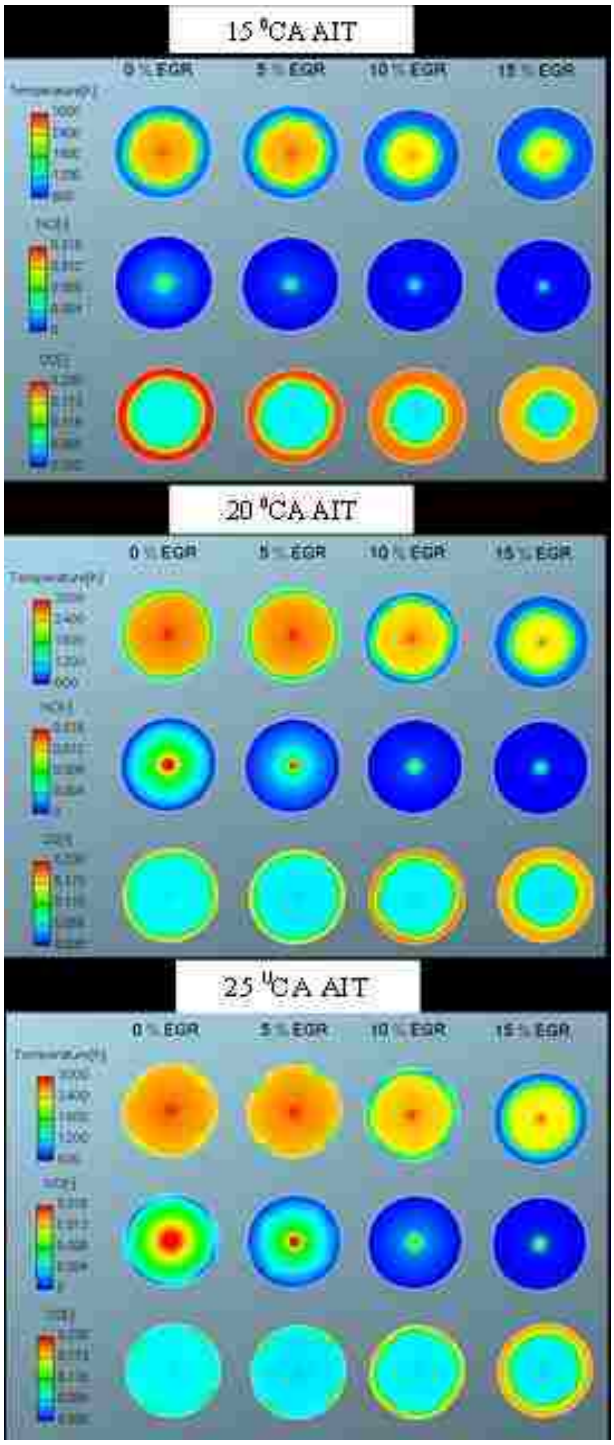

Figure 5 Variation of NO with O2 and temperature under different level of EGR with ignition timing of 5 OCA BTDC

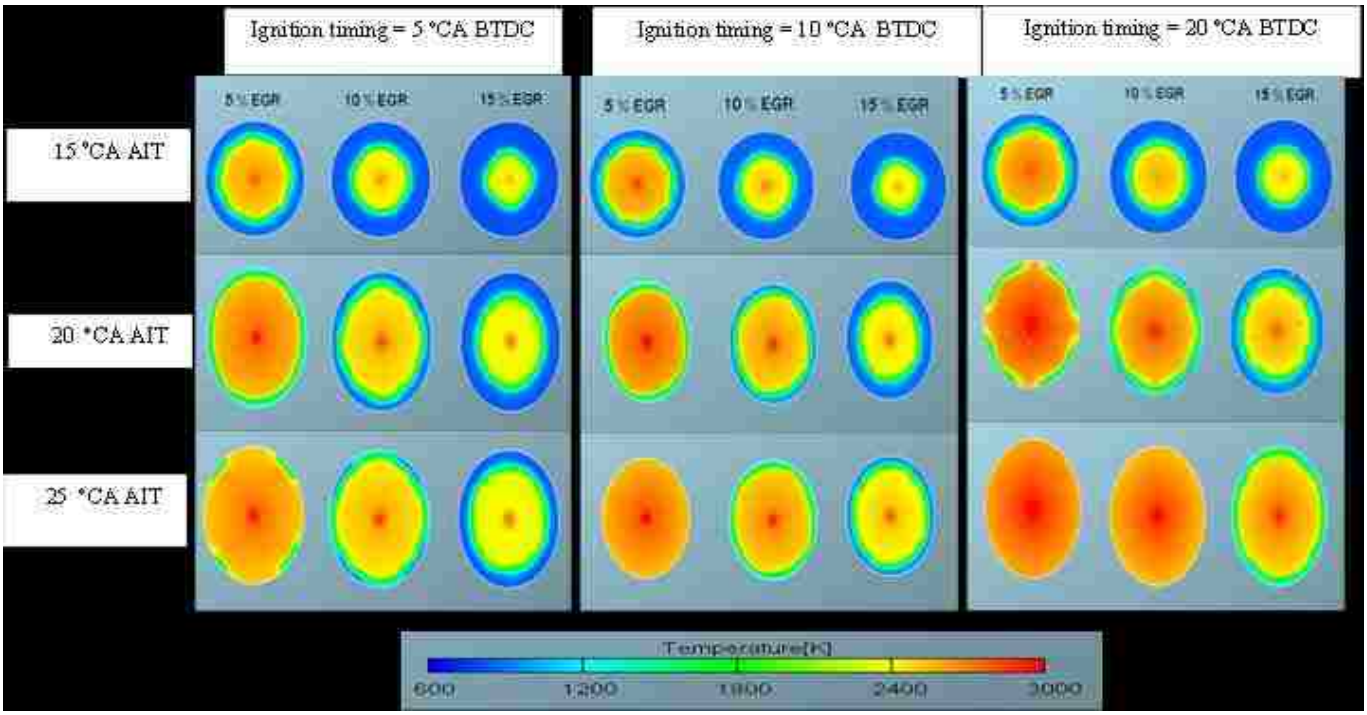

Figure 6 The development of average temperature under different level of EGR with various ignition timing

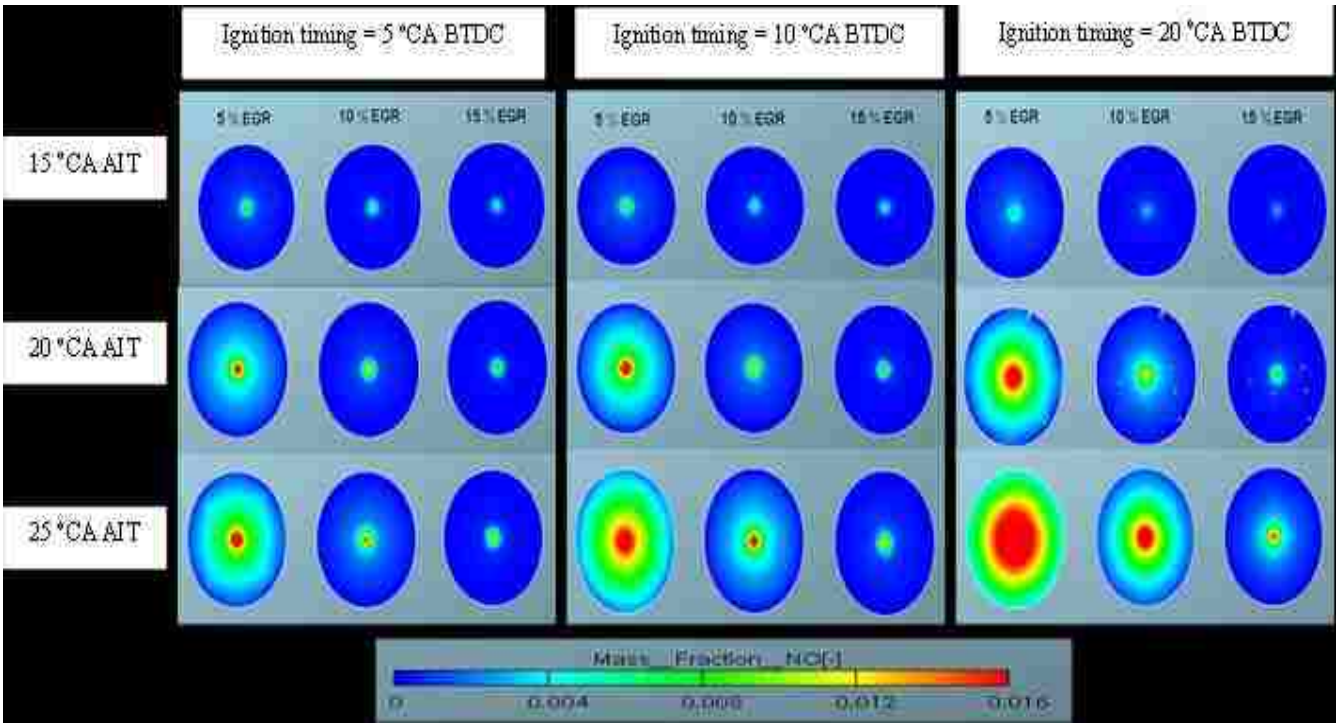

Figure 7 The development of NO mass fraction under different level of EGR with various ignition timing

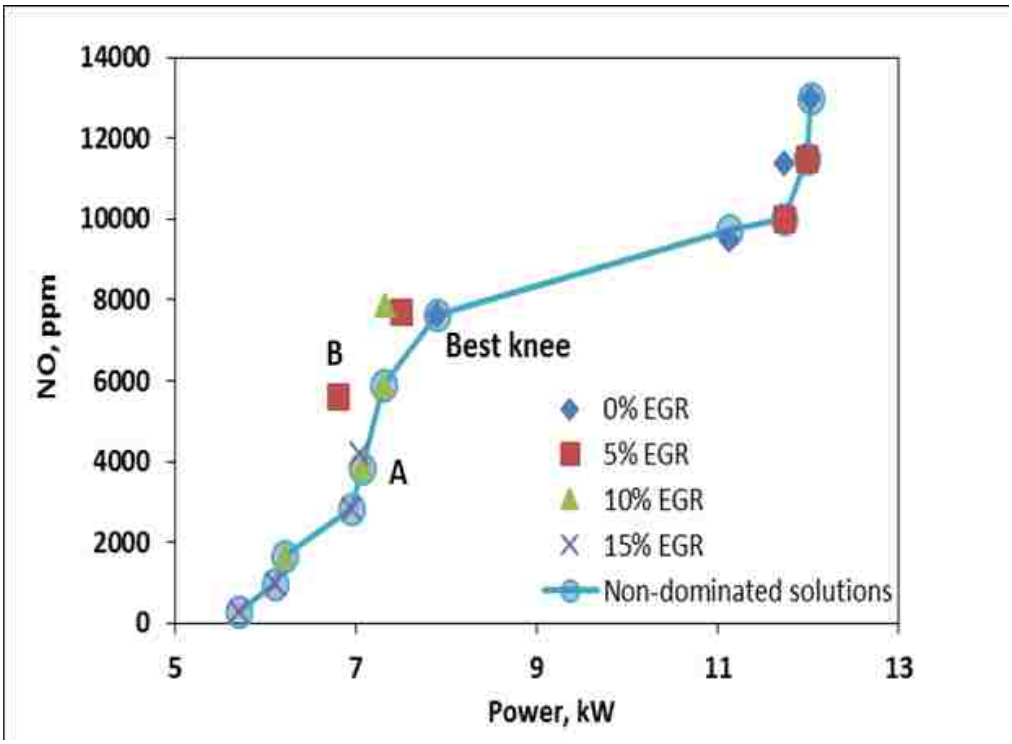

Figure 8 Engine power versus NO emissions for different operating conditions (EGR and ignition timing) with the best knee point being Point A.

III. COMPUTATIONAL INVESTIGATION OF IN-CYLINDER COMBUSTION CHARACTERISTICS AND EMISSION OF HYDROGEN-DIESEL DUAL FUEL ENGINE USING A 3D MODEL WITH CHEMICAL KINETICS

Hassan A. Khairallah[1] Umit O. Koylu[2]

[1]Graduate Student in Mechanical Engineering, Department of Mechanical and Aerospace Engineering, Missouri University of Science and Technology, Rolla, MO, USA

[2]Professor in Department of Mechanical and Aerospace Engineering, Missouri University of Science and Technology, Rolla, MO, USA

ABSTRACT

During the past decade, considerable efforts have been made to introduce alternative fuels for use in conventional diesel and gasoline engines. There is significant interest in adding hydrogen to a diesel engine to reduce emissions and improve efficiency. With the rapid increase in computational capabilities, computational fluid dynamics (CFD) codes have become essential tools for the design, control, and optimization of dual fuel engines. In the present study, a reduced chemical kinetics mechanism, consisting of 52 reactions and 29 chemical species for n-heptane fuel combustion, was incorporated with detailed chemical kinetics consisting of 29 reactions for hydrogen including additional nitrogen oxidation. This reaction mechanism was coupled with a 3D CFD model based on AVL FIRE software to investigate the performance and emission characteristics of a diesel engine with low amounts of hydrogen addition. Hydrogen was introduced at percentages of 37.5 %, 50 % 90 % by volume and compared our results with base fuel operation. The model was validated by the experimental results and then employed to examine important parameters that have significant effects on the engine performance. The simulation results showed that the variations of brake thermal efficiency, CO_2, CO and NO_X emissions reasonably agree with the experimental findings. NO_X emissions and exhaust gas

temperature increased with the rise in brake power for hydrogen-diesel mixtures. The CFD results quantified the degree of dependence of NO_X emissions on the average combustion temperature. The results also quantified that CO and CO_2 emissions decreased when adding hydrogen in diesel engine because the addition of hydrogen leads to reduction in the injected amount of diesel fuel that results in CO and CO_2 formation.

1. Introduction

Due to the depletion of fossil fuels and environmental degradation in recent years, there is considerable global effort to ensure continued availability of supplies of hydrocarbon fuels and to reduce exhaust emissions from all combustion devices, particularly internal combustion engines. Many studies by a number of research groups worldwide have focused attention on alternative transportation fuels to replace or supplement hydrocarbon fuels [1-4]. In this regard, hydrogen is considered one of the most promising alternate fuels due to its clean burning characteristics and better overall performance as compared to diesel. Some of the important properties of hydrogen are given in Table 1 [5, 6]. Hydrogen has a wide flammability range in comparison with all other fuels. As a result, hydrogen can be used in running an engine on a lean mixture that allows for greater fuel economy due to a more complete combustion of the fuel. Additionally, it allows for lower combustion temperature and hence decreases the amount of NO_x. The ignition energy required to ignite the hydrogen is also very low, which allows hydrogen engine to ignite lean mixtures and ensures prompt ignition even with a relatively weak spark. Although hydrogen has been mainly used in spark ignition engine applications it has capability to use in diesel engine, however it is very difficult to ignite it by only the compression process because the hydrogen has an appreciably lower cetane number than diesel fuel [6], and therefore it requires an ignition source such as spark plugs, glow plugs, or pilot fuel.

Various studies on internal combustion engines have been focused on substitution of diesel fuel by hydrogen to protect the global environment and to restore fossil fuels. The addition of H_2 to the intake air of diesel engines has shown to substantially reduce the emissions of CO, HC, CO_2, and particulate matters (PM). However, the addition of

relatively large amount of H_2 can significantly increase the emissions of NO_x [7] due to its high adiabatic flame temperature. Saravanan et al. [8, 9] have investigated and reported some studies using a DI diesel engine with hydrogen in the dual fuel mode. In general, they observed that a significant improvement in thermal efficiency and reduction in CO_2, CO and hydrocarbon (HC) emissions could be obtained under certain operating conditions by running a diesel engine in the dual fuel mode using hydrogen. Ghazal [10] investigated hydrogen-diesel co-combustion in a diesel engine. The results showed that, the hydrogen doses as enrichment to the diesel fuel can be improved engine performance and reduce emissions compared to the neat diesel operation. Köse and Ciniviz [11] carried out an experimental study to investigate the performance and emission characteristics of the diesel engine with hydrogen added to the intake air at rates of 2.5%, 5% and 7.5% as volume. Their results indicated that engine power for dual fuel mode increased averagely as 6.8%, 12.4% and 17% at 2.5 %, 5 % and 7.5 % H2, respectively compared with pure diesel mode. HC, CO_2 and CO emissions for all additional hydrogen rates were decreased while NOx was increased compared to pure diesel at full load. Similar conclusions were also drawn by [12, 13] who investigated the performance and emission characteristics of a diesel engine with hydrogen addition. They demonstrated that the HC, CO_2 and CO emissions could be reduced significantly by introducing amounts of hydrogen. They also observed that the NO_x emission increased with the additional hydrogen. Several studies have been demonstrated that exhaust gas recirculation (EGR), N_2 dilution and late injection timing were promising techniques to achieve substantial reduction of NO_X from diesel-hydrogen dual fuel engine [14-16].

Talibi et al. [17] reported a reduction in the particulates, CO and THC emissions when H_2 was used as a secondary fuel in a diesel engine. However, it was found a slight increase in CO_2 emissions with hydrogen addition, with fixed diesel fuel injection periods, which they ascribed to this factor; the addition of H_2 displaces some of the intake air and the subsequent oxidation of H_2 to water vapor, since the water vapor is condensed through cooling cycle to produce CO_2.

Zhou et al. [18] experimentally investigated the performance of regulated and unregulated emissions of a diesel engine with hydrogen addition. They concluded that

hydrogen addition also had the potential to reduce unregulated emissions, such as olefins (C_2H_4 and C_3H_6), BTX (C_6H_6, C_7H_8, and C_8H_{10}) and acetaldehyde (CH_3CHO).

Numerous experiments have been established on dual fuel engine to investigated and understand the in-cylinder combustion processes under different operating conditions [19]. However, there are difficult to obtain better knowledge about the in-cylinder combustion processes and pollutant experimentally. Also reduce the development costs and minimizing the time is needed with experimental investigations. In the past few years numerous studies focused on how to create an engine models in order to obtain an insight into the complex phenomena in-cylinder processes, and furthermore optimize engines development.

Computational fluid dynamics (CFD) has considered a powerful numerical tool to simulation of many processes in industry. It provides deeper understanding of what is happening inside the combustion cylinder. Consequently it will give the ability to predict the performance of new designs with much less time and costs compered to experimental investigation. There are some numerical studies have focused on using three-dimensional CFD tools to understand the in-cylinder processes in compression ignition engine (CI) fueled with hydrogen [20 - 23]. But there are appears much fewer detailed chemical reaction model has been developed for the combined combustion of hydrogen and diesel [24].

In the present work, a reduced reaction mechanism for diesel fuel was incorporated with detailed chemical kinetic reactions for hydrogen. This reaction mechanism was coupled with the AVL FIRE® CFD code to study the performance, combustion and emission characteristics of a hydrogen assisted diesel combustion under various engine operating conditions. An advantage of this model is the FIRE General Gas Phase Reactions Module was used for simulation of dual fuel engine that run on either diesel/hydrogen mixture or diesel with others conventional fuels (methane or gasoline), contrary to what it is done in most existing engines models.

2. Computational Methods

An integrated numerical model for diesel dual fuel combustion computations has been developed in this study; the numerical models are based on the AVL FIRE code.

2.1 Governing equations

Transient equations for the conservation of mass, Momentum and energy were solved using AVL FIRE [25]:

- Mass conservation equation:

$$\frac{\partial \rho}{\partial t} + \frac{\partial}{\partial x_j}(\rho U_j) = 0 \quad (1)$$

- Momentum conservation Equations (Navier-Stokes):

$$\frac{\partial}{\partial t}(\rho U_i) + \frac{\partial}{\partial x_j}(\rho U_i U_i) = \rho g_i - \frac{\partial p}{\partial x_i} + \frac{\partial}{\partial x_i}\left[\mu\left(\frac{\partial U_i}{\partial x_j} + \frac{\partial U_j}{\partial x_i} - \frac{2\partial U_k}{3\partial x_k}\delta_{ij}\right)\right] \quad (2)$$

On the left hand side, the first term represents the rate of change of the momentum; the second one is the net momentum flux through the volume boundary surfaces. On the right hand side, the first term represents the volume forces acting on the control volume, the second term the pressure gradient forces acting on the control volume, and the third one indicates the normal and shear stress tensor actions on the control volume surface, where δ_{ij} is the unit tensor (i.e. i = j then $\delta_{ij} = 1$ if i ≠ j then $\delta_{ij} = 0$) and μ is the dynamic viscosity coefficient.

- Energy conservation equation: ($H=h+ U^{\wedge 2}/2$)

$$\frac{\partial}{\partial t}(\rho H) + \frac{\partial}{\partial x_j}(\rho H U_j) = \rho \dot{q}_g + \frac{\partial p}{\partial t} + \frac{\partial(\tau_{ij} U_j)}{\partial x_i} + \frac{\partial}{\partial x_i}\left(\lambda \frac{\partial \hat{T}}{\partial x_j}\right) \quad (3)$$

On the right hand side, the first term represents the work due to body forces; the second term is the temporal change of pressure. The third term is work due to external forces, where τ_{ij} is the stress tensor. The last term is the heat influx through conduction.

- General transport equations

AVL FIRE® presents a general species transport model to allow the implementation of a detailed kinetic model and solves species transport equations for any arbitrary number of chemical species. The species mass conservation equation is expressed as

$$\frac{\partial}{\partial t}(\rho\varphi) + \frac{\partial}{\partial x_j}(\rho\varphi U_j) = \frac{\partial}{\partial x_j}\left(\left(\rho D_i + \frac{\mu}{\sigma_{ci}}\right)\frac{\partial}{\partial x_k}\right) + S_{w_i} \qquad (4)$$

Where,ρ, U_j are density and velocity , S_{w_i} is the source term of species by taking into account homogeneous chemical reactions, σ_{ci} is the stress tenser, and μ is the viscosity. Where φ scalar property (viscosity, density, specific heat, diffusion coefficient, thermal conductivity) shown in the equation above are calculated for each species and for gas mixtures by using the chemical kinetic databases (CHEMKIN™).

In this study the k-zeta-f model was chosen. This model recently developed by Hanjalic et al. [26] For IC-engine flows the k-z-f model leads to more accurate results than the much simpler two-equation eddy viscosity models of the k-e type by simultaneously exhibiting a high degree of numerical robustness. This model is based on Durbin's elliptic relaxation concept, which solves a transport equation for the velocity scales ratio $\zeta = \frac{\overline{v^2}}{k}$ instead of the equation for $\overline{v^2}$.[34] The $\overline{v^2}$ is the velocity scale and k is the turbulence kinetic energy. Durbin's model is described in refereance [27].

2.2 Chemical reaction mechanism

A reduced (52 reactions and 29 species) chemical reaction mechanism for n-Heptane was constructed from a comprehensive detailed n-Heptane mechanism (179 species and 1642 reactions) [28]. n-Heptane was chosen in this study because its cetane number (CN~56) is rather close to that of typical diesel fuels (CN~50).

The reduced reaction mechanism consisting of 52 reaction steps with 29 chemical species for n-Heptane fuel combustion was incorporated with detailed chemical kinetic reactions consisting of 29 reactions steps for hydrogen, which includes additional nitrogen oxidation reactions [29]. Figure 1 shows the skeletal chemistry mechanism for multi-fuels (hydrogen/diesel). The multi-chemical reaction mechanism (89 reactions and 32 species) was coupled with a 3D-CFD model based on AVL FIRE® software.

The CHEMKIN™ chemistry solver was integrated into the AVL FIRE® code for solving the chemistry during multidimensional engine simulation. The AVL FIRE® code provides CHEMKIN™ the species and thermodynamic information of each computation cell, and the CHEMKIN™ utilities return the new species information and energy release after solving for the chemistry. The detailed chemistry modeling scheme is shown in Figure 2. The general gas phase reaction module allows the simulation of various types of kinetic problems by interfacing property and reaction databases. The recommended way to calculate gas phase reactions in FIRE is to use the FIRE internal chemistry interpreter. Where the stoichiometries of the reactions and the kinetic Parameters (A, b and E) are defined. The reaction rates are calculated in the general form as the following [25]:

$$\sum_{k=1}^{K} v'_{ki} \, . k_k \leftrightarrow \sum_{k=1}^{k} v''_{ki} \, . k_k \qquad (i = 1, \ldots\ldots, I) \qquad (5)$$

where v are stoichiometric coefficients and k is the chemical symbol for the k^{th} species. K is the total number of gas phase species in the system, I is the total number of chemical reactions considered.

The stoichiometric coefficient of species k in reaction i is defined as the following:

$$v_{ki} = v'_{ki} - v''_{ki} \qquad (6)$$

The rate of production of species k is:

$$\dot{r}_k = \sum_{i=1}^{I} v_{ki}\, \dot{q}_i \qquad (7)$$

Where $\dot{q}_i$ is the reaction rate of reaction i.

The forward reaction rate constant k_{f_i} is defined by the following Arrhenius temperature dependence:

$$k_{f_i} = A.T^{b_i}.e^{\left(\frac{-E}{RT}\right)} \qquad (8)$$

The piston geometry and computational grid used for the simulations were built up using the commercial CFD tool AVL ESEDiesel. The mesh was composed of about 7680 computational cells with mesh size was 3 ×3×3 mm.

The convergence criterion is either maximum number of iterations 60 or reduction of residuals as 0.01 whichever achieves first. In this paper, the boundary conditions were as follows: the piston temperature was 570 K, cylinder liner temperature was 470 K, and cylinder head temperature was 570 K. The computational domain consists of one section of the modeled engine cylinder, which was used for simulations between inlet valve closing (IVC) and exhaust valve opening (EVO). This means that only the closed volume part of the engine cycle is computed. The injector located in the center of cylinder head. The hydrogen was substituted for diesel fuel with verity levels (37.5 %, 50 % and 90 % by volume). The injection timing of the pilot diesel (i. e. the crank angle of the start of diesel fuel injection) was kept constant as 23^o BTDC, and the injection duration was adjusted to 30 crank angle degrees. The computational time step used for simulation, during the compression stroke was 1 ^{o}CA. However during the combustion period, the time step was further decreased and becomes equal to 0.25 ^{o}CA. This occurs in order to increase the accuracy of the computational results.

2.3 Analysis procedure

After collecting the data sets at each diesel–hydrogen dual fuel mode, the dependent parameters are calculated according to the following equations:

- Theoretical combustion of fuel formula is given by;

$$(1-x)C_7H_{16} + xH_2 + a.(O_2 + 3.76N_2) \rightarrow y.CO_2 + z.H_2O + n.CO + f.NO + w.N_2 \quad (9)$$

- The brake thermal efficiency for dual fuel mode is given by:

$$\eta_{TE} = \frac{Power}{(\dot{m}_{f.diesel} \times CV_{diesel}) + (\dot{m}_{f.hydrogen} \times CV_{hydrogen})} \quad (10)$$

- Specific energy consumption (SEC) was calculated using the following equation

$$SEC = \frac{(\dot{m}_{f.diesel}.CV_{diesel}) + (\dot{m}_{f.hydrogen}.CV_{hydrogen})}{Power} \quad (11)$$

here $\dot{m}_{f.diesel}$ is the diesel flow rate (kg/s) and CV_{diesel} is the lower heating value of diesel (kg/kJ). $\dot{m}_{f.hydrogen}$ is the hydrogen flow rate (kg/s) and $CV_{hydrogen}$ is the lower heating value of hydrogen (kg/kJ).

3. Results and Discussion

In the present work, a multi-chemical reaction mechanism was implemented using 3-D computational fluid dynamics (CFD) based on AVL FIRE® and CHEMKIN™ to investigate the combustion and emission characteristics of a direct ignition (DI) diesel engine with gaseous hydrogen as a fuel and with diesel as the source of ignition. By using the experiment data, the model were run with same experiment engine condition at each brake power and the results found on good agreement with the experiment results. The operating conditions of the diesel engine modeled and simulated in this investigation were

similar to the independent experimental study by Saravanan et al. [30] because their reported test conditions and experimental data were well documented. The specifications of the compression ignition (CI) engine in this computational study are given in Table 2.

3.1. Combustion characteristics

Figure 4 depicts the variation of specific energy consumption with brake power. It is seen that the SEC of hydrogen/diesel operation was lower than that of diesel. At full load the SEC for hydrogen/diesel operation was 14.22 MJ/kWh compared to diesel, which it was 15.41 MJ/kWh at operating conditions. This is due to the premixing of hydrogen fuel with air due to its high diffusivity and better mixing with air resulting in complete combustion. Also the SEC decreased gradually with increasing hydrogen level, the reduction is more illustrious at higher loads.

The variation of brake thermal efficiency as function with engine power for different ratios of hydrogen was illustrated in Figure 5. The brake thermal efficiency can be defined as the ratio of the engine brake power to the input fuel energy. It was observed that highest brake thermal efficiency of 27 % was obtained for 37.5 % H_2 at full load compared to diesel of 22.7 %. The increase in brake thermal efficiency can be attributed to hydrogen's better mixing with air in addition to its faster burning characteristics. The brake thermal efficiency increased with increase in hydrogen level, but was limited to avoid knocking problem. For 90 % H2 approximately at 2.7 kW, the brake thermal efficiency was 27.5 %. The present simulations for the diesel/hydrogen mixture captured this trend and agreed well with the experiments reported under the same operating conditions [30, 9].

The variation of cylinder pressure as function with crank angle was illustrated in Figure 6. It can be seen that the peak cylinder pressure for a hydrogen/diesel mixture (37.5 % H_2 by volume) was higher (103.7 bar) than that for pure diesel (88.4 bar) for the same operational conditions. This is due to the higher flame speed of hydrogen which will lead to overall faster and more complete combustion, resulting in higher peak pressure, which corresponds well with the numerical results in reference [23]. Also the peak pressure occurrence in hydrogen/diesel operation is advanced by 3 crank angles compared to the peak pressure of diesel at full load. This is may be due to that hydrogen undergoes instantaneous combustion compared to diesel. The peak cylinder pressure decreased

gradually with increasing hydrogen level due to lean burn operation (equivalence ratio decreases) as observed in figure. The peak pressure with 90% H2 takes place definitely after TDC; this can be attributed to a longer ignition delay with lean mixture compared to 37.5 % H_2 operation. The ignition delay in diesel engine defined as the time lag between the start of diesel injection to start of the combustion.

Figure 7 displays hydrogen peroxide (H_2O_2) and hydroxyl (OH) radicals in the form of a mass fraction as a function of the crank angle during the combustion process. These radicals were selected as the most important for driving the ignition process [31]. H_2O_2 was produced during the compression stroke; then, with the increased temperature, most of the H_2O_2 that had formed began to dissipate and was converted to OH radicals via the reaction $H_2O_2 + M = OH + OH + M$. This involves the formation of two OH radicals, which enhanced the reduced the ignition delay. As can be seen in figure that the early formation time of OH with 37.5% and H2, 50% were observed and hence the combustion occurred at 10 BTDC and 5 BTDC respectively, while it was occurred at 4 ATDC with 90% H_2.

3.2. Emissions

3.2.1 NO_X emissions

Figure 8 illustrates the predicted and measured NO_X emissions as a function of engine power. It was observed that the NOx emissions increased with the additional power for the conditions considered. The NO_X emission with 37.5 % H_2 operation was 2500 ppm, which was higher than that of baseline diesel (2089 ppm) at full load. The main reason for the higher concentration of NOx in the hydrogen/diesel operation is the higher combustion temperatures compared to those in the pure diesel operation. The high combustion temperatures can be explained by the high adiabatic flame temperature and the combustion rates of hydrogen. Moreover, the high residence time of the high temperature gases in the cylinder led to the production of higher NOx emissions. The model-predicted trends of NOx emissions are very similar to the experimental results. Also we can see that as the hydrogen level increases, the lean limit of combustion is significantly prolonged, which in turn decreases the peak combustion temperature and hence lead to reduce NO_X , so the lower NO_X achieved was 490 ppm with 90 % H_2 at engine power of 99 Kw with equivalence ratio 0.4.

The present computational methods provide a better understanding of the NO formation, in relation to oxygen availability and the average in-cylinder temperature at the same instants of time. NO is formed mainly as a result of the following reactions:

$$N_2O + O = N_2 + O_2 \quad (R1)$$

$$N_2O + O = NO + NO \quad (R2)$$

$$N_2O + H = N_2 + OH \quad (R3)$$

$$N_2O + OH = N_2 + HO_2 \quad (R4)$$

$$N_2O + M = N_2 + O + M \quad (R5)$$

The other path to NOx formation can be described by reactions R6, R7, and R8, usually known as the extended Zel'dovich mechanism:

$$N_2 + O = N + NO \quad (R6)$$

$$N + O_2 = NO + O \quad (R7)$$

$$N + OH = NO + H \quad (R8)$$

Normally, these three reactions are only important at high temperatures because radicals O and OH are created in high temperature gases.

Figure 9 displayed the development process of NO mass fraction, oxygen mass fraction, and average in-cylinder temperature under three different levels of H_2 at various crank angles. As can be seen, the formation time of NO delayed with hydrogen increments, this is expected due to increase the ignition delay. Where the increase in the hydrogen level led to increase in ignition delay due to a high ignition temperature for hydrogen, and also the amount of diesel fuel to ignite the premixing of hydrogen with air was reduced and resulted in a late start of combustion and hence led to delay NO formation. The other reason to delay NO formation time was the lean burn operation with high hydrogen level. The NO formation time was shown in the central region of the cylinder near the injector where the local temperature was very high (in the flame region), and then it started to diffuse throughout the cylinder until it reached its maximum, which corresponds well with the numerical results in reference [21, 32]. It can be observed also, that the average in-cylinder temperature decreased gradually with increasing hydrogen level due to lean burn operation

(equivalence ratio decreases). The local gas temperature becomes more homogeneous with 90 % H2 as shown in figure. After the in-cylinder temperature reached its maximum for three cases (37.5, 50 and 90 %H2) the temperature gradually decreased as the crank angle increased during the expansion stroke; hence, the rate of NO decomposition rapidly decreased, because the rates of R6, R7, and R8 (Zel'dovich mechanism) became small. Consequently, the concentration of NO remained almost frozen and did not change during the remainder of the expansion stroke.

Figure 9 also showed oxygen mass fraction which considered another factor contributes to NO formation. Although oxygen mass fraction increased along with the enhancement of H2 level, NO formation decreased. This is indicated that the NO formation was influenced, primarily, by a reduction in temperature rather than the availability of O_2. For three cases, it was observed that the oxygen mass fraction began to consume at the central area of the cylinder where regions combustion reaction occurs [33], then starts to decrease significantly as crank angles increased during combustion processes simultaneous with increased in-cylinder temperature and that leads to the extended the region of NO towards the chamber walls.

3.2.2 Carbon monoxide (CO) emissions:

The variation of carbon monoxide emissions with load is shown in Figure 10. The CO level with hydrogen/diesel (37.5 % H2 by volume) operation was 0.05 % by volume, which was lower than that of baseline diesel 0.16 % by volume at full load. The CO level gradually decreased with increase in the hydrogen level. The CO level is reduced by 30 %, 40 % and 80 % with 37.5 % H2, 50 % H2 and 90 % H2 by volume respectively as shown in Figure. The CO emission decrease with increasing hydrogen level because of the reason that hydrogen does not contain any carbon in its structure and also because the addition of hydrogen led to reduction in the injected amount of diesel fuel that resulted in CO formation.

3.2.3 Carbon dioxide (CO2) emissions:

The variation of carbon dioxide emissions with load is shown in Figure 11. The CO2 emissions are lower compared to that of baseline diesel, the minimum being 7.9% by

volume at full load at the flow rate of hydrogen as 37.5 % by volume as depicted in Figure. The CO2 emission in hydrogen is lowered because of better combustion of hydrogen fuel and also due to the absence of carbon atom in hydrogen flame.

The CO2 value is found to be 8 % by volume with 37.5 H2 % by volume. Further increase in hydrogen flow rate 50 % H_2 and 90 % H2 reduces the CO2 value to 6.6 and 1.06 by volume respectively as shown in Figure. This is because as H2 is added to the intake manifold, the amount of diesel fuel injected is reduced. Many researchers found similar results in the literature [13].

More demonstrate can be seen in Figure 12 which presents the spatial and temporal distribution of the in-cylinder CO and CO2 formations at TDC, 10 ^{o} ATDC, 30 ^{o}ATDC, 50 ^{o}ATDC and 70 ^{o}ATDC for three different modes. As can be seen the CO formation time was observed around the burnt region of fuel near the injector for three mode. After that, the CO formation region was extended in the cylinders; then, most of the CO formed began to decrease with an increase in the crank angle; along with extended the region of CO_2 towards the cylinder walls. This due to oxidation of CO to CO2 by OH radical, where the key reaction pathway for CO oxidation is CO + OH = CO_2 + H, (See R26 in Appendix 1), and it was activated by the increased combustion temperature.

4. Conclusions

To investigate performance, in-cylinder combustion, and pollutant characteristics of a hydrogen-fueled diesel engine, a three-dimensional numerical simulation was employed with detailed chemical kinetics. The following conclusions can be drawn from the present research:

- The multi-fuel mechanism successfully predicted NO_x, CO and CO_2 emissions in the simulated engine over the four engine loads tested.
- The unwanted emissions were reduced drastically with increase hydrogen.
- NO_x formation was higher with 37.5% hydrogen level, but beyond this level, it decreased due to lean burn operation.

- An increase in the duration of ignition delay was observed with increase in H2 addition, which could be attributed to the decreasing O2 concentration in the intake charge.
- The present model successfully demonstrated the capability of describing multi-fuel combustion operations.

5. References:

1- Lata D, Misra A, Medhekar S. Effect of hydrogen and LPG addition on the efficiency and emissions of a dual fuel diesel engine. Int J Hydrogen Energy 2012;37: 6084-96.

2- Kahraman N, Ceper B.A, Akansu S , Aydin K., Investigation of combustion characteristics and emissions in a spark-ignition engine fuelled with natural gas–hydrogen blends. Int J Hydrogen Energy 2009; 34: 1026-34.

3- Wei F, Bin H, Kittelson D, Northrop W. Dual-fuel diesel engine combustion with hydrogen, gasoline, and ethanol as fumigants: effect of diesel injection timing. J Engineering for Gas Turbines and Power 2014; 136:0815-02.

4- Chokri B, Ridha E, Rachid S, Jamel B. Experimental study of a diesel engine performance running on waste vegetable oil biodiesel blend. J Energy Resour Technol 2012;134:0322-27.

5- Verhelst S. Recent progress in the use of hydrogen as a fuel for internal combustion engines Int. J. Hydrogen Energy 2014; 39: 1071-85.

6- Karim G. Hydrogen as a spark ignition engine fuel. Int J Hydrogen Energy 2003;56:256-63.

7- McWilliam L, Megaritis T, Zhao H. Experimental Investigation of the Effects of Combined Hydrogen and Diesel Combustion on the Emissions of a HSDI Diesel Engine. SAE Technical Paper 2008-01-1787.

8- Saravanan N, Nagarajan G. Performance and emission study in manifold hydrogen injection with diesel as an ignition source for different start of injection. Renewable Energy 2009; 34: 328-334.

9- Saravanan N, Nagarajan G. An experimental investigation of hydrogen-enriched air induction in a diesel engine system. Int J Hydrogen Energy 2008;33: 1769-75.

10- Ghazal O. Performance and combustion characteristic of CI engine fueled with hydrogen enriched diesel. Int J Hydrogen Energy 2013; 38: 15469-76.

11- Köse H, Ciniviz M. An experimental investigation of effect on diesel engine performance and exhaust emissions of addition at dual fuel mode of hydrogen. Fuel Processing Technology 2013; 114:26–34.
12- An H, Yang W, Maghbouli A, Li J, Chou S, Chua K. A numerical study on a hydrogen assisted diesel engine. Int J Hydrogen Energy 2013;38: 2919-28.
13- Sandalcı T, Karagoz Y, Experimental investigation of the combustion characteristics, emissions and performance of hydrogen port fuel injection in a diesel engine. Int J Hydrogen Energy 2014;39: 18480-89.
14- Singh Yadav, V., Soni, S.L., "Performance and emission studies of direct injection C.I. engine in duel fuel mode (hydrogen-diesel) with EGR," Int. J Hydrogen Energy 2012; 37: 3807-17.
15- Christodoulou F, Megaritis A, Experimental investigation of the effects of simultaneous hydrogen and nitrogen addition on the emissions and combustion of a diesel engine. Int J Hydrogen Energy 2014;39: 2692-02.
16- Miyamoto T, Hasegawa H, Mikami M, Kojima N, Kabashima H, Urata Y. Effect of hydrogen addition to intake gas on combustion and exhaust emission characteristics of a diesel engine. Int J Hydrogen Energy 2011; 36: 13138-49.
17- Talibi M, Hellier P, Balachandran R, Ladommatos N. Effect of hydrogen-diesel fuel co-combustion on exhaust emissions with verification using an in-cylinder gas sampling technique. Int J Hydrogen Energy 2014; 9: 15088-02.
18- Zhou J, Cheung C, Leung C. Combustion, performance, regulated and unregulated emissions of a diesel engine with hydrogen addition. Applied Energy 2014;126:1–12 .
19- Mueller C, Martin G, Briggs T, Duffy K. An Experimental Investigation of In-Cylinder Processes under Dual-Injection Conditions in a DI Diesel Engine. SAE Technical paper 2004:011843.
20- An H, Yang W, Maghbouli A, Li J, Chou S, Chua K, Wang J, Li L. Numerical investigation on the combustion and emission characteristics of a hydrogen assisted biodiesel combustion in a diesel engine. Fuel 2014;120:186–194.
21- Yang Z, Chu C, Wang L, Huang Y. Effects of H2 addition on combustion and exhaust emissions in a diesel engine. Fuel 2015;139:190–97.
22- An H, Yang W.M, Maghbouli, A, Li J, Chou S, Chua K. A numerical study on a hydrogen assisted diesel engine," International Journal Hydrogen Energy 2013;38: 2919-28.
23- Xiao F, Karim G. An Investigation of the combustion in an IDI diesel engine with low concentrations of added hydrogen," SAE Paper 2011:010676.
24- Singh S. Numerical investigation of NO2 formation mechanism in H2-diesel dual-fuel engine. SAE Paper 2012:010655.
25- FIRE Version 8.1 Manual, AVL List GmbH Graz, Austria, 2011.

26- Hanjalic K, Popovac M, Hadziabdic M. A robust near-wall elliptic relaxation eddy-viscosity turbulence model for CFD. Int. J. Heat and Fluid Flow, 2004;25:1047–51.
27- Durbin P. Near-wall turbulence closure modelling without damping functions. Theoretical and Computational Fluid Dynamics. 1991:3113.
28- Patel A, Kong S, Reitz R., Development and validation of reduced reaction mechanism for HCCI engine simulations. SAE Paper 2004:010558.
29- https://github.com/OpenCFD/OpenFOAM1.7.x/blob/master/tutorials/combustion/dieselFoam/aachenBomb/chemkin/chem.inp_15.
30- Saravanan N, Nagarajan G, Sanjay G, Dhanasekaran C. Combustion analysis on a DI diesel engine with hydrogen in dual fuel mode. Fuel 2008;87: 3591–99.
31- Aggarwal S, Awomolo O, Akber K. Ignition characteristics of heptane-hydrogen and heptane-methane fuel blends at elevated pressures. Int J Hydrogen Energy 2011; 36: 15392-02.
32- Yang B, Yao M, Cheng W, Li Y, Zheng Z, Li S. Experimental and numerical study on different dual-fuel combustion modes fuelled with gasoline and diesel. Applied Energy 2014;113:722–73

Table 1 Properties of hydrogen in comparison with diesel

Properties	Hydrogen	Diesel
Auto-ignition temperature (K)	858	530
Minimum ignition energy (mJ)	0.02	-
Flammability limits in air (vol. %)	4-75	-
Net heating value (MJ/kg)	119.9	42.2
Stoichiometric air/fuel (mass)	34.3	14.5
Density at ambient temperature (kg/m^3) @ 1.01 bar	0.083	824
Quenching gap in NTP air (cm)	0.064	-
Stoichiometric flame speed (m/s)	2.65-3.25	0.3

Table 2 Engine specifications and operation conditions

Engine Specifications	
No. of cylinders	1
Bore	80 mm
Stroke	110 mm
Speed	1500 rpm
Compression ratio	16.5:1
Rated output	3.7 kW
Piston type	Flat
Number of injector holes	4
Hole diameter	0.000169 m
Spray angle	160º
Operating Conditions	
Fuel amounts by volume %	4.83%
Initial temperature	333 K
Initial pressure	1 bar
Start of injection	23o BTDC
Duration of injection	30 degrees

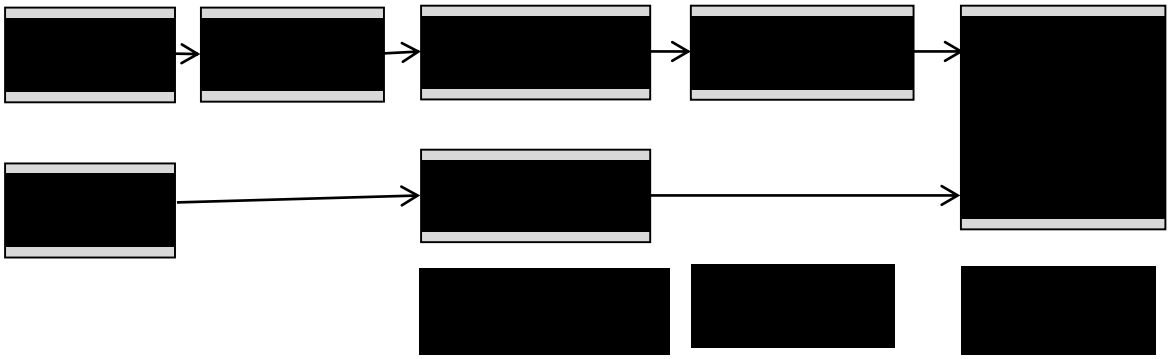

Figure 1 Skeletal chemistry mechanism for multi-fuels

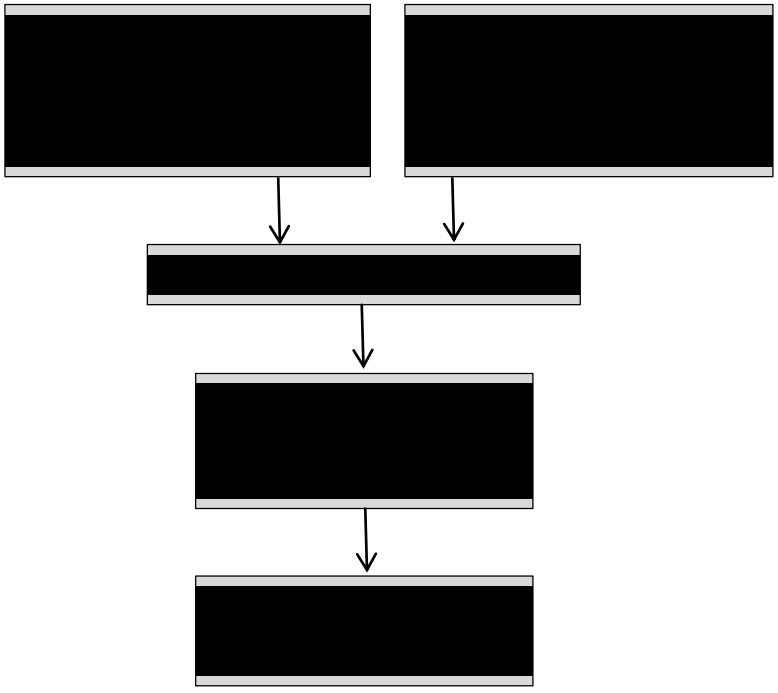

Figure 2 Detailed chemistry modeling scheme

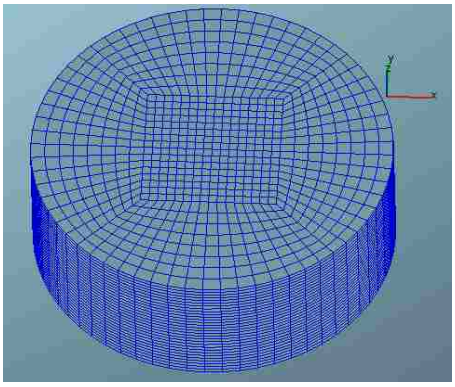

Figure 3 Computational mesh (50 sectors at TDC).

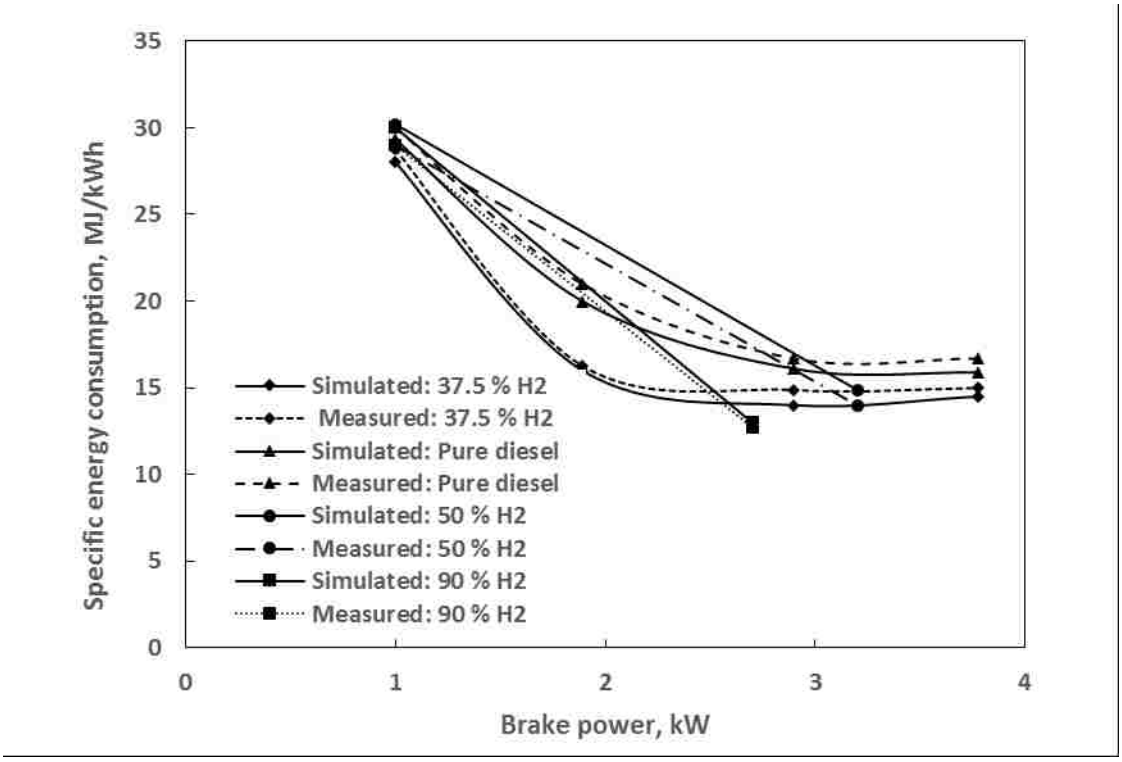

Figure 4 Variation of specific energy consumption with brake power at different levels of hydrogen

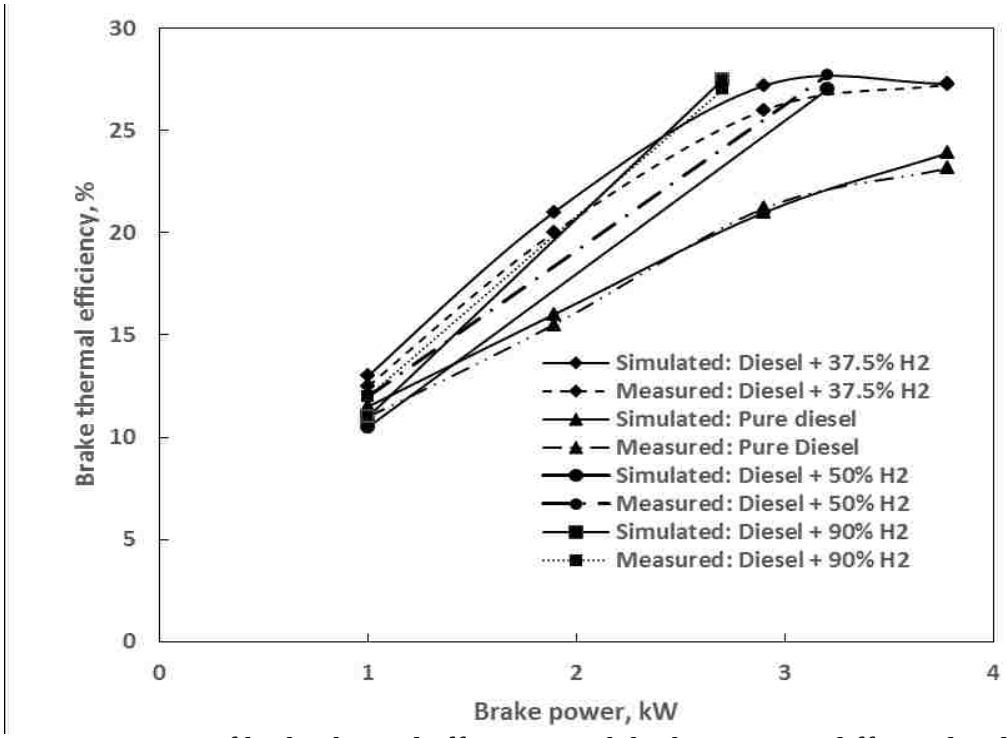

Figure 5 Variation of brake thermal efficiency with brake power at different levels of hydrogen

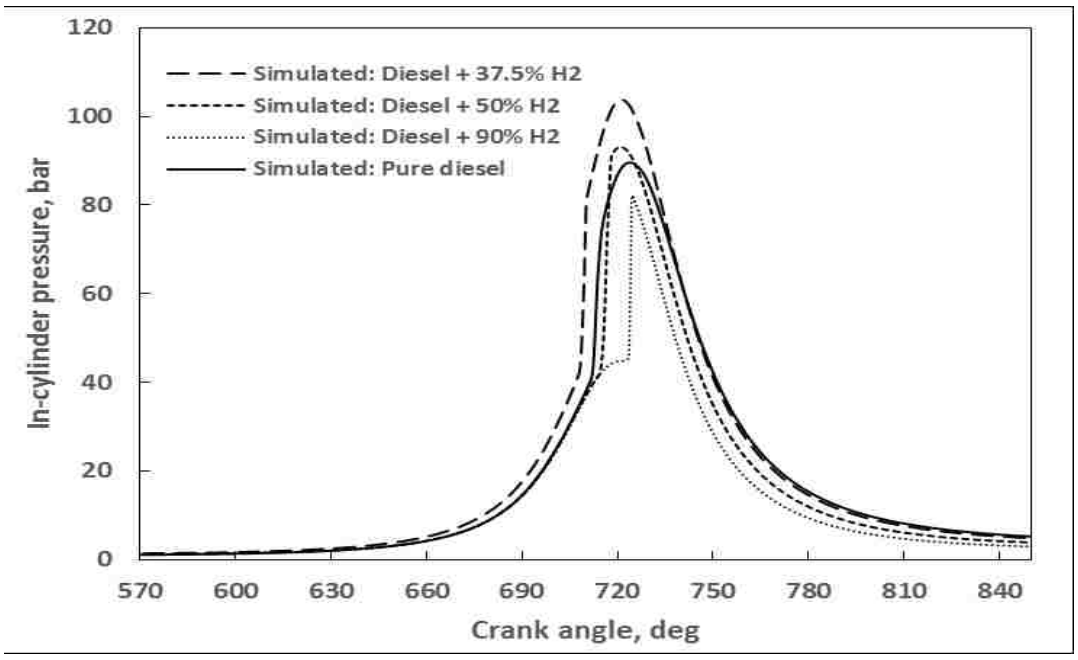

Figure 6 Variation of cylinder pressure with crank angle at different levels of hydrogen

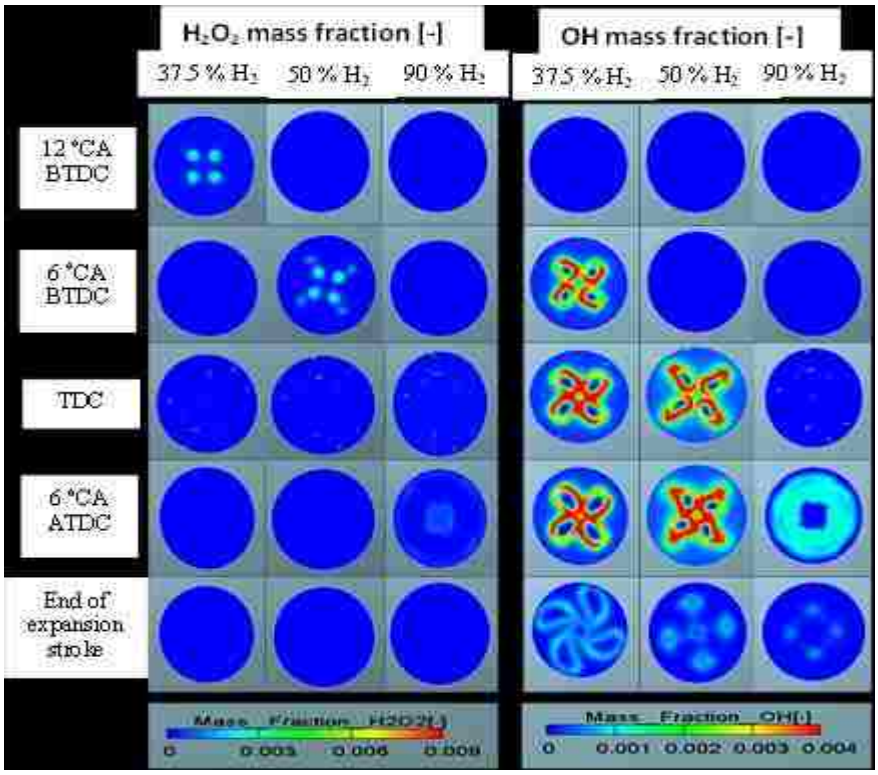

Figure 7 Variation of H_2O_2 with OH with three different levels of hydrogen

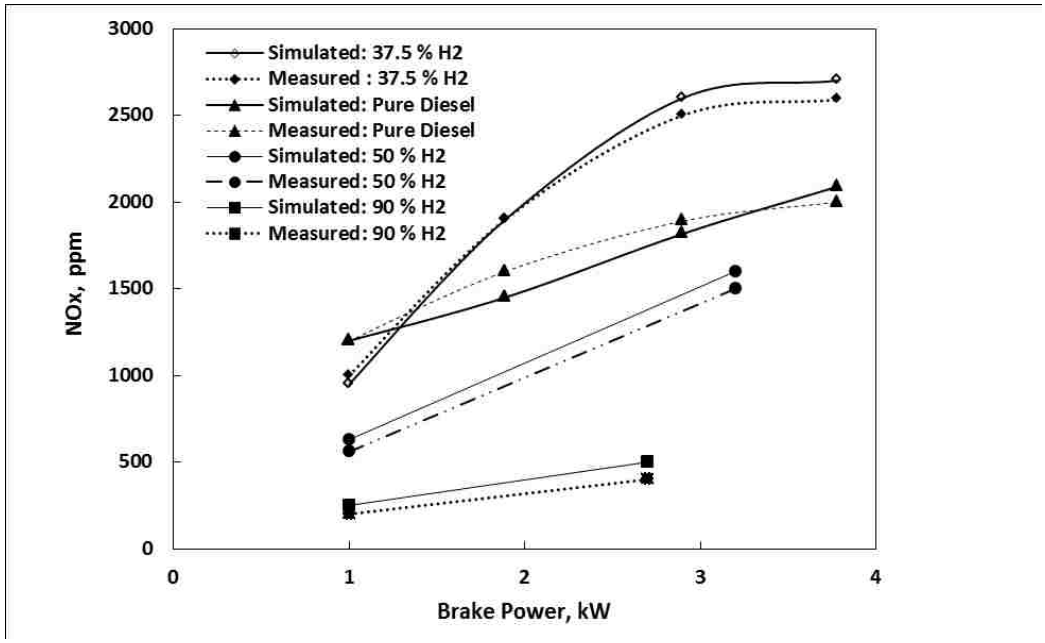

Figure 8 Variation of oxides of nitrogen with brake power at different levels of hydrogen

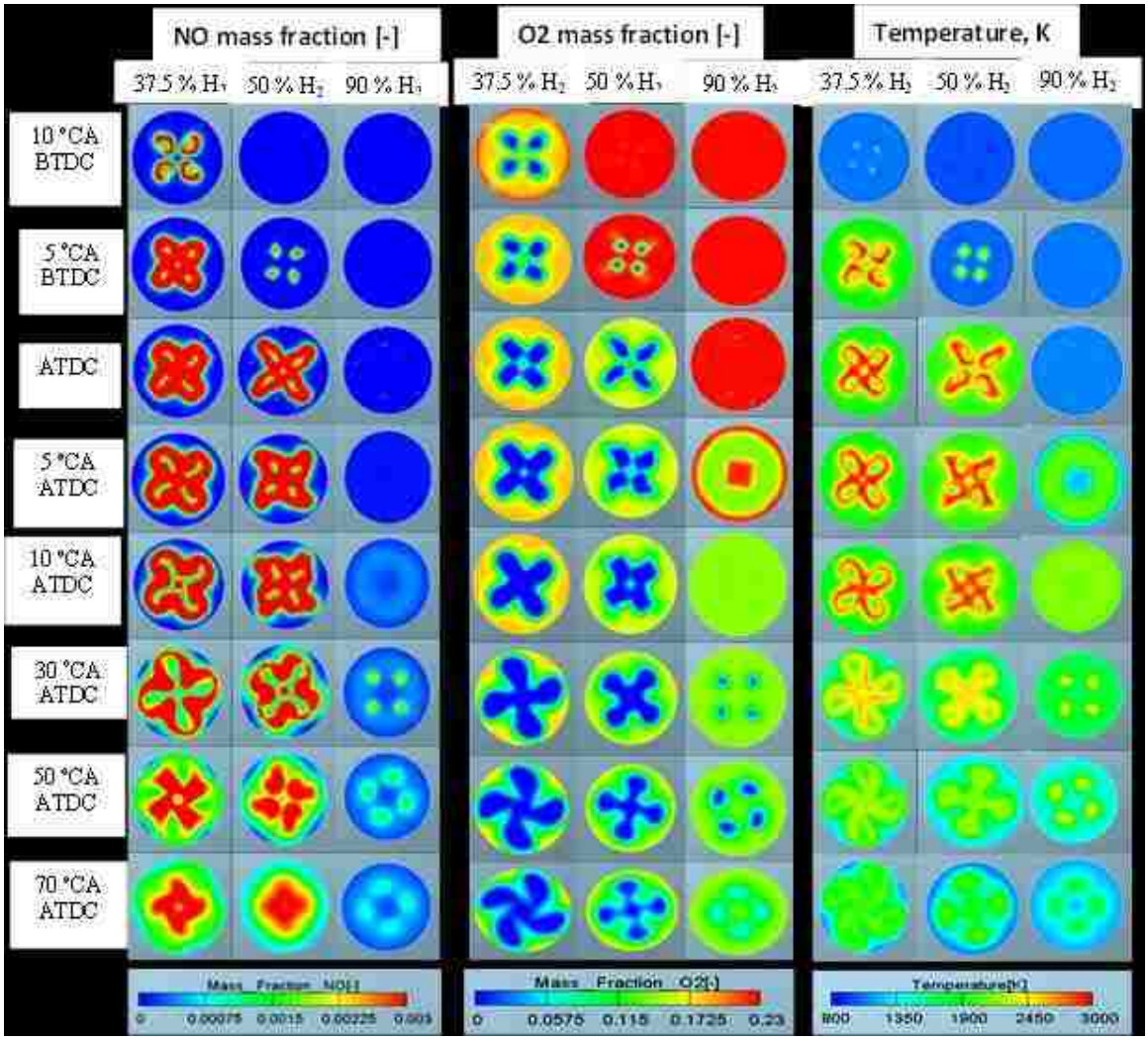

Figure 9 Variation of NO with O_2 and temperature with three different levels of hydrogen

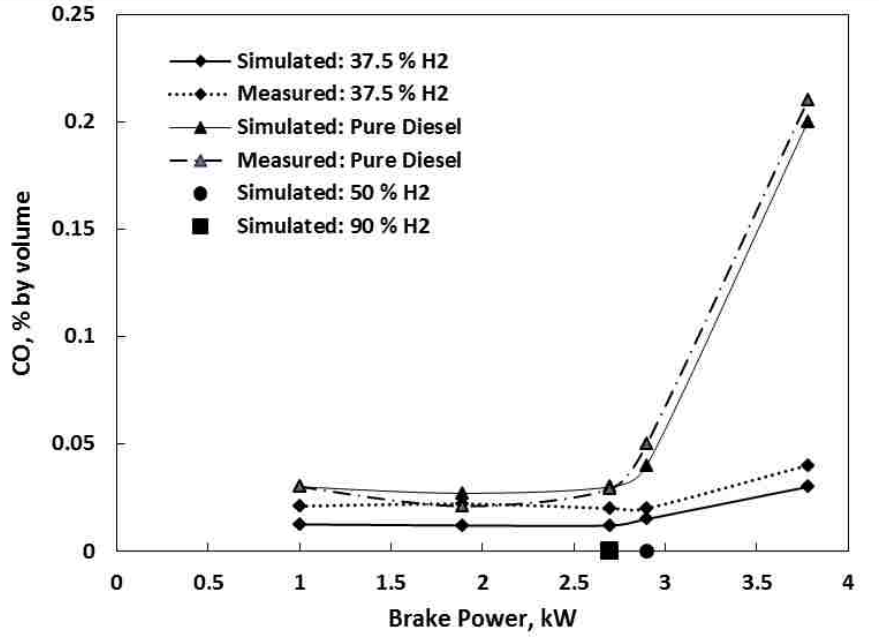

Figure 10 Variation of carbon monoxide with brake power at different levels of hydrogen

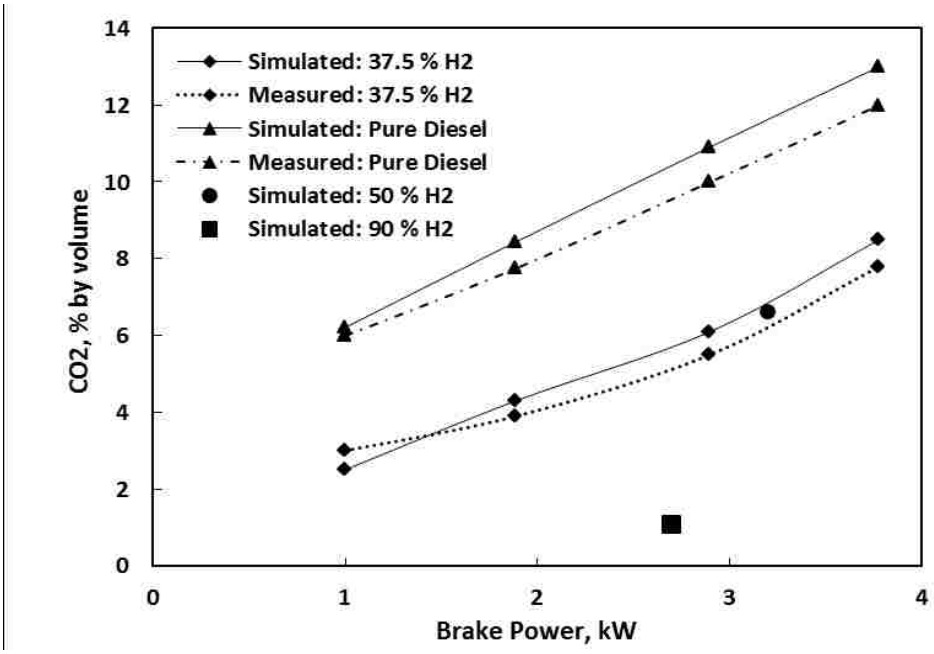

Figure 11 Variation of carbon dioxide with brake power at different levels of hydrogen

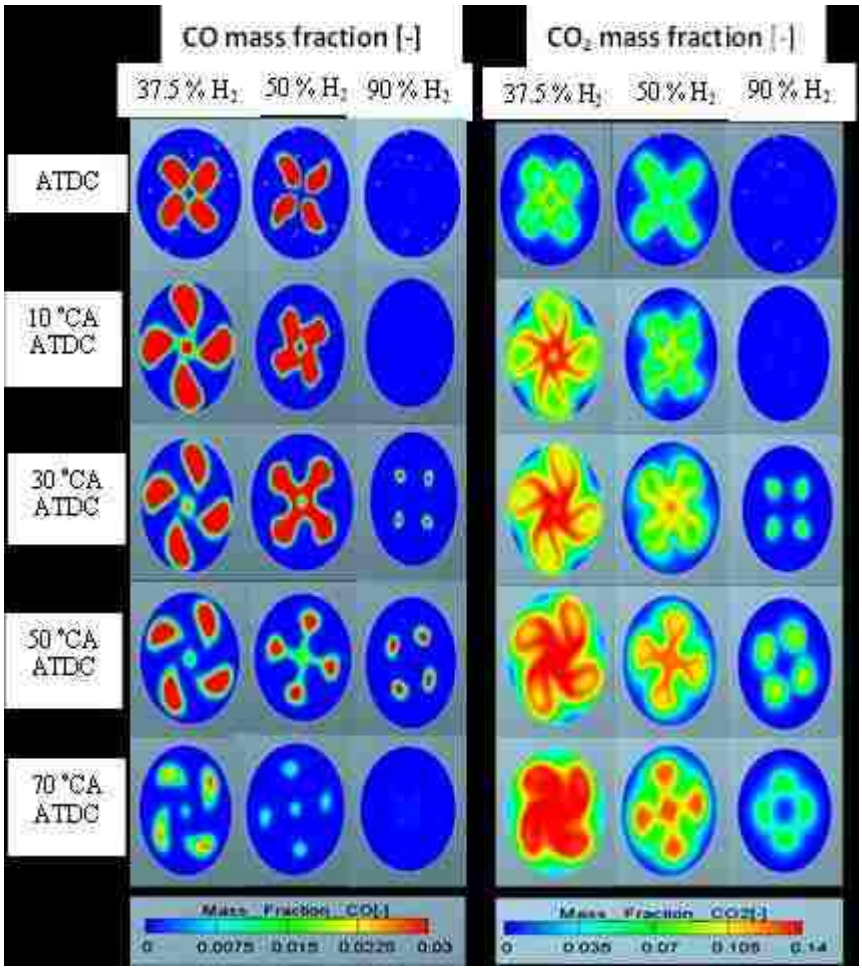

Figure 12 Variations of CO and CO_2 with three different levels of hydrogen

IV. A COMPUTATIONAL STUDY OF IN-CYLINDER NOX REDUCTION STRATEGIES FOR A COMPRESSION-IGNITION ENGINE FUELED WITH DIESEL/HYDROGEN MIXTURES

Hassan A. Khairallah
Department of Mechanical and Aerospace Engineering,
Missouri University of Science and Technology,
Rolla, MO, USA

Umit O. Koylu
Department of Mechanical and Aerospace Engineering,
Missouri University of Science and Technology,
Rolla, MO, USA

ABSTRACT

Considerable efforts have been made to introduce alternative fuels for use in conventional diesel and gasoline engines. There is significant interest in adding hydrogen to a diesel engine to reduce emissions and improve efficiency. However, the main challenge associated with the use of hydrogen in diesel engines is high nitrogen oxide (NO_X) emissions. In the present study, a reduced chemical kinetics mechanism, consisting of 52 reactions and 29 chemical species for n-heptane fuel combustion, was incorporated with detailed chemical kinetics consisting of 29 reactions for hydrogen as well as additional nitrogen oxidation. This reaction mechanism was coupled with 3-D advanced CFD software to investigate the performance and emission characteristics of a diesel-hydrogen dual-fuel engine. Computational results showed good agreements with the experimental results for brake thermal efficiency, CO_2, CO, and NO_X emissions. The model was then employed to examine the effects of exhaust gas recirculation (EGR) and N_2 dilution on NO_X emissions. The computational results quantified the reduction in NO_X emissions with EGR and N_2 dilution, and a more remarkable reduction was found with 30% N_2 dilution. However, in terms of the N_2 dilution, a general decreasing trend was observed for both NO_X and CO_2 emissions, while CO emissions increased. In relation to the EGR, the NO_X emissions decreased while CO_2 and CO emissions significantly increased. Additionally, the results showed that the indicated mean effective pressure (IMEP) and indicated power

decreased as the N_2 dilution increased. The same trend was observed for the EGR but the reduction was less compared to that of the N_2 dilution.

Introduction

During the past decade, a number of researchers have investigated the replacement of hydrocarbon fuels by hydrogen as a technique to improve the performance and emissions of internal combustion engines. Numerous studies have reported on the performance of spark-ignition (SI) engines with hydrogen-natural gas fuel [1-2] and hydrogen-gasoline fuel [3]. Several researchers have investigated the replacement of diesel fuel by hydrogen in diesel engines for reducing pollutant formations and emissions. The addition of H_2 to the intake air of diesel engines has been shown to substantially reduce the emissions of CO, HC, CO_2, and soot. However, as reported by [4], adding a relatively large amount of H2 could significantly increase the emissions of NO_X. The high NO_X emissions associated with hydrogen addition are probably due to the higher combustion temperatures inside the chamber. Saravanan et al. [5-8] have reported studies using hydrogen in the dual-fuel mode a DI diesel engine. In general, they observed that a significant improvement in thermal efficiency and a reduction in hydrocarbon (HC), CO, and CO_2 emissions could be obtained under certain operating conditions by running a diesel engine in the dual-fuel mode using hydrogen. Zhou et al. [9] experimentally investigated the performance of regulated and unregulated emissions of a diesel engine with hydrogen addition. They concluded that hydrogen addition also had the potential to reduce unregulated emissions, such as olefins (C_2H_4 and C_3H_6), BTX (C_6H_6, C_7H_8, and C_8H_{10}) and acetaldehyde (CH_3CHO). An et al. [10] also studied the performance and emission characteristics of a dual-fuel (hydrogen/diesel) engine. They found that the CO and soot emissions decreased under most engine operating conditions due to the "carbon-free" nature of hydrogen, while the NO_X emissions increased. Sandalci and Karagoz [11] conducted an experimental study on a four-stroke, single cylinder diesel engine fueled by hydrogen at different levels. Their results indicated that specific CO, CO_2, and smoke emissions decreased with increasing hydrogen levels. However, specific NO_X emissions increased with hydrogen. Singh [12]

carried out a numerical analysis to investigate the impact of H_2 addition on NO_2 emissions from an H_2-diesel dual-fuel engine using a CFD model integrated with a reduced chemistry model as well as a NO_X formation model. They showed that the addition of H2 up to 4% by volume led to an increase in NO2. Nguyen and Mikami [13] investigated the characteristics of combustion noise from a dual-fuel (hydrogen/diesel) engine and reported that the diesel engine noise with hydrogen addition was lower than that with diesel fuel alone at late diesel-fuel injection timings.

The main challenges of using hydrogen in an internal combustion (IC) engine in the dual-fuel mode with diesel fuel are high in-cylinder peak pressures and temperatures that result in greater amounts of NO_X emissions and high self-ignition temperatures [14, 15]. Currently, there are global demands to reduce NO_X emissions, which have been discharged from IC engines fueled by hydrogen. Several approaches have been applied to reduce such emissions. Exhaust gas recirculation (EGR) and N_2 dilution techniques were very useful in reducing the NO_X emission level for dual fuel engine operation with hydrogen induction. SinghYadav and Soni [16] used hydrogen in a diesel engine with 10% and 20% EGR levels. They showed that, at 80% load, the NO_X concentration for hydrogen enrichment without EGR was 470 ppm whereas it was 447 ppm with 20% EGR. Bose and Maji [17] conducted an experimental study on a single-cylinder compression-ignition engine using a hydrogen-diesel blend with exhaust gas recirculation. NO_X emissions for the hydrogen-diesel operation with 10% and 20% EGR were 760 ppm and 710 ppm, respectively, at 80% load, compared to neat diesel fuel at 810 ppm. Christodoulou and Megaritis [18, 19] studied the effect of hydrogen/nitrogen blend on the emissions and combustion of an HSDI diesel engine. They reported that a great reduction of NO_X was achieved by nitrogen dilution but this came at the expense of smoke and CO. Roy et al. [20] found a dramatic reduction in NO_X emissions with certain percentages of N_2 dilutions.

Today, computational fluid dynamics (CFD) has become an essential tool in the process of designing and developing engineering devices [21]. Advanced 3-D CFD codes have become a common means to gain a better understanding of the complex combustion processes inside engine cylinder. CFD offers successful assessment of new technologies, e.g., new fuel preparation methods, new combustion concepts, and/or alternative fuels.

With the relatively recent development of computer processors and the expansion of allowable memory, researchers and engineers are now able to integrate detailed chemical kinetics with CFD software to simulate IC engines. Many studies have investigated and reported on the integration of detailed chemical kinetics with the three-dimensional computational fluid dynamics (CFD) tools to understand the in-cylinder flow field and mixing process [26,27,28]. Few studies have focused on integrated multi-fuel mechanism with CFD code to study dual fuel combustion engine [29, 30].

In the present work, a reduced reaction mechanism consisting of 52 reaction steps with 29 chemical species for n-heptane fuel combustion was incorporated with detailed chemical kinetic reactions consisting of 29 reaction steps for hydrogen, including additional nitrogen oxidation reactions. This reaction mechanism was coupled with the AVL FIRE® CFD code to investigate in-cylinder combustion and pollutant characteristics in a dual-fuel engine. One focus of this study was to investigate the effects of EGR and N2 dilution on engine performance and emissions. An advantage of this model is the FIRE® General Gas Phase Reactions Module used to simulate a dual-fuel engine that ran on either a diesel/hydrogen mixture or diesel with other conventional fuels (methane or gasoline), contrary to what occurs in most existing engine models. Also the present computational provide a better understanding of the NOx emissions production, in association with the mean in-cylinder gas temperature and oxygen availability at the same instants of time.

Computational Methods

AVL FIRE® presents a general species transport model to allow the implementation of a detailed kinetic model [22] and solves species transport equations for any arbitrary number of chemical species. The species mass conservation equation is expressed as

$$\frac{\partial(\rho w_i)}{\partial t} + \frac{\partial}{\partial x_k}(\rho(U_k - U_{\delta k})w_i) = \frac{\partial}{\partial x_k}\left(\left(\rho D_i + \frac{\mu}{\sigma_{ci}}\right)\frac{\partial}{\partial x_k}\right) + S_{w_i} \quad (1)$$

$$S_{w_i} = r_i$$

here w_i is the mass fraction, S_{w_i} is the source term of species i by taking into account homogeneous chemical reactions, σ_{ci} is the stress tenser, and μ is the viscosity. The thermophysical properties (i.e., viscosity, density, specific heat, diffusion coefficient, thermal conductivity) shown in the equation above were calculated for each species and for gas mixtures by using the chemical kinetic databases (CHEMKIN™). The chemistry effect (level of elementary reactions) was taken into account such that at the beginning of each CFD time step (Δt), a single zone reactor model was calculated for each computational cell. At the last CFD time step for the properties (pressure, volume, temperature), the following conservation equations were integrated by the model for the time step, considering the volume cell as a function of time. The species conservation equation was computed using

$$\rho \frac{\partial w_i}{\partial t} = M_i \omega_i \tag{2}$$

here, M_i is the molecular weight of ith species, and ω_i is the molar production rate of species. The source term, S_{w_i}, was taken into account due to the homogeneity assumption. The energy conservation equation was expressed as

$$\rho c_v \frac{\partial T}{\partial t} + \frac{P}{V}\frac{\partial V}{\partial t} = -\sum_{i=1}^{N_y} u_i M_i \omega_i \tag{3}$$

On the left-hand side, the first term represents the temporal change of the energy content, and the second term represents the volume work. The terms on the right-hand side represent the consideration of the change of internal energy due to production and consumption of chemical species. By using an interface to the CHEMKIN™ libraries, the molar species production rate, ω_i, can be calculated, and the source terms can be calculated by neglecting any effect of turbulence/mixing on the chemical reaction, as follows:

$$r_i = \frac{\rho^{n+1} w_i^{n+1} - \rho^n w_i^n}{\Delta t} \tag{4}$$

where the superscripts n and n+1 indicate the first and the last values of the single-zone reactor model. Keeping the source terms constant for the following CFD time step was the most important advantage of this approach because it made the CFD simulation 100% conservative, fast, and valid. This approach considered the effects of both mixing and chemical kinetics by assuming that the reaction rate was determined via a kinetic time scale τ_{kin} (an equilibrium assumption under perfect mixed conditions) and turbulent time scale τ_{turb} (an eddy break-up assumption). Furthermore, it was assumed that the equilibrium concentration of the fuel wass zero and the kinetic time scale was equal to the scale used for the fuel for all species. The time scale of CO was used as a rate-limiting kinetic time step if the fuel concentration approached zero. By taking these assumptions into account, the above equation becomes

$$\mathrm{r_i} = \frac{\tau_{\mathrm{kin}}}{\tau_{\mathrm{kin}} + \mathrm{f}\tau_{\mathrm{turb}}} \frac{\rho^{\mathrm{n+1}}\mathrm{w_i^{n+1}} - \rho^{\mathrm{n}}\mathrm{w_i^{n}}}{\Delta \mathrm{t}} \tag{5}$$

$$\tau_{kin,i} = \Delta t \frac{\rho^{n+1} w_i^{n+1}}{\rho^{n+1} w_i^{n+1} - \rho^{n} w_i^{n}} \tag{6}$$

$$\tau_{kin} = \max\left(\tau_{kin,f}, \tau_{kin,CO}\right) \tag{7}$$

The turbulent time scale, τ_{turb}, was calculated using:

$$\tau_{\mathrm{turb}} = \mathrm{C_t}\frac{\mathrm{k}}{\varepsilon} \tag{8}$$

The variable f is a delay coefficient that is used to simulate the influence of turbulence on combustion after ignition has occurred [23], and can be calculated as:

$$f = \frac{1 - e^{-r}}{0.632} \tag{9}$$

$$r = \frac{w_{CO_2} - w_{H_2O} - w_{CO} - w_{H_2}}{1 - w_{N_2}} \quad (10)$$

A reduced (52 reactions and 29 species) chemical reaction mechanism for n-heptane was constructed from a comprehensive detailed mechanism (179 species and 1642 reactions) [24]. This study uses n-heptane because its cetane number (CN~56) is rather close to that of typical diesel fuels (CN~50). This reduced reaction mechanism for n-heptane fuel combustion was incorporated with detailed chemical kinetic reactions consisting of 29 reaction steps for hydrogen, which includes additional nitrogen oxidation reactions [24]. The multi-chemical reaction mechanism (89 reactions and 32 species) was coupled with a 3-D CFD model based on AVL FIRE® software. The CHEMKIN™ chemistry solver was integrated into the AVL FIRE® code for solving the chemistry during the multidimensional engine simulation. The piston geometry and computational grid used for the simulations are shown in Figure 1. The mesh was composed of about 7680 computational cells with mesh dimensions of 3.33 × 3.33 × 3.56 mm.

Results and Discussion

In the present work, a multi-chemical reaction mechanism was implemented using a comprehensive 3-D CFD to investigate the combustion and emission characteristics of a direct ignition (DI) diesel engine with gaseous hydrogen as a fuel and with diesel as the source of ignition. The hydrogen was substituted for diesel fuel on an energy basis of 37.5%. By using the experimental data, the model was run at the same engine conditions at various brake power. The operating conditions of the diesel engine modeled and simulated in this investigation were similar to the independent experimental study by Saravanan et al. [8] because their reported test conditions and experimental data were well documented. The specifications of the compression-ignition (CI) engine in this computational study are given in Table 1.

Model Validation

The brake thermal efficiency can be defined as the ratio of the engine brake power to the input fuel energy. The variation of the brake thermal efficiency with the brake power

is shown in Figure 2 for a diesel/hydrogen mixture. The brake thermal efficiency increased with the brake power for the conditions considered. Specifically, the brake thermal efficiency reached 27.3% at the highest brake power of about 4 kW. The present simulations for the diesel/hydrogen mixture captured this trend and agreed well with the experiments reported under the same operating conditions.

Figure 3 shows the predicted and measured NO_X emissions as a function of brake power. It was observed that the NO_X emissions increased with the additional brake power for the conditions considered. The NO_X emissions reached 2700 ppm at the highest brake power of about 4 kW. In general, the amount of NO_X formed in the hydrogen/diesel mixture operation was greater than what was formed in the case of pure diesel [6]. The higher concentration of NO_X in the hydrogen/diesel mixture was mainly the result of the higher combustion temperatures compared to those in the pure diesel operation. Moreover, the long residence time of the high temperature gases in the cylinder led to the production of greater NO_X emissions. The model-predicted trends were very similar to the experimental results.

The emissions of carbon monoxide and carbon dioxide were generally reduced in the hydrogen-diesel mixture operation compared to what would occur in a conventional diesel operation [6, 17]. This was due to the addition of hydrogen, which led to a reduction in the amount of diesel (carbon-based fuel injected). Figure 4 shows the variation of carbon monoxide with brake power. It was observed that carbon monoxide emissions were almost constant below a brake power of approximately 2.9 kW. When the brake power increased beyond this value, the CO emissions increased and reached a peak value of around 0.05% by volume at the highest brake power of about 3.7 kW.

Figure 5 illustrates the variation of carbon dioxide with brake power. Carbon dioxide increased with the brake power for the conditions considered. In particular, CO_2 reached 8.5% by volume at the highest brake power. The emissions of carbon monoxide and carbon dioxide were generally reduced in the hydrogen-diesel mixture operation compared to a conventional diesel operation [6, 17]. This was due to the addition of hydrogen, which led to a reduction in the amount of diesel (carbon-based fuel injected).

Effect of EGR and N2 Dilution on Engine Performance and Emissions

After its development and validation, the computational model could be employed to investigate various aspects of hydrogen-diesel dual-fuel engines. One possibility is to use the model to study the effect of injection time and different compression ratios on engine performance and emissions. Another possibility is to computationally study the effect of EGR levels and N_2 dilution on NO_X emissions. In the present study, different levels of EGR and N_2 dilution were applied. Hydrogen-enriched air was used as the intake charge in a diesel engine with 10%, 20%, and 30% EGR or N_2 dilution, the hydrogen percentage was set at 4.83% by volume. The engine was operated at full load.

Indicated Thermal Efficiency, Indicated Power, and IMEP .Engine performance parameters were obtained using the measured cylinder pressure and engine geometry at a constant engine speed. Indicated work (W_i), indicated mean effect pressure (IMEP), indicated power (IP), and indicated thermal efficiency (ITE) were calculated using the measured cylinder pressure versus engine crank angle at different operating conditions, as shown in the following equations:

$$W_i\ (kj) = \int_{IVC}^{EVO} pdV \tag{11}$$

$$IMEP\ (kPa) = \frac{1}{V_d} \int_{IVC}^{EVO} pdV \tag{12}$$

$$P_i\ (kW) = \frac{W_i\ .N}{2\ \times 60} \tag{13}$$

here, N is the engine speed (rpm), $\bar{S}_p$ is the mean piston speed (m/s), and V_d is the displacement volume (m3). The indicated thermal efficiency was calculated as the ratio of the power output from the engine to the combined energy input from both diesel fuel and hydrogen, as follows:

$$\eta_{ITE} = \frac{P_i}{\left(\dot{m}_{f,diesel} \times CV_{diesel}\right) + \left(\dot{m}_{f,H2} \times CV_{H2}\right)} \quad (14)$$

As the EGR level increased, the indicated thermal efficiency and indicated power decreased. The same trend was observed with the N_2 dilution, but the reduction was more than occurred with EGR (Table 2). The reductions in the indicated thermal efficiency and indicated power with dilution (i.e., EGR or N_2) were due to deficiency in the oxygen concentration, which had a significant negative effect on combustion; this, in turn, led to a decrease in the peak pressure and temperature, resulting in the degradation of the work done per cycle. Moreover, the retarded ignition with the N_2 dilution (compared to the EGR cases) led to more reduction in the indicated thermal efficiency and the indicated power.

Ignition Delay

Ignition delay is defined as the period between the start of the diesel injection and the inflammation of the air-fuel mixture. Figure 6 shows that the ignition delay without dilution was about 13o after injection time (AIT), whereas it was about 18.4o AIT with 30% EGR, and 25o AIT with a 30% N2 dilution. The reduction in the oxygen availability (a dilution effect) increased the specific heat capacity of the in-cylinder mixture (a thermal effect). This led to an increase in ignition delay and a reduction in combustion temperature. However, the ignition delay with the EGR was shorter than that with the N2 dilution; this might be due to the fact that oxygen reduction is the dominant factor in ignition delay rather than in specific heat capacity [25].

In-cylinder Pressure

Figures 7 and 8 display the variations of in-cylinder pressure as a function of crank angle at full load for various EGR levels and N_2 dilutions, respectively. In general, the peak pressure decreased as the EGR increased. The same trend was observed with N_2 dilution [17, 18], but the reduction was more than that occurred with EGR. At full load, the lowest peak pressure of 90 bar was observed with 30% EGR, compared to the peak pressure of

98.5, 103, and 103.6 bar with 20%, 10% and without EGR, respectively (Figure 7). The lowest peak pressure of 87 bar was observed with 30% N_2, compared to the peak pressure of 95.7, 102.3, and 103.6 bar with 20% and 10% and without N_2, respectively (Figure 8). This reduction in peak pressure was due to the substitution of air by the exhaust gas that led to increases in the amount of the combustion-accompanying gases, which in turn increased the heat capacity and lowered the in-cylinder pressure and combustion temperature. Moreover, the burning velocity decreases when an in-cylinder mixture is diluted with exhaust gases, and this also leads to a decrease in peak pressure. Due to the increase in the ignition delay with N_2 dilution, the peak cylinder pressures for N_2 dilution occurred after the EGR.

NOX Emissions

NO is formed mainly as a result of the following reactions:

$$N2O + O = N2 + O2 \qquad (R1)$$

$$N_2O + O = NO + NO \qquad (R2)$$

$$N_2O + H = N_2 + OH \qquad (R3)$$

$$N_2O + OH = N_2 + HO_2 \qquad (R4)$$

$$N_2O + M = N_2 + O + M \qquad (R5)$$

The other path to NOX formation can be described by reactions R6, R7, and R8, usually known as the extended Zel’dovich mechanism [31]:

$$N_2 + O = N + NO \qquad (R6)$$

$$N + O_2 = NO + O \qquad (R7)$$

$$N + OH = NO + H \qquad (R8)$$

Normally, these three reactions are only important at high temperatures because radicals O and OH are created at high temperatures.

Figure 9 displays the variations of NO as a function of crank angle at full load for various EGR levels. At full load without EGR, the NO concentration was 2700 ppm (Figure 2) compared to 1600, 1000, and 900 ppm with 10%, 20% and 30% EGR, respectively. The NO emission decreased with an increase in the EGR level. This is due to the presence of inert gas in the engine cylinder that replaces the oxygen in the combustion chamber, which reduces the peak combustion temperature. As a result of a reduction in both parameters, NO reduced drastically with EGR.

Figure 10 displays variations of NO with N_2 dilution levels. The same trend was observed with N_2 dilution, where NO formation decreased with an increase in the N_2 dilution, but the reduction was comparatively greater with EGR. At full load without N2 dilution, the NO was 2700 ppm (Figure 3) compared to 1500, 900, and 800 ppm with 10%, 20%, and 30% EGR, respectively. There are two reasons for this reduction in NO: Nitrogen dilution replaces the oxygen in the combustion chamber, and there is a retarded ignition time with N_2 dilution compared to EGR. Hence, there is more reduction in the in-cylinder temperature with N2 dilution that leads to a greater reduction in NO. These results were in confirmation with observations reported recently [16-19].

Figure 11 shows the development process of NO mass fraction, in association with the mean in-cylinder gas temperature and oxygen availability at the same instants of time for hydrogen-diesel operation without dilution and with dilution by 30 % EGR and 30 % N_2. It was easy to see that the in-cylinder temperature and oxygen mass fraction gradually decreased with dilution operations, and hence NO emissions reduced. As shown in figure the formation time of NO delayed with the dilution operations (i.e. EGR and N_2), compared to that at without dilution. This is may be due to the increase in the ignition delay with dilution operation as shown above (Fig. 5). The peak NO value was attained just near the top dead center (TDC) in the post-flame region because the temperature and oxygen concentration were very high in that region. As observed, the NO formation rate inside the cylinder varied with the crank angle that was dependent on the temperature history of each crank angle. The temperature and oxygen mass fraction gradually decreased as the crank angle increased during the expansion stroke; hence the rate of NO decomposition rapidly decreased. This is because the rates of R6, R7, and R8 (Zel'dovich mechanism) became

small, due to the reduction in O and OH radicals. With N_2 dilution, NO value became very small due to combustion retardation, which, in turn, led to reductions in the peak pressure and temperature.

CO and CO2 Emissions

Figures 12 and 13 display the variations of carbon monoxide as a function of crank angle at full load for various EGR levels and N_2 dilutions, respectively. In general, CO concentration increased with the EGR level. At full load, the CO emission was 0.05% by volume without EGR, while it was 0.4%, 0.6%, and 0.73% by volume with 10%, 20%, and 30% EGR, respectively (Figure 12). The increase in CO concentration was due to the deficiency in oxygen concentration and the increased inert gas inside the cylinder with a rise in the EGR. As a result, lower oxygen concentrations led to a less complete combustion, increasing CO emission.

CO emission also rose as the N_2 dilution level increased, as illustrated in Figure 13, but the increase was greater than that of the EGR cases. This is due to the deficiency in oxygen concentration and the retarded ignition with the N_2 dilution compared to the EGR cases. These results were in confirmation with observations reported by [18].

Figures 14 and 15 display the variations of carbon dioxide as a function of crank angle at full load for various EGR levels and N2 dilutions, respectively. Figure 13 quantifies the increase in CO_2 level with a rise in the EGR level. At full load, the CO_2 emission was 9% by volume without EGR while it was 9.3%, 10.2%, and 11% by volume with 10%, 20%, and 30% EGR, respectively (Figure 37). The reason for this increase in CO_2 was the presence of CO_2 in the exhaust gas [16, 17].

Carbon dioxide emissions decreased with increasing level of N_2 dilution. At full load, the CO_2 emission was 9% by volume without the N_2 dilution, while it was 8.4%, 7.5%, and 7% by volume with 10%, 20%, and 30% N_2 dilution, respectively (Figure 15).

Figure 16 illustrates iso-counters of CO and CO_2 for a hydrogen-diesel mixture with 30% EGR and 30% N_2. These images quantified the evolution of the formed CO and CO_2 along with temperature. It was observed that CO mainly formed around the center of the cylinder due to combustion of the pilot fuel and oxidation of the pre-mixture. After that,

the CO formation region extended into the cylinder and reached its peak value at around 12 BTDC with no dilution, 15 BTDC with 30% EGR, and 17 BTDC, with 30% N_2. With the increase in the crank angle during the expansion stroke, the in-cylinder temperature started to decline; then, most of the CO that had formed began to dissipate due to the conversion of CO to CO_2. This was due to the key reaction pathway for CO oxidation, CO + OH = CO_2 + H, which was activated by the increased combustion temperature. Thus, for no dilution at the end of the expansion stroke, the temperature was higher compared to the EGR and N_2 operations, which led to a reduction in CO. Additionally, it could be seen that CO_2 for the EGR operation covered the entire cylinder at 10 ATDC compared to what occurred for no dilution and N_2 dilution; this was due to the presence of CO_2 in the fresh mixture, which explained the higher CO_2 with EGR. The significant decrease in CO_2 with 30% N_2, this is due to the combined effect of lower pressure and temperature inside the cylinder, which lead to the lower conversion ratio of the CO to CO_2 and the shift in the reaction CO + OH = CO_2 + H toward the reverse direction.

Conclusions

To investigate performance, in-cylinder combustion, and pollutant characteristics of a hydrogen-fueled diesel engine with EGR and N_2 dilution, a three-dimensional numerical simulation was employed with detailed chemical kinetics. The following conclusions can be drawn from the present research:

- Computational results showed good agreements with the experimental results for brake thermal efficiency, NOX emissions, CO emissions, and CO_2 emissions.
- The present model successfully showed the capability of describing a hydrogen-fueled diesel engine with EGR or N_2 dilution operations.
- In terms of N2 dilution, the simulation results demonstrated that NOX and CO_2 emissions decreased, while CO emissions increased.
- In relation to the EGR level, the NO_X emissions decreased while the CO_2 and CO emissions significantly increased.
- N_2 dilution was more efficient in reducing NO_X emissions than the EGR method because of relatively low in-cylinder temperatures.

References

1. Lata, D.B., Misra, A., Medhekar, S., "Effect of hydrogen and LPG addition on the efficiency and emissions of a dual fuel diesel engine," International Journal of Hydrogen Energy 37: 6084-6096 (2012).
2. Kahraman, N., Ceper, B.A., Akansu, S. O., Aydin, K., "Investigation of combustion characteristics and emissions in a spark-ignition engine fuelled with natural gas–hydrogen blends," International Journal of Hydrogen Energy 34: 1026-1034 (2009).
3. Wei, F., Bin, H., Kittelson, D.B., Northrop, W.F., "Dual-fuel diesel engine combustion with hydrogen, gasoline, and ethanol as fumigants: effect of diesel injection timing," Journal of Engineering for Gas Turbines and Power, 136/081502 (2014).
4. McWilliam, L., Megaritis, T., Zhao, H., "Experimental Investigation of the Effects of Combined Hydrogen and Diesel Combustion on the Emissions of a HSDI Diesel Engine," SAE Technical Paper 2008-01-1787.
5. Saravanan, N., Nagarajan, G., "Performance and emission study in manifold hydrogen injection with diesel as an ignition source for different start of injection," Renewable Energy 34: 328-334 (2009).
6. Saravanan, N., Nagarajan, G., Narayanasamy, S., "An experimental investigation on DI diesel engine with hydrogen fuel," Renewable Energy 33: 415-421 (2008).
7. Saravanan, N., Nagarajan, G., "An experimental investigation of hydrogen-enriched air induction in a diesel engine system," International Journal Hydrogen Energy 33: 1769-1775 (2008).
8. Saravanan, N., Nagarajan, G., Sanjay, G., Dhanasekaran, C., "Combustion analysis on a DI diesel engine with hydrogen in dual fuel mode," Fuel 87: 3591–3599 (2008).
9. Zhou, J.H., Cheung, C.S., Leung, C.W., "Combustion, performance, regulated and unregulated emissions of a diesel engine with hydrogen addition," Applied Energy 126: 1–12 (2014).
10. An, H., Yang, W.M., Maghbouli, A., Li, J., Chou, S.K., Chua, K.J., "A numerical study on a hydrogen assisted diesel engine," International Journal Hydrogen Energy 38: 2919-2928 (2013).
11. Sandalcı, T., Karagoz, Y., "Experimental investigation of the combustion characteristics, emissions and performance of hydrogen port fuel injection in a diesel engine," International Journal Hydrogen Energy 39: 18480-18489 (2014).
12. Singh S., "Numerical investigation of NO_2 formation mechanism in H_2-diesel dual-fuel engine," SAE Paper 2012-01-0655.
13. Nguyen, T.A., Mikami, M., "Effect of hydrogen addition to intake air on combustion noise from a diesel engine," International Journal Hydrogen Energy 38: 4153-4162 (2013).
14. Naber, J.D., Szwaja, S., "Statistical approach to characterize combustion knock in the hydrogen fuelled SI engine," Journal of Kones - Powertrain Transport 14: 443-50 (2007).
15. Welch, A.B., Wallace, J.S., "Performance characteristic of a hydrogen-fueled diesel engine with ignition assist," SAE Paper No. 902070.

16. Singh Yadav, V., Soni, S.L., "Performance and emission studies of direct injection C.I. engine in duel fuel mode (hydrogen-diesel) with EGR," International Journal Hydrogen Energy 37 3807-3817 (2012).
17. Bose, P.K., Maji, D., "An experimental investigation on engine performance and emissions of a single cylinder diesel engine using hydrogen as inducted fuel and diesel as injected fuel with exhaust gas recirculation," International Journal Hydrogen Energy 34: 4847-4854 (2009).
18. Christodoulou, F., Megaritis, A., "Experimental investigation of the effects of separate hydrogen and nitrogen addition on the emissions and combustion of a diesel engine," International Journal Hydrogen Energy 38: 10126-10140 (2013).
19. Christodoulou, F., Megaritis, A., "Experimental investigation of the effects of simultaneous hydrogen and nitrogen addition on the emissions and combustion of a diesel engine," International Journal Hydrogen Energy 39: 2692-2702 (2014).
20. Roy, M.M., Eiji, T., Kawahara, N., Harada, Y., Sakane, A., "An experimental investigation on engine performance and emissions of a supercharged H2-diesel dual-fuel engine," International Journal Hydrogen Energy 35: 844-853 (2010).
21. Verhelst, S., Wallner, T., "Hydrogen-fueled internal combustion engines," Progress in Energy and Combustion Science 35: 490-527 (2009).
22. Priesching, P., Wanker, R., Cartellieri, P., Tatschl, R., "Detailed and reduced chemistry CFD modeling of premixed charge compression ignition engine combustion," International Multidimensional Engine Modeling User's Group Meeting (2003).
23. Kong, S.C., Marriott, C.D., Reitz, R.D., Christensen, M., "Modeling and experiments of HCCI engine combustion using detailed chemical kinetics with multidimensional CFD," SAE Paper 2001-01-1026.
24. Patel, A., Kong, S.C., Reitz. R.D., "Development and validation of reduced reaction mechanism for HCCI engine simulations," SAE Paper 2004-01-0558.
25. Tie Li, Hiroyuki Izumi, Toshio Shudo, Hideyuki Ogawa, Yukihiro Okabe, "Characterization of low temperature diesel combustion with various dilution gases," SAE Paper 2007-01-0126.
26. Vincent, K., Adlène, B., Stéphane, J., and Olivier, C., "Modelling of combustion and nitrogen oxide formation in hydrogen-fuelled internal combustion engines within a 3D CFD Code," International Journal Hydrogen Energy. 33 :5083-5097(2008)
27. Pitsch, H., Barths, H., and Peters, N., "Three-dimensional modeling of NOx and soot formation in DI-Diesel engines using detailed chemistry Based on the interactive flamelet approach," SAE Paper 1996 -96-2057,.
28. Xiao, F., and Karim, G.A. "An Investigation of the combustion in an IDI diesel engine with low concentrations of added hydrogen," SAE Paper 2011-01-0676,.
29. Jessica L. Brakora, Ra Youngchul and ReitzmR.D., "Development and validation of a reduced reaction mechanism for biodiesel-Fueled engine simulations," SAE Paper 2008 01-1378.
30. An, H., Yang, W.M., Maghbouli, A., Li, J., Chou, S.K., Chua, K.J., Chua, J.X. Wang , L. Li "Numerical investigation on the combustion and emission characteristics of a hydrogen assisted biodiesel combustion in a diesel engine" Fuel 120-186–194 (2014)

31. Lavoie GA, Heywood JB, Keck JC. Experimental and theoretical study of nitric oxide formation in internal combustion engines. Combustion Science Technology 1970;1(4)313- 26.
32. Gregory K. Lilik , Hedan Zhang , Jose´ Martin Herreros, Daniel C. Haworth, Andre´ L. Boehman “Hydrogen assisted diesel combustion” International Journal Hydrogen Energy 35: 4382-4398 (2010).

Table 1 Engine specifications and operating conditions

Engine Specifications	
No. of cylinders	1
Bore	80 mm
Stroke	110 mm
Speed	1500 rpm
Compression ratio	16.5:1
Rated output	3.7 kW
Piston type	Flat
Number of injector holes	4
Hole diameter	0.000169 m
Spray angle	160o
Operating Conditions	
Fuel amounts by volume %	4.83%
Initial temperature	333 K
Initial pressure	1 bar
Start of injection	23o BTDC
Duration of injection	30 degrees

Table 2 Various engine performance parameters

Case	Indicated power (kW)	Indicated thermal eff. (%)	IMEP (kPa)
No dilution	7.20	0.57	1129
10% EGR	6.98	0.51	1010
20% EGR	6.51	0.47	942
30% EGR	6.03	0.44	872
10% N2	6.99	0.51	1011
20% N2	6.43	0.47	931
30% N2	5.89	0.43	853

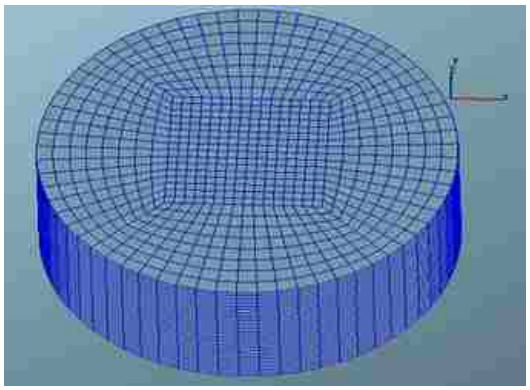

Figure 1 Computational mesh (50 sectors at TDC)

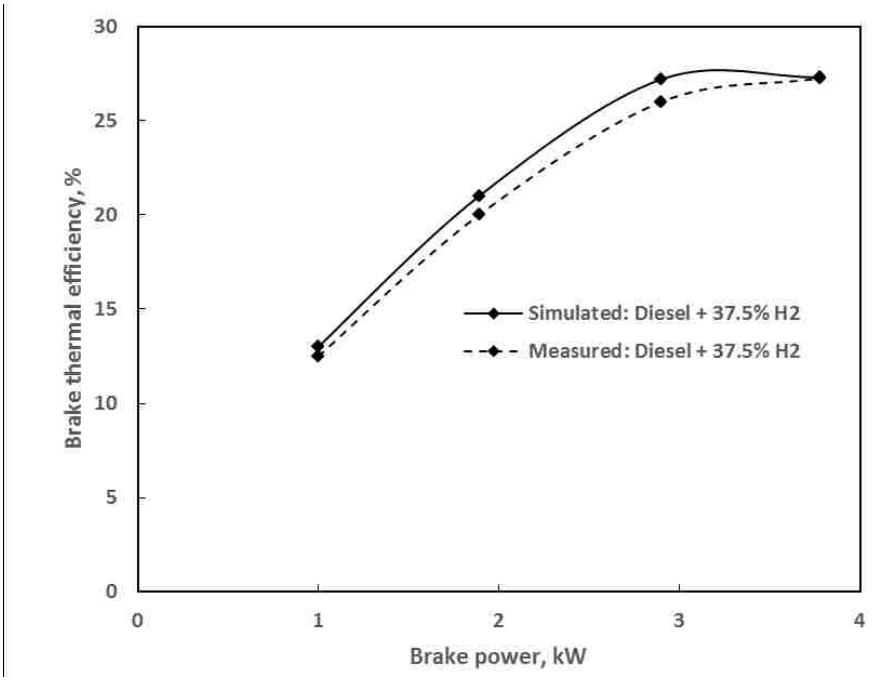

Figure 2 Variation of brake thermal efficiency with brake power

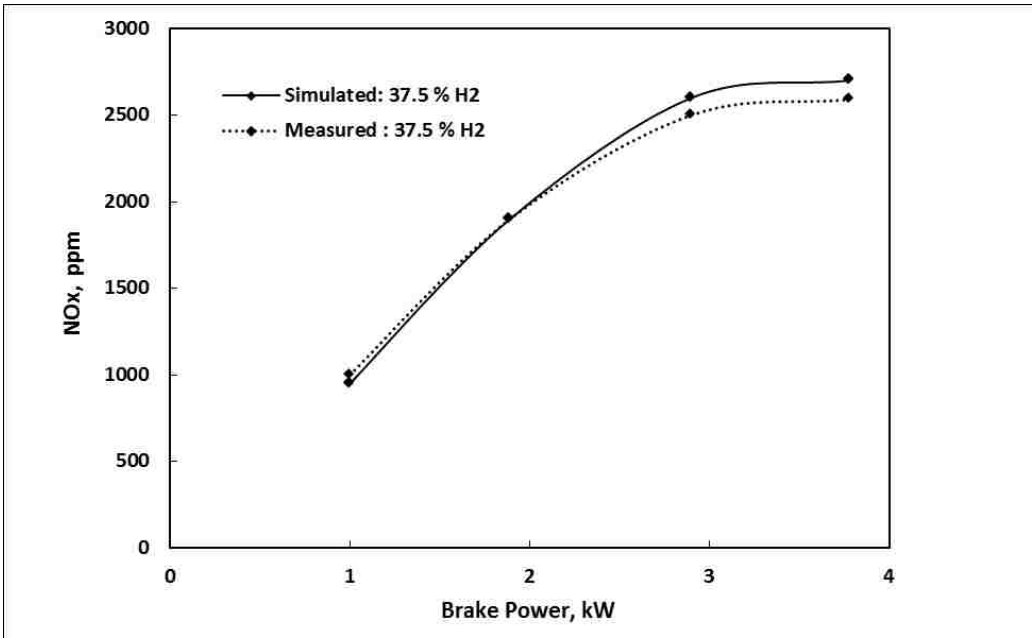

Figure 3 Variation of oxides of nitrogen with brake power

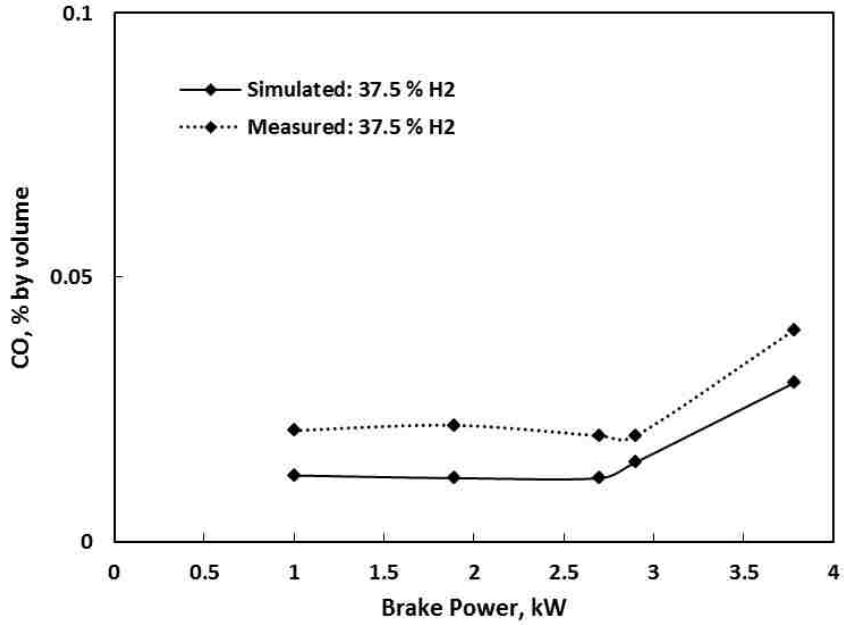

Figure 4 Variation of carbon monoxide with brake power

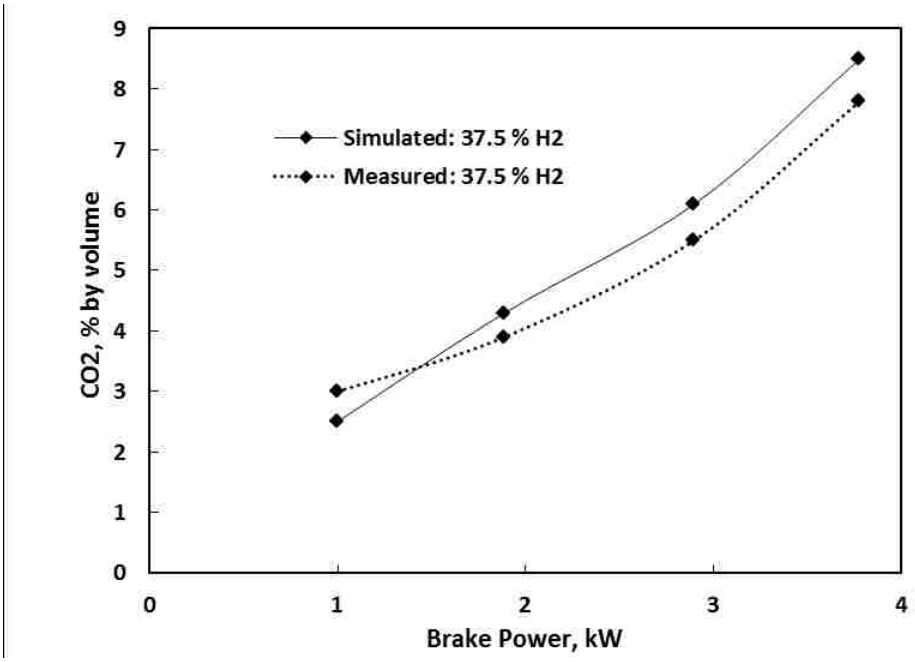

Figure 5 Variation of carbon dioxide with brake power

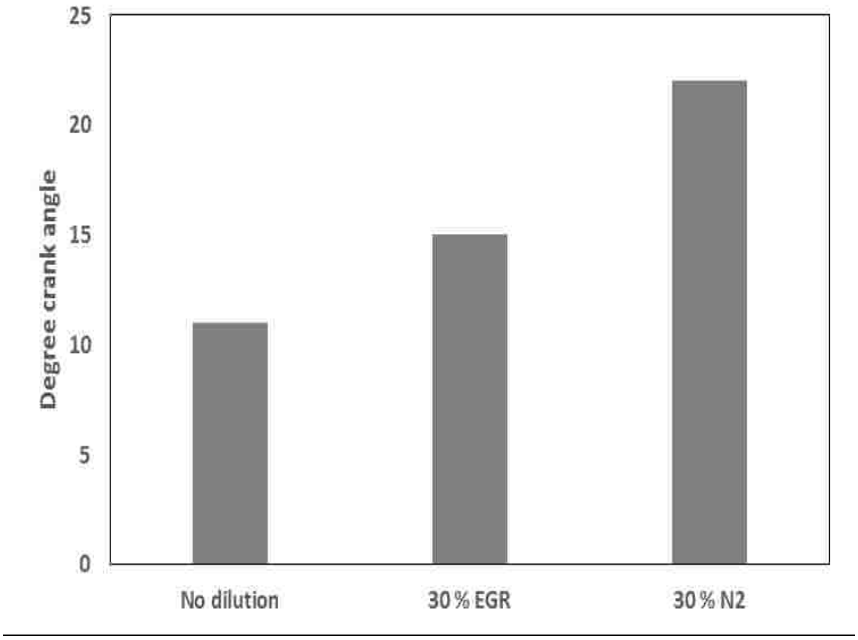

Figure 6 Ignition delay at no dilution, 30% EGR and, 30% N2

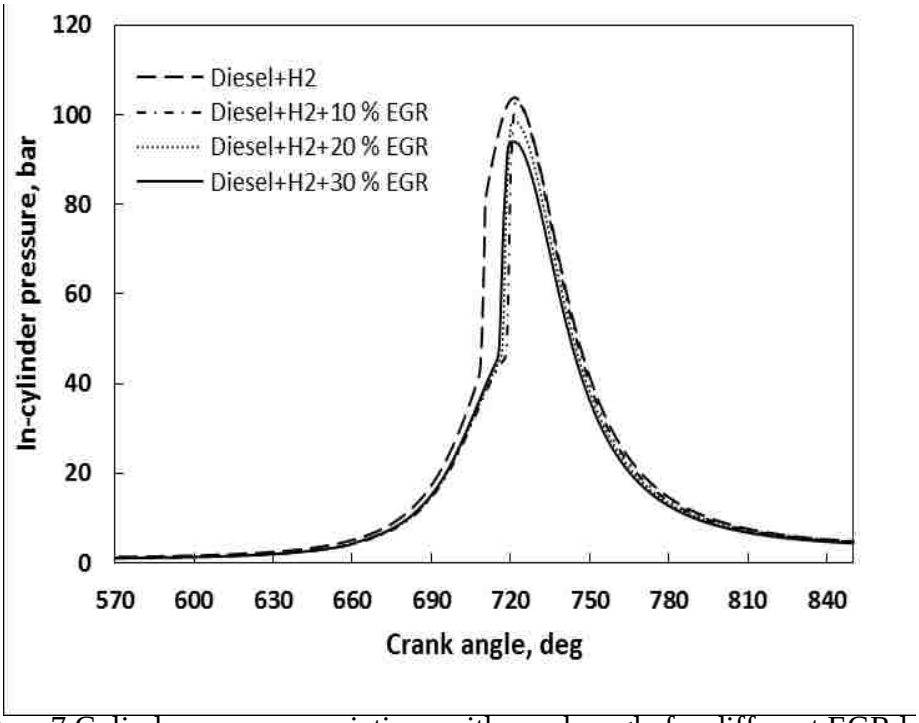

Figure 7 Cylinder pressure variations with crank angle for different EGR levels

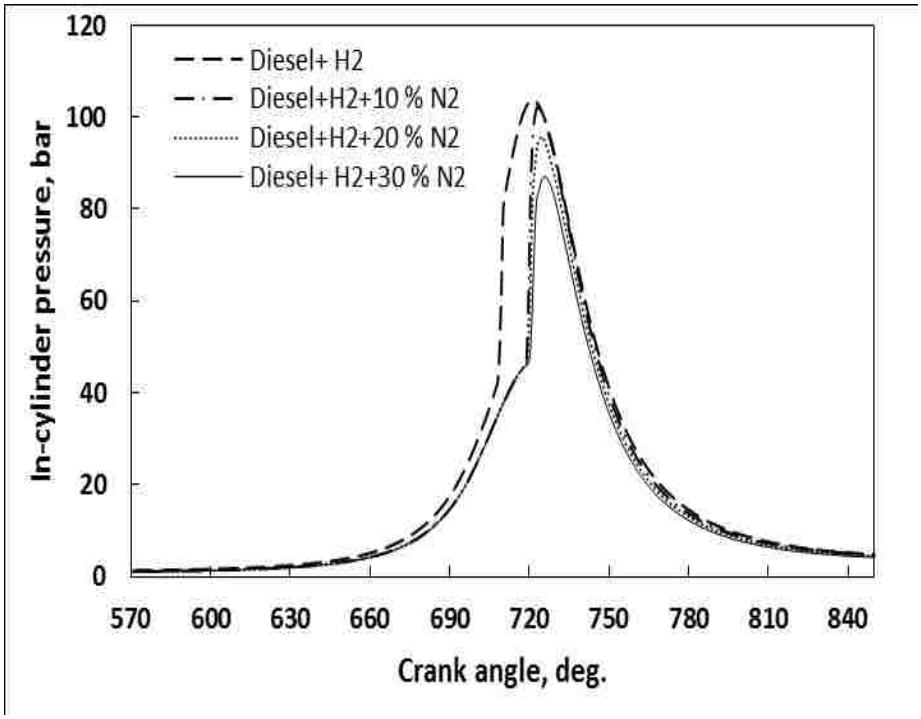

Figure 8 Cylinder pressure variations with crank angle for different N2 dilution levels

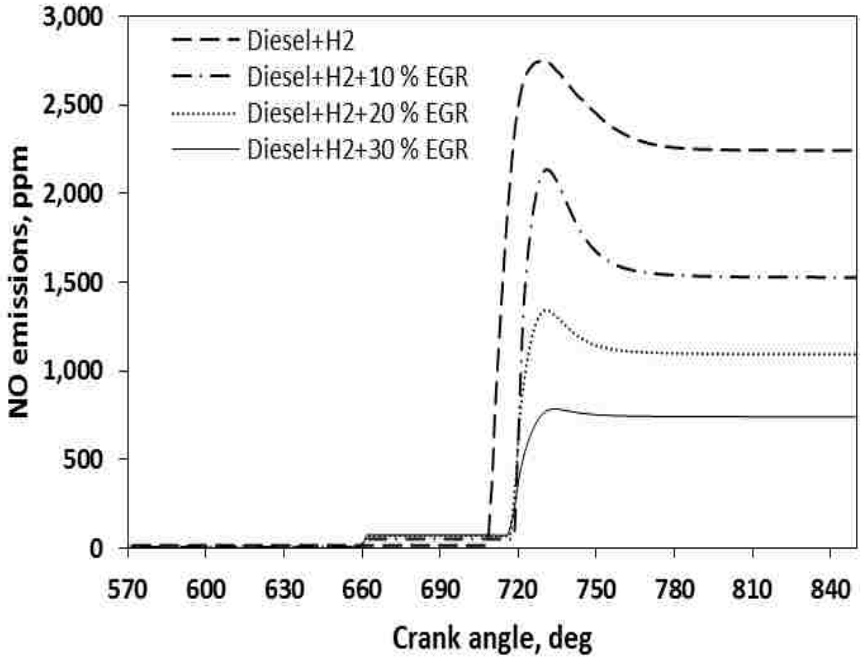

Figure 9 NO concentration as function of crank angle for different EGR levels

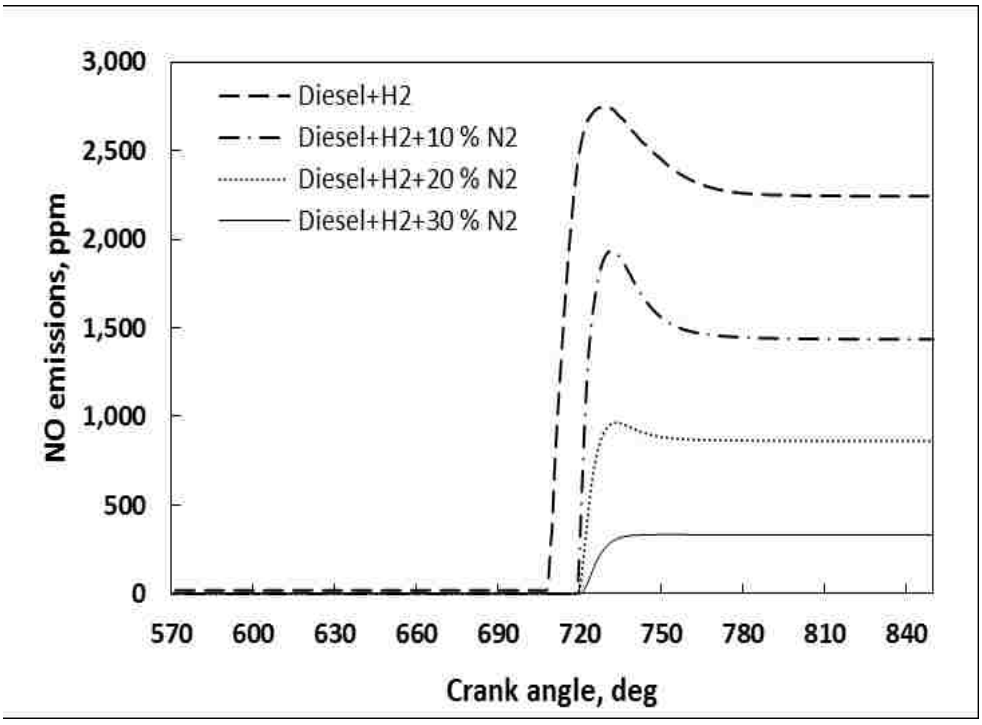

Figure 10 NO concentration as function of crank angle for different N2 levels

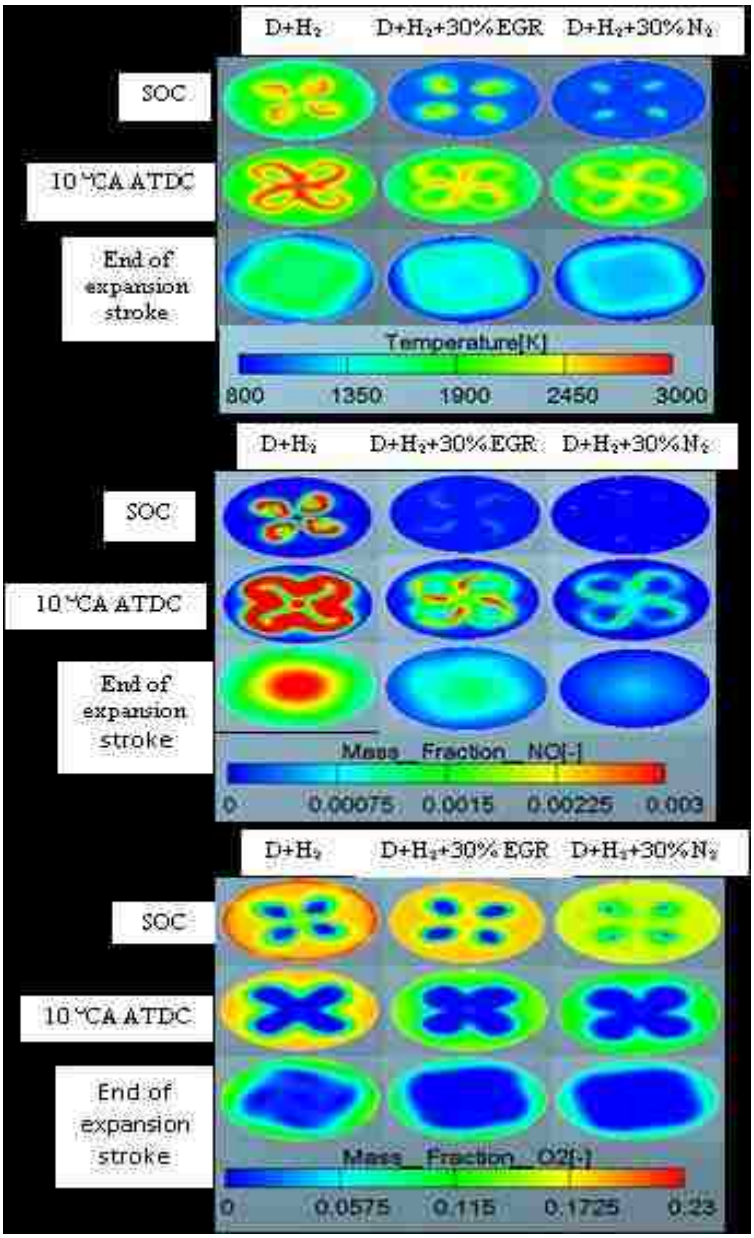

Figure 11 Variation of NO with O2 and temperature for no dilution, 30% EGR and 30% N2

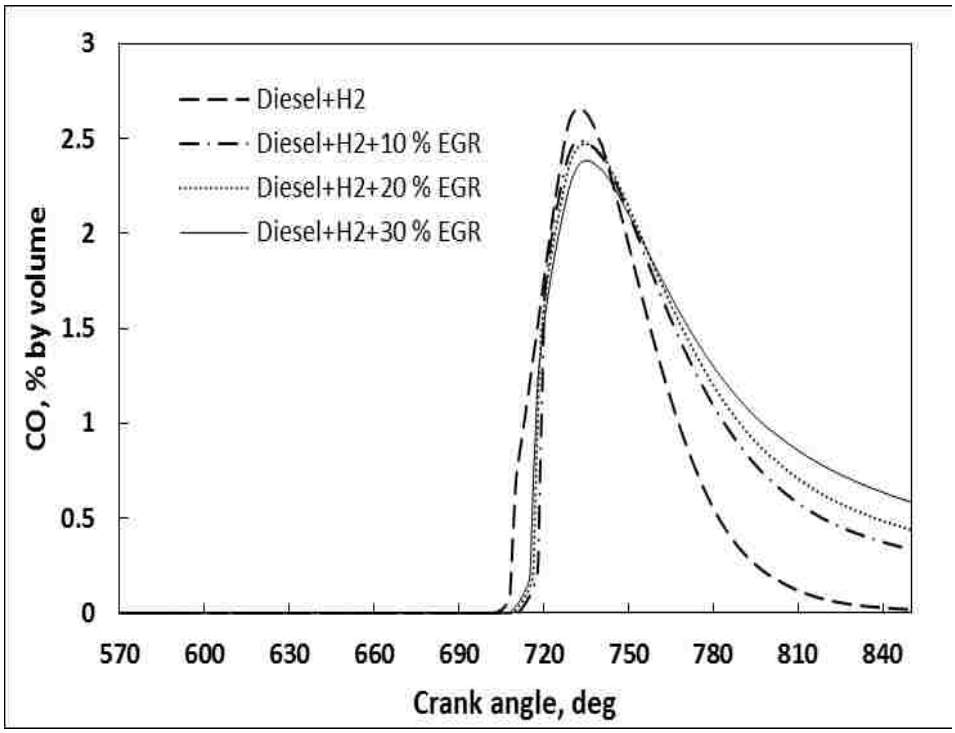

Figure 12 CO concentration as function of crank angle for different EGR levels

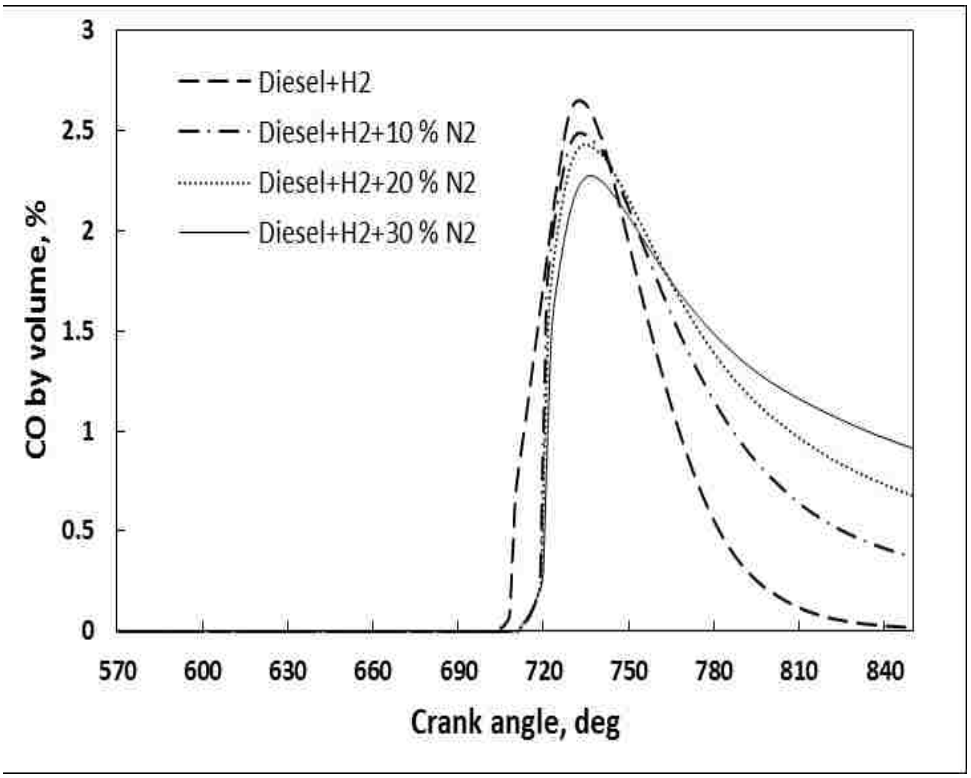

Figure 13 CO concentration as function of crank angle for different N2 dilution levels

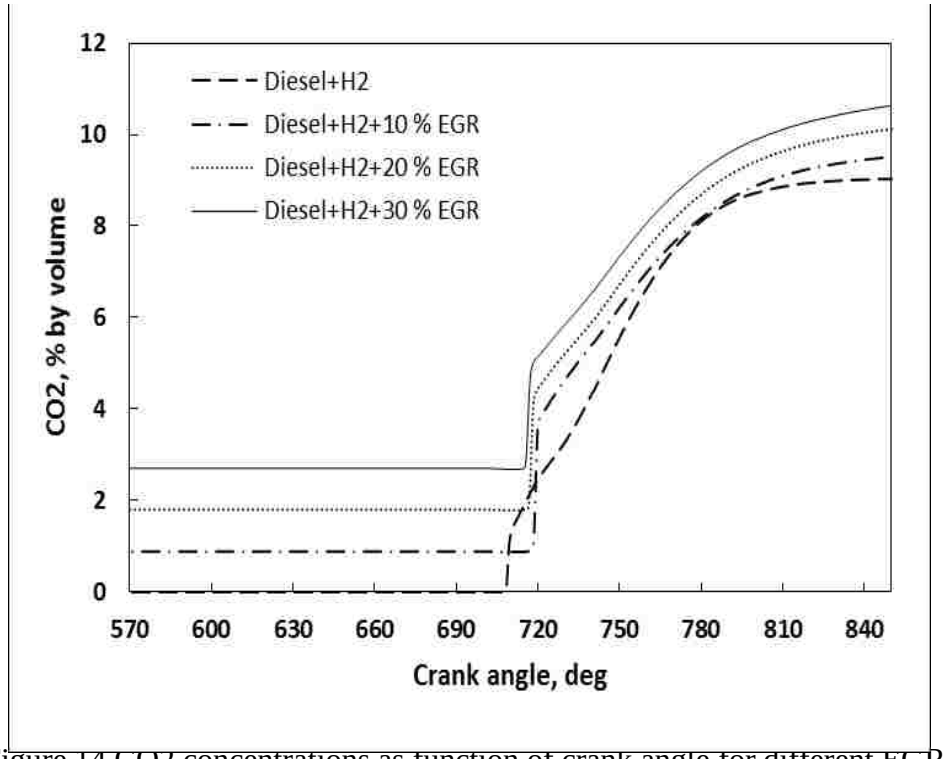

Figure 14 CO2 concentrations as function of crank angle for different EGR levels

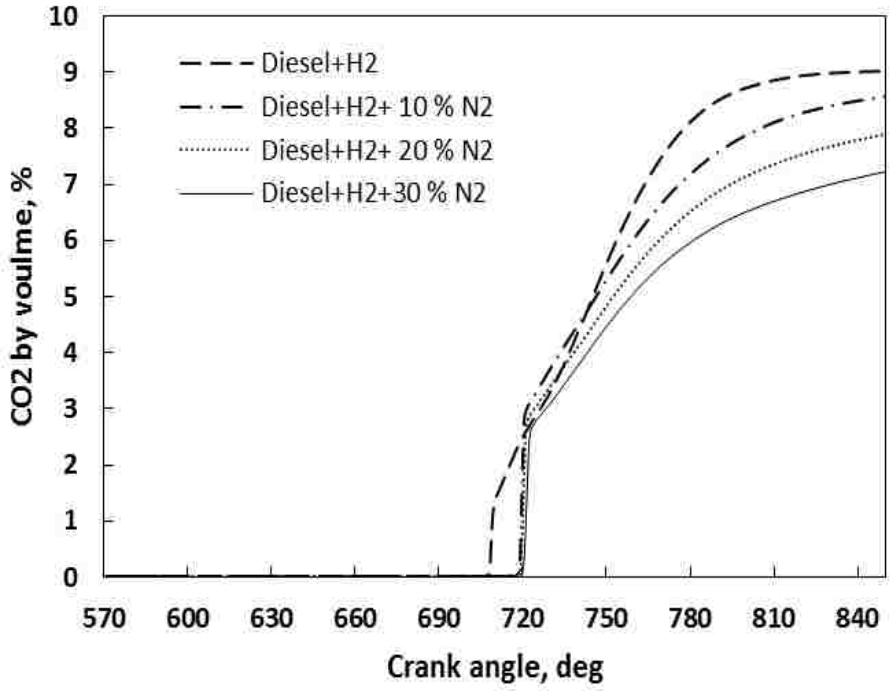

Figure 15 CO2 concentrations as function of crank angle for different N2 dilution levels

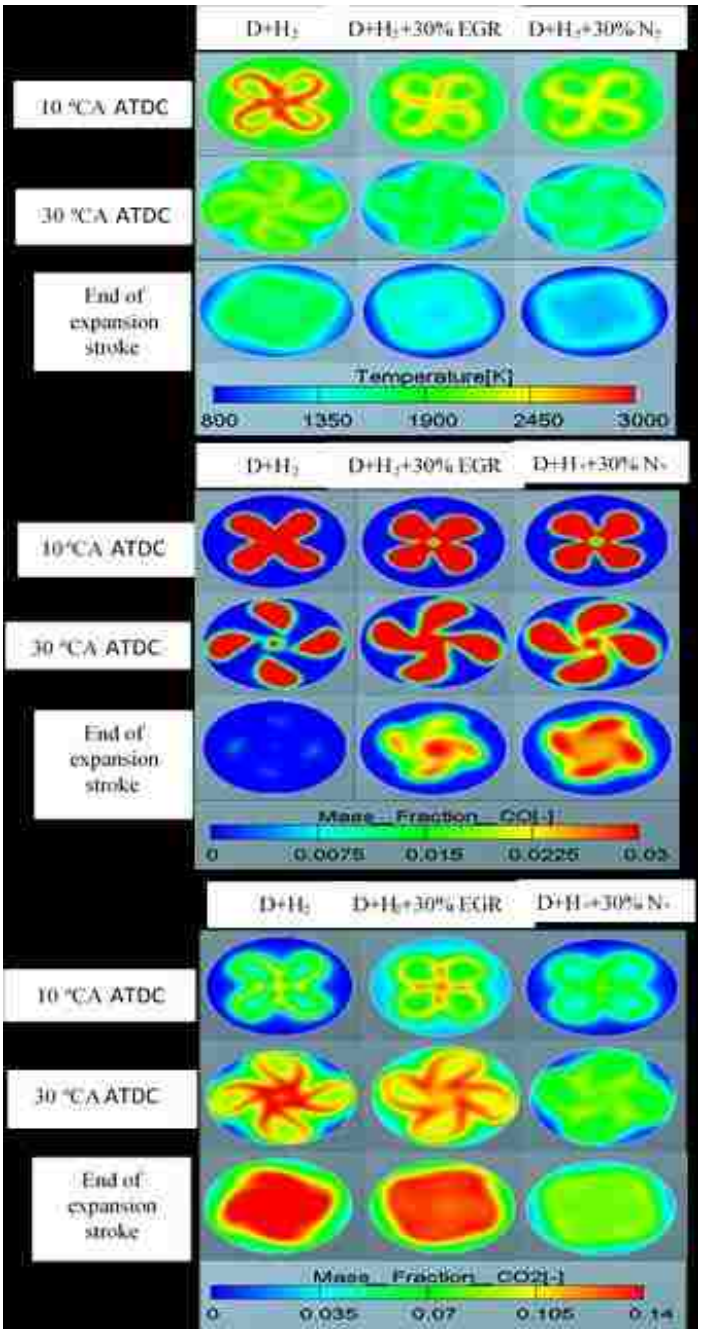

Figure 16 Variations of CO with O2 and temperature for no dilution, 30% EGR and 30% N2

2. SUMMARY AND CONCLUSIONS

The present work aims to numerically study the in-cylinder combustion process, emission and engine performance of spark ignition engine (SI) fueled with hydrogen and compression ignition engine (CI) with a dual fuel (diesel-hydrogen). Simulations were performed using multi-dimensional software AVL FIRE coupled with CHEMKIN. The models have been highly successful in describing the complex in-cylinder combustion processes that are often difficult or impossible to understand experimentally.

In the first part, the model was successfully showed the capability of describing a hydrogen-fueled IC engine with different equivalence ratios. Additionally, the pollutant model, namely the extended Zeldovich model, was also adapted to be able to quantitatively predict the NOx emissions. Once validated, the proposed model provide an insight into the in-cylinder combustion and pollutant formation processes occurring in a hydrogen-fuelled engine with different ignition timings and various levels of EGR.

In the second part in this thesis, three-dimensional simulations were conducted to numerically study the performance, combustion and emission characteristics of a hydrogen assisted diesel engine. A detailed reaction mechanism was developed to include the chemical kinetics of diesel and hydrogen. The developed reaction mechanism was validated against the experimental results with 0%, 37.5 %, 50 % and 90 % of hydrogen induction. Combustion characteristics such as ignition delay, the thermal efficiency, specific energy consumption and exhaust emissions (including NOx, CO_2, CO and soot) were investigated. The model has been applied to examine effects of EGR and N2 dilution on the NOx emissions, and it observed that the model has great potential to predict the effect of EGR and N2 dilution on NOx emission. The present model successfully shows

the capability of describing multi-fuel combustion operations, which provides guidance for selecting experimental test conditions.

The subject for future work will be studies on the effect of combing the ignition timing with other important parameters such as engine speed and equivalence ratio and to find an optimized range of operation conditions for hydrogen-fueled IC engine.

In dual fuel engine model (diesel/hydrogen mixture), the future work will be to investigate the effect of injection timings on engine performance and emissions. Also future work includes optimization of injection parameters such as nozzle geometry and injection strategy.

APPENDIX A

REACTION MECHANISM FOR HYDROGEN

```
elements
h   c    o   n
end

specie
H2    H     O2     O    OH    HO2    H2O    H2O   N    N2    NO
end
```

(k = A T**b exp(-E/RT))

	REACTIONS	A	b	E
53.	h2 + o2 = oh + oh	1.700E+13	0.00	47780
54.	h2 + oh = h2o + h	1.170E+09	1.30	3626
55.	o + oh = o2 + h	4.000E+14	-0.50	0.0
56.	o + h2 = oh + h	5.060E+04	2.67	6290
57.	h + ho2 = o + h2o	3.100E+10	0.00	3590
58.	o + oh + M = ho2 + M	1.000E+16	0.00	0.0
59.	h + o2 + M = ho2 + M	2.800E+18	-.86	0.0
60.	h + o2 + o2 = ho2 + o2	2.080E+19	-1.24	0.0
61.	h + o2 + h2o= ho2 + h2o	11.26E+18	-.76	0.0
62.	h + o2 + n2 = ho2 + n2	2.600E+19	-1.24	0.0
63.	oh + ho2 = h2o + o2	7.500E+12	0.00	0.0
64.	h + ho2 = oh + oh	1.700E+14	0.0	875
65.	o + ho2 = o2 + oh	1.400E+13	0.00	1073
66.	oh + oh = o + h2o	6.000E+08	1.30	0.0
67.	h + h + M = h2 + M	1.000E+18	-1.00	0.0
68.	h + h + h2 = h2 + h2	9.200E+16	-0.60	0.0
69.	h + h + h2o= h2 + h2o	6.000E+19	-1.25	0.0
70.	h + oh + M = h2o + M	1.600E+22	-2.00	0.0
71.	h + o + M = oh + M	6.200E+16	-0.60	0.0
72.	o + o + M = o2 + M	1.890E+13	0.00	-1788
73.	h + ho2 = h2 + o2	1.250E+13	0.00	0.0
74.	ho2 + ho2 = h2o2 + o2	2.000E+12	0.00	0.0
75.	oh + oh (+M) = h2o2 (+M)	7.600E+13	-.37	0.0
	LoW / 4.300E+18 -.900 -1700.00/			
	TRoE/ .7346 94.00 1756.00 5182.00 /			
76.	h2o2 + h = ho2 + h2	1.600E+12	0.00	3800
77.	h2o2 + oh = h2o + ho2	1.000E+13	0.00	1800
78.	h2o2 + h = h2o + oh	1.000E+13	0.00	3590
79.	h2o2 + o = h2o + o2	8.400E+11	0.00	4260
80.	h2o2 + o = oh + ho2	2.000E+13	0.00	5900
81.	h2 + ho2 = h2o + oh	6.500E+11	0.00	18800
82.	n2o + o = n2 + o2	1.400E+12	0.00	10810
83.	n2o + o = no + no	2.900E+13	0.00	23150
84.	n2o + h = n2 + oh	4.400E+14	0.00	18880
85.	n2o + oh = n2 + ho2	2.000E+12	0.00	21060
86.	n2o + M = n2 + o+ M	1.300E+11	0.00	59620
87.	n + no = n2 + o	3.270E+12	0.30	0.0
88.	n + o2 = no + o	6.400E+09	1.00	6280

```
 89. n      + oh       = no     + h       7.333E+13  0.00    1120
end
```

APPENDIX B

REACTION MECHANISM OF HYDROGEN-DIESEL

```
elements
h   c    o   n
end

specie
nc7h16    o2    n2    co2    h2o  co   h2 oh  h2o2  ho2     h
o
ch3o    ch2o   hco  ch2  ch3   ch4 c2h3 c2h4  c2h5 c3h4 c3h5 c3h6
c3h7
c7h15-2   c7h15o2    c7ket12  c5h11co  n2o  no  n
end

                                          (k = A T**b exp(-E/RT))
 REACTIONS                                   A       b        E

 1. nc7h16 + h  = c7h15-2 + h2          4.380e+07  2.0     4760.0
 2. nc7h16 + oh = c7h15-2 + h2o         9.700e+09  1.3     1690.0
 3. nc7h16 + ho2= c7h15-2 + h2o2        1.650e+13  0.0    16950.0
 4. nc7h16 + o2 = c7h15-2 + ho2         2.000e+15  0.0    47380.0
 5. c7h15-2 + o2 = c7h15o2              1.560e+12  0.0     0.0
 6. c7h15o2 + o2  = c7ket12 + oh        4.500E+14  0.0   18232.71
 7. c7ket12      = c5h11co + ch2o + oh  9.530e+14 0.0   4.110e+4
 8. c5h11co      = c2h4  + c3h7 + co    9.84E+15  0.0   4.02E+04
 9. c7h15-2      = c2h5 + c2h4  + c3h6  7.045E+14  0.0  3.46E+04
 10. c3h7        = c2h4 + ch3           9.600e+13  0.0  30950.0
 11. c3h7        = c3h6 + h             1.250e+14  0.0  36900.0
 12. c3h6 + ch3  = c3h5 + ch4           9.000e+12  0.0  8480.0
 13. c3h5 + o2   = c3h4 + ho2           6.000e+11  0.0  10000.0
 14. c3h4 + oh   = c2h3 + ch2o          1.000e+12  0.0  0.0
 15. c3h4 + oh   = c2h4 + hco           1.000e+12  0.0  0.0
 16. ch3   + ho2 = ch3o  + oh           5.000e+13  0.0  0.0
 17. ch3   + oh  = ch2   + h2o          7.500e+06  2.0  5000
 18. ch2   + oh  = ch2o  + h            2.500e+13  0.0  0.0
 19. ch2   + o2  = hco   + oh           4.300e+10  0.0  -500
 20. ch2   + o2  = co2   + h2           6.900e+11  0.0  500
 21. ch2   + o2  = co    + h2o          2.000e+10  0.0  -1000
 22. ch2   + o2  = ch2o  + o            5.000e+13  0.0  9000
 23. ch2   + o2  = co2   + h     + h    1.600e+12  0.0  1000
 24. ch2   + o2  = co    + oh    + h    8.600e+10  0.0  -500
 25. ch3o  + co  = ch3   + co2          1.570e+14  0.0  11800
 26. co    + oh  = co2   + h            8.987e+07  1.38 5232.877
 27. o     + oh  = o2    + h            4.000e+14 -0.50 0.0
 28. h     + ho2 = oh    + oh           1.700e+14  0.0  875
 29. oh    + oh  = o     + h2o          6.000e+08  1.30 0.0
 30. h     + o2  + m  = ho2   + m       3.600e+17 -0.72 0.0
       h2o/21./  co2/5.0/  h2/3.3/  co/2.0/
 31. h2o2  + m   = oh    + oh    + m    1.000e+16  0.00 45500
       h2o/21./  co2/5.0/  h2/3.3/  co/2.0/
 32. h2    + oh  = h2o   + h            1.170e+09  1.30 3626
```

```
33. ho2   + ho2 = h2o2  + o2          3.000e+12  0.00  0.0
34. ch2o  + oh  = hco   + h2o         5.563e+10  1.095 -76.517
35. ch2o  + ho2 = hco   + h2o2        3.000e+12  0.00  8000
36. hco   + o2  = ho2   + co          3.300e+13 -0.40  0.0
37. hco   + m   = h     + co   + m    1.591E+18  0.95  56712.32
38. ch3   + ch3o= ch4   + ch2o        4.300e+14  0.00  0.0
39. c2h4  + oh  = ch2o  + ch3         6.000e+13  0.0   960
40. c2h4  + oh  = c2h3  + h2o         8.020e+13  0.00  5955
41. c2h3  + o2  = ch2o  + hco         4.000e+12  0.00  -250
42. c2h3  + hco = c2h4  + co          6.034e+13  0.0   0.0
43. c2h5  + o2  = c2h4  + ho2         2.000e+10  0.0   -2200
44. ch4   + o2  = ch3   + ho2         7.900e+13  0.00  56000
45. oh    + ho2 = h2o   + o2          7.50E+12   0.0   0.0
46. ch3   + o2  = ch2o  + oh          3.80E+11   0.0   9000
47. ch4   + h   = ch3   + h2          6.600e+08  1.60  10840
48. ch4   + oh  = ch3   + h2o         1.600e+06  2.10  2460
49. ch4   + o   = ch3   + oh          1.020e+09  1.50  8604
50. ch4   + ho2 = ch3   + h2o2        9.000e+11  0.00  18700
51. ch4   + ch2 = ch3   + ch3         4.000e+12  0.00  -570
52. c3h6        = c2h3 + ch3          3.150e+15  0.0   85500
53. h2    + o2  = oh    + oh          1.700E+13  0.00    47780
54. h2    + oh  = h2o   + h           1.170E+09  1.30    3626
55. o     + oh  = o2    + h           4.000E+14 -0.50    0.0
56. o     + h2  = oh    + h           5.060E+04  2.67    6290
57. h     + ho2 = o     + h2o         3.100E+10  0.00    3590
58. o     + oh  + M  = ho2   + M      1.000E+16  0.00    0.0
59. h     + o2  + M  = ho2   + M      2.800E+18  -.86    0.0
60. h     + o2  + o2 = ho2   + o2     2.080E+19 -1.24    0.0
61. h     + o2  + h2o= ho2   + h2o    11.26E+18  -.76    0.0
62. h     + o2  + n2 = ho2   + n2     2.600E+19 -1.24    0.0
63. oh    + ho2      = h2o   + o2     7.500E+12  0.00    0.0
64. h     + ho2      = oh    + oh     1.700E+14  0.0     875
65. o     + ho2      = o2    + oh     1.400E+13  0.00    1073
66. oh    + oh       = o     + h2o    6.000E+08  1.30    0.0
67. h     + h   + M  = h2    + M      1.000E+18 -1.00    0.0
68. h     + h   + h2 = h2    + h2     9.200E+16 -0.60    0.0
69. h     + h   + h2o= h2    + h2o    6.000E+19 -1.25    0.0
70. h     + oh  + M  = h2o   + M      1.600E+22 -2.00    0.0
71. h     + o   + M  = oh    + M      6.200E+16 -0.60    0.0
72. o     + o   + M  = o2    + M      1.890E+13  0.00    -1788
73. h     + ho2      = h2    + o2     1.250E+13  0.00    0.0
74. ho2   + ho2      = h2o2  + o2     2.000E+12  0.00    0.0
75. oh    + oh  (+M) = h2o2 (+M)      7.600E+13  -.37    0.0
    LoW  /  4.300E+18    -.900  -1700.00/
    TRoE/   .7346   94.00  1756.00  5182.00 /
76. h2o2  + h        = ho2   + h2     1.600E+12  0.00    3800
77. h2o2  + oh       = h2o   + ho2    1.000E+13  0.00    1800
78. h2o2  + h        = h2o   + oh     1.000E+13  0.00    3590
79. h2o2  + o        = h2o   + o2     8.400E+11  0.00    4260
80. h2o2  + o        = oh    + ho2    2.000E+13  0.00    5900
81. h2    + ho2      = h2o   + oh     6.500E+11  0.00    18800
```

```
 82. n2o   + o       = n2    + o2      1.400E+12  0.00    10810
 83. n2o   + o       = no    + no      2.900E+13  0.00    23150
 84. n2o   + h       = n2    + oh      4.400E+14  0.00    18880
 85. n2o   + oh      = n2    + ho2     2.000E+12  0.00    21060
 86. n2o   + M       = n2    + o+ M    1.300E+11  0.00    59620
 87. n     + no      = n2    + o       3.270E+12  0.30    0.0
 88. n     + o2      = no    + o       6.400E+09  1.00    6280
 89. n     + oh      = no    + h       7.333E+13  0.00    1120
end
```

VITA

Hassan Khairallah was born in Tobruk, Libya. He was admitted to Omer Al-Mokhtar University, Libya in 1996 and received his Bachelor's degree in Mechanical Engineering in 2001. He continued his graduate study at Tabbin Institute for Metallurgical Studies, Cairo, Egypt, and received his M.S. degree in Mechanical Engineering in 2005. He worked at Omer Al-Mokhtar University, Libya as a lecturer in Mechanical Engineering Department between 2005 and 2008.

Since May 2009, Mr. Khairallah has been enrolled in the Ph.D. Program in the Department of Mechanical and Aerospace Engineering at Missouri University of Science and Technology, Rolla, Missouri, USA. In August 2015, he received his Ph.D. in Mechanical Engineering from Missouri University of Science and Technology.